"A NEW APPROACH TO THE INITIAL MASS FUNCTION OF YOUNG STELLAR CLUSTERS"

By

Bertha Alicia Porras Juárez

A thesis submitted in partial fulfilment of the Requirements for the degree of Doctor in astrophysics at the National Institute for Astrophysics, Optics and Electronics

Advisors:

Dra. Irene Cruz-González Espinosa
Dr. Luis Salas Casales

Instituto de Astronomía, UNAM

Tonantzintla, Pue.

June 2001

"A NEW APPROACH TO THE INITIAL MASS FUNCTION OF YOUNG STELLAR CLUSTERS"

Por

Bertha Alicia Porras Juárez

Tesis sometida como requisito parcial para obtener el grado de **Doctor en Ciencias** en la especialidad de **Astrofísica** en el Instituto Nacional de Astrofísica Óptica y Electrónica.

Supervisada por:

Dra. Irene Cruz-González Espinosa

Dr. Luis Salas Casales

Instituto de Astronomía, UNAM

Tonantzintla. Pue.

Junio de 2001

ABSTRACT

The main goal in this thesis is to study the IMF in a sample of embedded star formation regions along the Perseus Arm, at an average distance of ∼3.5 kpc. Selection criteria were established in order to do near-infrared observations (J, H, K-bands) with the 2.1m telescope at the Observatorio Astronómico Nacional in San Pedro Mártir, Baja California, México.

The survey of the 38 star forming regions provided information on 6298 stars in 40 young stellar clusters (YSCs). The intrinsic error achieved in the photometry is less than 7%.

We obtain cluster parameters such as surface density ($3< \Sigma <220$ stars/pc^2), cluster radius ($0.26< r_c <2.34$ pc), and average concentration parameter (∼3 times smaller than globular clusters).

We develop a method to estimate ages based on a comparison between observed and theoretical luminosity function histograms. The estimated ages for clusters yield a mean value of 2.42 ± 1.20 Myr in an interval from 1.1 to 5.5 Myr.

The computation of the extinction to individual stars and their masses depend on its location in the J-H/H-K diagram. For stars along the reddened MS, the J/J-H diagram is used taking each star along the A_V vector direction to the corresponding isochrone, the mass value is obtained from the scale along this isochrone. While for reddened CTT and Ae/Be stars, they are dereddened directly based on their distance to the CTTS line (Meyer 1996) in the J-H/H-K diagram and their mass is estimated using the relations $\log M = -0.25\ M_H + 0.44$ and $\log M = -0.24\ M_K + 0.24$, where M_H and M_K are the uncorrected for extinction H- and K-band magnitudes (Carpenter et al. 1993).

All clusters show average extinction values greater than ∼4 magnitudes and about 20% of the YSC sample have $< A_V >$ grater than 10 mag.

Stellar masses are obtained to construct the mass distributions that yield the cluster IMF, i.e. the number of stars per logarithmic mass interval. This study concludes that young stellar clusters have an IMF composed of three segments:

$$\Gamma = \begin{cases} -0.20 & \text{for } 0.3 < M < 0.6 M_\odot \\ -0.75 \pm 0.10 & \text{for } 0.6 < M < 1 M_\odot \\ -0.96 \pm 0.14 & \text{for } M > 1 M_\odot \end{cases}$$

where the first value, from Scalo 1998, is suggested from the study of 6 YSCs, the second arises from 14 YSCs and the final one from the most complete sample of IMF indices of 40 YSCs.

Spatial mass distributions of YSCs and correlations between physical cluster parameters, show two types of clusters, massive and less massive. The less massive clusters present an IMF that is steeper than the IMF of the massive ones.

Properties and a richness of information is summarized in a Catalog of the 40 YSCs.

RESÚMEN

La meta principal de esta tesis es estudiar la IMF en una muestra de regiones de formación estelar enterradas a lo largo del Brazo de Perseo, a una distancia promedio de ∼3.5 kpc. Establecimos criterios de selección con el propósito de llevar a cabo observaciones (en las bandas J, H y K) con el telescopio de 2.1m en el OAN/SPM.

Las observaciones de 38 regiones de formación estelar nos dieron información de 6298 estrellas en 40 cúmulos estelares jóvenes (YSCs). Los errores intrínsecos en la fotometría son menores del 7%.

Obtenemos parámetros de los cúmulos tales como su densidad superficial ($3< \Sigma <220$ stars/pc^2), radio del cúmulo ($0.26< r_c <2.34$ pc), y el parámetro de concentración promedio (∼3 veces menor que los cúmulos globulares).

Dessarrollamos un método de estimación de edades basado en la comparación entre histogramas de funciones de luminosidad teóricas y observadas. Las edades estimadas para los cúmulos en promedio es de 2.42 ± 1.20 Myr en un rango de 1.1 a 5.5 Myr.

El cálculo de la extinción a estrellas individuales y su masa dependen de su localización en el diagrama J-H/H-K. Para estrellas a lo largo de la MS enrojecida, el diagrama J/J-H es usado para llevar cada estrella a lo largo del vector de extinción A_V, a la isocrona correspondiente, el valor de la masa es obtenido de la escala a lo largo de esta isocrona. Mientras que para las estrellas CTT y Ae/Be, son desenrojecidas directamente en el diagrama J-H/H-K, basándonos en su distancia a la línea de CTTS (Meyer 1996), y su masa es estimada usando las relaciones $\log M = -0.25\ M_H + 0.44$ y $\log M = -0.24\ M_K + 0.24$, donde M_H y M_K son las magnitudes absolutas en la banda H y K no corregidas por extinción (Carpenter et al. 1993).

Todos los cúmulos muestran una extinción interestelar mayor a ∼4 magnitudes y cerca del 20% de la muestra de YSCs tiene $< A_V >$ mayor a 10 mag.

Las masas estelares se obtienen para construir las distribuciones de masa que llevan a la IMF de los cúmulos, es decir, al número de estrellas por intervalo de masa logarítmico. Este estudio concluye que los cúmulos estelares jóvenes tienen una IMF compuesta por tres segmentos:

$$\Gamma = \begin{cases} -0.20 & \text{for } 0.3 < M < 0.6 M_\odot \\ -0.75 \pm 0.10 & \text{for } 0.6 < M < 1 M_\odot \\ -0.96 \pm 0.14 & \text{for } M > 1 M_\odot \end{cases}$$

donde el primer valor,de Scalo 1998, es sugerido del estudio de 6 YSCs, el segundo de 14 YSCs y el último de la muestra mas completa de índices IMF de 40 YSCs.

Las distribuciones espaciales de masa y las correlaciones entre parámetros físicos, muestran dos tipos de cúmulos, masivos y menos masivos. Los menos masivos presentan una IMF que es mas empinada que la IMF de los masivos.

Las propiedades y una riqueza de informacion es resumida en un Catalogo de los 40 YSCs.

AGRADECIMIENTOS

Deseo extender mi mas profundo agradecimiento a todos los investigadores, familiares y amigos que hicieron posible con su ayuda profesional y moral que este trabajo llegara a su termino.

A la Dra. Irene Cruz-González y al Dr. Luis Salas, por su entrega y profesionalismo para mostrarme en la práctica, la metodología de la investigación astronómica y el trabajo conjunto, desde la obtención de datos y la operación de CAMILA, hasta la escritura de nuestros resultados en artículos internacionales y su divulgación en congresos especializados.

Al Dr. Leonid Georgiev, quien me mostró el manejo del paquete de reducción de datos IDL/DAOPHOT, mismo que sirvió para realizar la fotometría de todas mis observaciones.

A la Dra. Irene Cruz-González, Dr. Jorge Cantó, Dr. Stan Kurtz, Dr. Luis Carrasco, Dr. Divakara Mayya y al Dr. Jose Guichard, quienes como miembros de mi comité asesor de tesis tanto en el IA-UNAM como en el INAOE, estuvieron pendientes de mi avance semestral y me hicieron importantes comentarios para considerar en la misma, incluso en el escrito final.

A mis profesores del INAOE, Dr. Alfonso Serrano, Dr. Luis Carrasco, Dr. Octavio Cardona, Dra. Elsa Recillas, Dr. Manuel Corona, Dr. Alberto Carramiñana, Dr. Alberto Buzzoni, Dr. Jose Guichard, Dr. Alejandro Palma, Dr. Nicolai Silantiev, Dr. Alejandro González y el Dr. William Wall, por heredarme su saber en materias de Astronomia y Astrofisica, formadores de mi gusto por la búsqueda de respuestas (y nuevas preguntas) en el universo que hoy me es posible escudriñar.

A mis padres, Sra. Lucía Juárez Morado y Sr. Héctor Díaz Briseño, que con su apoyo incondicional y su confianza en mi perseverancia, me alentaron en todo momento.

A mis familiares, Norma, Pili, Abraham, Hector, Paty, Rafa, Angel, Alba y Elva, tios y tias, quienes sin ser especialistas, pero con inquietante curiosidad, preguntaban continuamente por la culminación de este trabajo.

A CONACyT, que como institución de apoyo a estudiantes de posgrado, tuvo a bien otorgarme una beca doctoral (de 3 años, mas una prorroga de 6 meses), que sirvió para mi manutención durante $\sim$80% del tiempo usado en la elaboración de esta tesis.

Al INAOE y al IA-UNAM, como instituciones, por brindarme todos sus espacios (cubículo, biblioteca, computadora, apoyo a congresos y viajes de observación, acceso a observatorio, etc.) indispensables para mi trabajo.

A mis compañeros de grado (y de desvelos) y amigos de ambas instituciones: Aarón, César, Leobardo, Ricardo, Abraham, Daniel, Olga, Gaby López, Pablo, César G., Jose Luis, Rosario, Fidel, Ari, Erika, Lorena, Lalo, Ricardo, Jose Luis, Vicente y Migue.

A mi pareja, Miguel Angel Trinidad, por su oportuna llegada a mi vida, por compartir conmigo los momentos finales de este anhelo y por apoyarme en convertirlo, en una meta alcanzada.

Finalmente, considero que no estaría completa esta lista si no menciono mi agradecimiento a la Vida, sin ella habría sido literalmente imposible esta tarea. Por ello, agradezco al grupo de donadores de sangre que solidaria y desinteresadamente me ayudaron a conservar mi vida, en los momentos difíciles de 1989.

Sin importar el orden en que los he mencionado, a todos, muchas gracias.

.

To those who read and improve this work

Contents

List of Figures

List of Tables

Chapter 1

Introduction

Observations indicate that stars frequently form in clustered environments - in rich clusters of hundreds to many thousands of stars, or in smaller groups and aggregates containing of order ten to a few tenths of stars. It is only recently, however, that the properties of young clusters are beginning to be well characterized. Deeply embedded clusters of young stars offer an excellent laboratory to study the earliest phases in stellar evolution. These rich clusters have been revealed through near-infrared array observations of nearby molecular clouds.

The general theory of cluster formation is really at its infancy. In a review paper by Clarke et al. 2000 a scenario prior to cluster formation consists of an ensemble of dense lumps of mass M_J (the mass of thermally supported lumps that are marginally Jeans stable), which are not gravitationally bound and are later on destabilized externally which induce their collapse. Two extreme cases in the possibilities of cluster formation are described: The top-down fragmentation which produces coeval structures that end up in a Jeans mass close to the protocluster mass. And the bottom-up case where the Jeans mass is close to the stellar mass and has an age spread between clumps which depends on the timescale at which the discrete lumps are destabilized. Studies of star forming clusters show that the low-mass molecular cloud cores are possibly produced by top-down fragmentation while more populous clusters result from a bottom-up process.

The collection of young stars with ages of 10 Myr or less found in association with molecular clouds are referred to as the **initial stellar population**. Studying this initial stellar population in our Galaxy is a fundamental problem, because the determination of the individual and global characteristics may provide a better understanding of the effects of molecular clouds fragmentation in the formation of **young stellar clusters (YSCs)** and how the individual stellar masses are

acquired and distributed. Furthermore, they may lead to the knowledge of the mass contribution of the young stellar population in the Milky Way and other galaxies.

Studies of age and mass distribution of single star-forming events, associated with the individual molecular cloud cores at the earliest stages of stellar evolution, are crucial to our understanding of young stellar clusters. Several studies of the stellar content in nearby YSCs have characterized their physical parameters such as: size ($\sim$0.2 - 0.8 pc), spatial distribution (centrally concentrated), stellar content ($\sim$100 stars), age ($\leq$ 10 Myr) and total mass (20 - 160 $M_{\odot}$). The age and individual stellar mass are the most important parameters and require special techniques to derive them. Rough mass and age distributions can be obtained from near-IR photometry alone. While more reliable values of stellar masses require combining photometry and spectral types from near-IR spectroscopy to place stars directly in the H-R diagram.

One global characteristic of YSCs is how the parent cloud mass gets distributed into stars. This initial distribution of stellar masses is known as the **initial mass function (IMF)**. Our knowledge of the IMF comes from studies of volume-limited samples of stars. The IMF was first studied in the solar neighborhood and in this case evolutionary corrections to the observed mass distribution were required. In young stellar clusters the observed mass distributions reveal the history of star formation from the cloud fragmentation up to now, but since on-going star formation is present the integrated final outcome of the cloud core and in consequence the true IMF are really unknown.

Young stellar clusters provide the best laboratories to study the IMF in a range of 0.5 to 15 $M_{\odot}$. The observational advantages are (Meyer et al. 2000): 1) because of their youth, there are minimum evolutionary corrections to the present day mass distribution, and so, the present mass distribution can be considered as the IMF; 2) youth precludes wandering of cluster members far from their birth-sites due to peculiar motions; 3) observations are more sensitive to low-mass objects because the M-L relationship for stars in the PMS phase is not as steep function of mass as for stars on the main sequence; 4) they are not contaminated by foreground stars due to their compactness; 5) they are not contaminated by background stars due to the presence of molecular gas which provides a natural veil to avoid them.

The solar neighborhood IMF was first studied in a now classical work by Edwin E. Salpeter in 1955. The IMF for the whole range of masses was first obtained by Miller & Scalo 1979. As a result, the generally accepted concept of IMF is the number of stars per logarithmic mass interval, and the power law

notation more commonly used is:

$$\Gamma = \frac{d\,log\Phi(log M)}{d\,log M}, \tag{1.1}$$

where Γ is called the **IMF index**. Another used notation is $\gamma = d\phi/dM$ and so, Γ and γ are related by $\Gamma = \gamma + 1$.

In this notation the Salpeter IMF yields Γ_{Sal} = -1.35 in a mass interval of 3 to 10 $M_{\odot}$. Miller & Scalo 1979 found a three-segment power law IMF in the solar neighborhood, Γ=-0.4 in an interval of 0.1 to 1 $M_{\odot}$, -1.5 in an interval of 1 to 10 $M_{\odot}$ and -2.3 for masses $>$ 10 $M_{\odot}$. This third interval was later corrected to the value of Γ = -1.2 by Scalo 1986. Kroupa et al. 1993 solar neighborhood (within 5.2 pc of the Sun) study of stars with masses between 0.08 and 100 $M_{\odot}$ shows that the IMF can be approximated with Γ: 0.3 to -0.85 for $0.08 < M < 0.5$ $M_{\odot}$, -1.2 for $0.5 \leq M \leq 1$ $M_{\odot}$ and -1.7 for $M >$1 $M_{\odot}$. Either of these IMFs, specially the first two, have been used in the literature and assumed as universal laws, nevertheless the universality of the IMF is still an open question (e.g. Scalo 1998).

Recent reviews on the IMF based on theoretical and observational work have been presented by Scalo 1998, Clarke 1998, Larson 1998 and 1999, Elmegreen 1999 and Meyer et al. 2000. Important reviews on the IMF in the galactic and extragalactic context are contained in the ASP conference by Gilmore & Howell 1998.

The IMF index as a function of the average $\log M$ of 61 clusters and associations in the Milky Way and the LMC presented by Scalo 1998 (Figure 5) and reproduced here in Fig. 1.1, summarizes several papers on the IMF on a wide mass interval and includes both field stars, young and older clusters. This plot suggests that $0 < \Gamma < -0.5$ for $0.1 < M < 0.8$ $M_{\odot}$ which is in agreement with field stars. Above about 1 $M_{\odot}$ the spread in the IMF index is quite large ($\Delta\Gamma \sim 1$). Scalo concludes that there is no evidence for a clustering of points around the Salpeter value (-1.35). Also that the uncertainties are so large that either the IMF is not yet known or the significant variations observed are real. He further points out that if the IMF variations are real they "apparently do not depend much on metallicity, stellar density, or galactocentric radius, but must either depend on some unknown combination of environmental variables or else the IMF, as usually conceived, is not a statistically well-defined probability function." This point of view contrasts with Larson 1999, who based on the same figure concludes "no clear evidence has been found for any systematic dependence of the IMF on any property of the systems studied, and this has lead to the current widely held view that the IMF is universal, at least in the local universe."

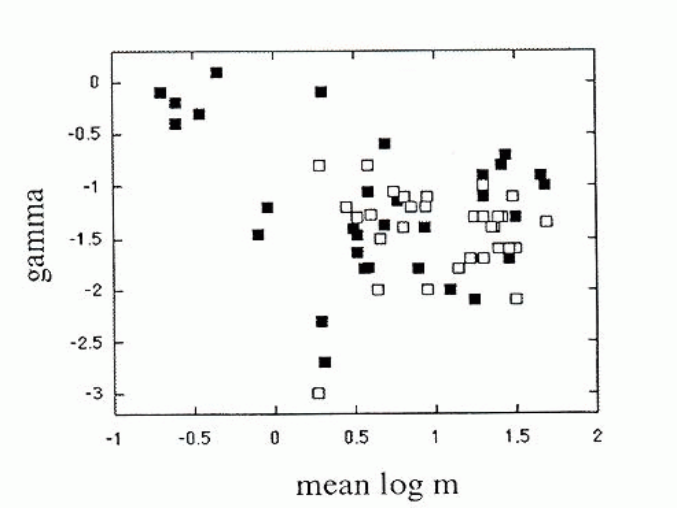

Figure 1.1 IMF index Γ as a function of average $\log m$ for 61 clusters and associations. Filled and open symbols refer to the Milky Way and the LMC, respectively. Reproduction of Figure 5 in Scalo 1998.

For galactic evolution studies Scalo 1998 suggests the use of the following three-segment power law form:

$$\begin{array}{rcll} \Gamma & = & -0.2 \pm 0.3 & 0.1 - 1\ M_\odot \\ & & -1.7 \pm 0.5 & 1 - 10\ M_\odot \\ & & -1.3 \pm 0.5 & 10 - 100\ M_\odot \end{array} \tag{1.2}$$

where the $\pm$ symbols can be interpreted as a measure of the empirical uncertainties and/or the real IMF variations.

The minimal requirement for collapse to occur is the classical Jeans criterion that the self-gravity of a dense core must overcome its thermal pressure. For a given temperature and density, this Jeans mass is fixed. Considering a critically stable "Bonnor-Ebert sphere" (Larson 1998), with typical molecular cloud temperature (10 K) and a non-thermal pressure (3×10^5 cm $^{-3}$ K), the resulting radius and Jeans mass are about 0.03 pc and 0.7 $M_\odot$, respectively. The latter is typically observed in the structure of molecular clouds (see reviews by Evans 1999 and Williams et al. 2000).

Molecular clouds are dominated by turbulent and magnetic pressures on large scales and by thermal pressure on small scales. The transition between the two regimes is in fact what defines the Jeans scale when the latter is calculated by

assuming pressure balance between a thermally supported isothermal clump and the turbulent ambient medium. The Jeans mass is proportional to $T^2/P^{1/2}$, where T is the temperature and P is the pressure in star-forming clouds. In these terms, clouds with higher temperatures might be expected to form stars with a higher characteristic mass (Larson 1985). But in fact, clouds with higher temperatures generally also have much higher pressures, so there is a partial cancellation of this effect when the Jeans mass is calculated (Larson 1999). This suggests that $T^2/P^{1/2}$ is approximately constant for different environments (Elmegreen 1999). Nevertheless, a still open and difficult question is if the distribution of stellar masses depend weakly or strongly on the initial physical conditions in the molecular cloud environment (e.g. ambient temperature and density, fragmentation conditions).

On the other hand, accretion and agglomeration processes are important in particular to form massive stars, but a clear understanding of these processes is an open problem. Thus, a reliable modeling of the upper IMF is needed. Observations will certainly provide important constrains. Also, theoretical studies that provide PMS evolutionary tracks are crucially needed for stellar masses above 5 $M_\odot$.

Relevant observational evidence shows that newly formed massive stars are always found to be surrounded by clusters of less massive stars, where the more massive stars tend to have larger associated clusters (Hillenbrand 1995, Testi et al. 1999, Garay & Lizano 1999). The most massive stars in young clusters tend to be centrally located, e.g. the Trapezium system. Massive stars also have a high frequency of massive companions, and even the runaway O stars must have been formed in close proximity to other massive stars in very dense stellar systems (Larson 1999; Stahler 2000).

With the use of IR arrays, in the last 10 years, the studies of the initial stellar population, i.e. the collection of young stars with ages $\leq$10 Myr found in association with molecular clouds, are providing valuable information on the IMF. This research subject is currently very active with most studies being carried out in the near-IR. A review on this subject is presented in Zinnecker et al. 1993, where the initial theoretical and observational work is summarized both in giant molecular clouds where OB associations are found and in intermediate mass cloud complexes. In the review by Meyer et al. 2000, the most recent work related to the IMF is presented.

Meyer et al. 2000 points out that a fundamental question in star formation studies is the distribution of stellar masses formed within molecular clouds. Quantitative IMF estimations have been made via parallactic, photometric and spectroscopic techniques, as well as a combination of them. Two important issues

are highlighted by these authors. Whether the IMF changes from a pure power law to a more complex distribution between 1-5 $M_{\odot}$ is crucial since it provides an important constrain on theories for the origin of stellar masses. And the clear demonstration of a peak in the IMF at the low mass end, which is of greater importance. Considerable observational effort has been focussed on establishing whether or not such a peak exists, and if so, characterizing its location and width. For example, an optical spectroscopic survey of about 1000 stars located $\sim$ 2 pc from the Trapezium stars, reveals that the cluster mass function turns over at $\sim$0.2 $M_{\odot}$ (Hillenbrand 1997).

Since the detailed IMF is not available for many young stellar clusters, Meyer and co-workers provide a gross characterization of the IMF by the ratio of high-to-low-mass stars in the few well studied nearby YSCs. They "conservatively" conclude that "most extremely young, compact star-forming regions exhibit emergent mass distributions consistent with having been drawn from the field star IMF within our ability to distinguish any differences". Which supports the IMF universality, but their cluster sample is quite small and further work is still needed. Finally, they address the complexity of the theoretical framework in the formidable problem of the origin of the IMF.

In this thesis we study the IMF in a sample of 38 young stellar clusters along the Perseus Arm. The Perseus Arm was selected because it is located far from the galactic center and Orion regions, avoiding possible contamination. Also, previous studies show evidence of on-going star formation along it and a region in the outer arms of the Galaxy provides a set of YSCs in a small distance interval (Chapter 2). The description of the observations and data reduction process are presented in Chapter 3. The study provides information on 6298 stars in YSCs. We propose a multi-color photometrical method to estimate cluster sizes, stellar densities (Chapter 4) and ages (Chapter 5), as well as individual extinction and masses of cluster stars (Chapters 5 and 6) . We use luminosity functions to estimate cluster age and diagnostic diagrams to distinguish stellar populations in clusters. The distributed population or local field star ages are obtained and compared to cluster ages. Stellar masses are obtained to construct the mass distributions that yield the cluster IMF, relying on a uniform treatment of the data. A comparison of clusters is discussed both in the IMF index and in the spatial distribution of masses (Chapter 6). Images, programs and photometry data tables are presented in Appendixes A, B and C, respectively. We have compiled a catalogue presented in Appendix D, that contains all the important individual cluster data obtained in our work, which we believe will be useful for future work. Finally, a summary and conclusions are presented in Chapter 7.

Chapter 2

Sample Selection Criteria

2.1 Previous work

Our main interest in this work is to study the young stellar population in star forming regions (SFRs). We chose to survey sources in the Perseus Arm because it cointains several well known SFRs (e.g. W3-5, Gem OB1, Cyg OB1), its location in the outer part of the Galaxy guarantees less contamination from Population II stars and it is observable from a Northern observatory.

Since the IRAS survey and the publication of the Point Source Catalog, criteria based mainly on IRAS fluxes have been proposed to succesfully search for star formation tracers. For example, Beichman et al. 1986 used criteria to search for candidate solar-type proto-stars in nearby (D $<$ 0.5 kpc) molecular cores of CO and NH_3. Wood and Churchwell 1989 selected a sample of radio UC HII regions and from IRAS flux ratios criteria were able to find massive stars embedded in dense cores from warm galactic molecular clouds (GMC). Hughes and MacLeod 1989 use color-color criteria to select HII regions embedded in SFRs for a study of methanol masers association. Finally, Palagi et al. 1993 clasify H_2O masers in two groups: stellar and SFR associated, based on parameters defined also by IRAS fluxes.

In Table 2.1 we summarize criteria adopted from different groups where star formation tracers such as protostars, H_2O masers, GMC cores, UC HII regions, HII regions, bright IRAS sources and compact molecular clouds (CMCs) + UC HII have been succesfully found (see also Table 4 by Palagi et al. 1993). These guidelines lead us to a adopt our own criteria, listed at the bottom of Table 2.1 and described in detail in next section, to seach for young stellar clusters (YSCs), which are the main subject of our work.

Table 2.1 SELECTION CRITERIA FOR STAR FORMATION TRACERS

Class of Object	log (F_{25}/F_{12})	log (F_{60}/F_{25})	log (F_{100}/F_{60})	log (F_{60}/F_{12})	Ref.
Protostars	-	0.52	0.7	-	a
H_2O Maser	0.5 - 1.1	0.4 - 1.7	-0.1 - 0.5	-	b
Cores	0.4 - 1.0	0.4 - 1.3	0.1 - 0.7	-	c
UC HII Regions	≥ 0.57	≥ 0.73	-	≥ 1.3	d
HII Regions	≥ 0.4	≥ 0.25	-	-	e
Bright IRAS	0.5 - 1.2	0.6 - 1.6	0.0 - 0.6	-	f
CMC + UC HII	≥ 0.57	0.61 - 1.74	0.087 - 0.52	≥ 1.3	g
YSCs	$\gtrsim 0.4$	$\gtrsim 0.3$	> 0	> 0	h

[a] Beichman et al. 1986.
[b] Wouterloot & Walmsley 1986.
[c] Emerson 1987.
[d] Wood & Churchwell 1989.
[e] Hughes & MacLeod 1989.
[f] Braz et al. 1989.
[g] Palla et al. 1991.
[h] This work.

2.2 Selection criteria

Based on criteria from different authors and in succesful findings in previous studies, we adopted four criteria for candidate sources associated to multiple star forming regions (YSCs) from the IRAS/PSC.

1. **In the Perseus Arm**. We restricted our search of IRAS candidates to the Perseus Arm region. We consider the Perseus Arm as the sky proyected in the interval of galactic coordinates $\boldsymbol{l} \in$ (70°,200°) and $\boldsymbol{b} \in$ (-5°,5°). Fig. 2.1 shows this region of the sky. It includes some known places of star formation, Sharpless HII regions, candidate sources for YSCs and those studied in the NIR in this work (■).

2. **Nearby a small HII region**. Candidate sources were chosen to be close to a small diameter (d $\lesssim$ 6 pc) HII region included in the Sharpless Catalog (Sharpless 1959). About 50 Sharpless HII regions (SHRs) were searched within a radius of $\sim 1°$ (which at 3.5 kpc corresponds to $\sim$ 60 pc) from the SHR positions looking for IRAS point sources. A second generation of stars

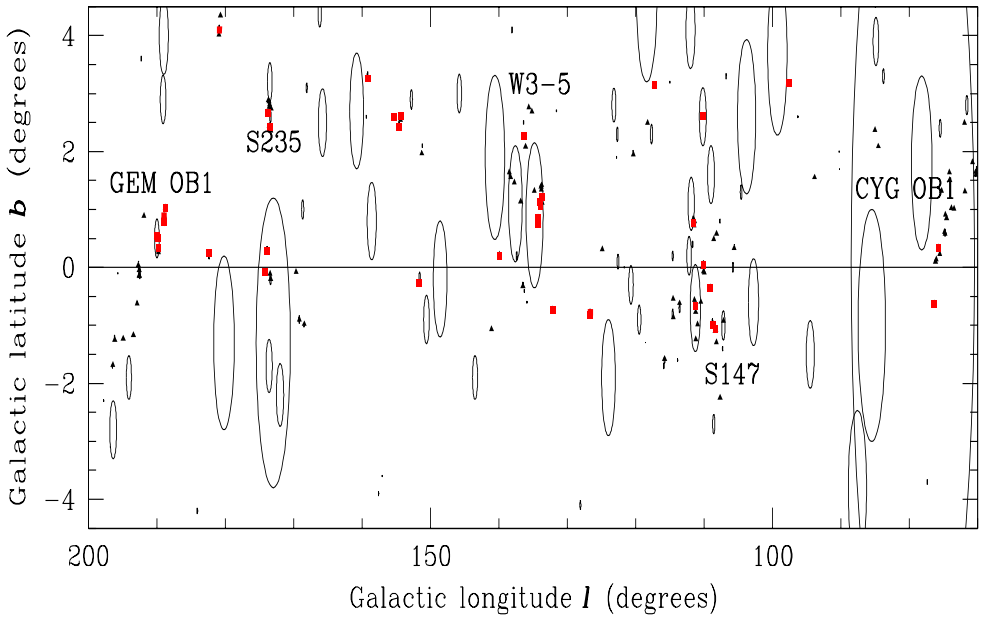

Figure 2.1 Location in the Galaxy of the Perseus Arm region. The symbols correspond to Sharpless HII regions (ellipses), ∼150 IRAS candidate sources for young clusters (▲) and YSCs observed in the NIR subject of this work (■).

may be triggered around these SHRs and a study of its stellar population is important.

3. **Colors**. We chose IRAS point sources having SED (spectral energy distribution) such that fluxes 1 $Jy \lesssim F_{12\mu m} < F_{25\mu m} < F_{60\mu m} < F_{100\mu m}$. This is a general characteristic of massive young stellar objects (YSOs), as noted by Chan & Henning 1996. The IRAS flux ratios in the 12, 25 and 60 μm bands should satisfy the conditions:

$$\begin{aligned} log(F_{60\mu m}/F_{25\mu m}) &\gtrsim 0.3 \\ log(F_{25\mu m}/F_{12\mu m}) &\gtrsim 0.4 \end{aligned} \qquad (2.1)$$

4. **High** $F_{100\mu m}$. We considered candidate sources with $F_{100\mu m} \gtrsim 1000\ Jy$, because dust grains in molecular clouds absorb radiation from embedded stars and re-emit in the far-infrared (FIR) regime. At the beginning we

considered $F_{100\mu m} \gtrsim 500Jy$, but we realized that sources with $F_{100\mu m} > 1000Jy$ had more succeful findings of embedded stellar clusters.

Under these criteria we present in Fig. 2.2 the IRAS color-color diagram, $\log(F_{60}/F_{25})$ vs. $\log(F_{25}/F_{12})$, of selected candidate and observed sources, the dashed box represents the intersection region that satisfies the criteria presented in Table 2.1. About 150 IRAS candidate sources satisfy the four criteria listed above, where short exposures at K were done (c.f. chapter 3). Of these candidates, we observed 50 regions in the near-infrared JHK bands under photometric conditions. The remaining sources include about 10-15% of good candidates to be observed in the future. We also estimate that ∼10% could be deeply embedded young stellar objects ideal to be observed in the mid-infrared. Finally, we found that about 30% of the candidate sources are associated to a stellar group or cluster, which gives us confidence in our selection criteria.

From the 50 observed sources, we constrained our sample to 38. The remaining 12 sources were rejected because they lie outside the Perseus Arm limits, the photometry was not complete or the number of detected stars was too small.

Table 2.2 lists the sample of 38 sources where clear evidence of a young stellar cluster (YSC) was found. It contains the following data: consecutive number of young stellar cluster (YSC) to be used hereon, corresponding IRAS name and galactic coordinates. Cols. (5) to (8) list IRAS colors, flux and quality numbers from the IRAS/PSC. We also include the nearest Sharpless HII region and the adopted distance to the observed region, obtained from the literature. In most cases the IRAS source distance is quoted and if unavailable, the adopted distance corresponds to the HII region. The FIR luminosities were calculated from IRAS fluxes and distance values (e.g. Tokunaga 2000).

The selected sample has a mean distance value of 3.4 ± 1.6 kpc, with a minimum and maximum values of 1 and 9 kpc, respectively. The FIR luminosities are in the $2 < L_{IR}/(10^3\ L_\odot) < 900$ range.

Fig. 2.3 shows the distribution in the galactic plane of the 38 YSC sources studied in this work. We note a concentration of sources in longitudes 110° and 135° which are well known sites of star formation (c.f. Fig. 2.1) and an acceptable coverage of the Perseus Arm.

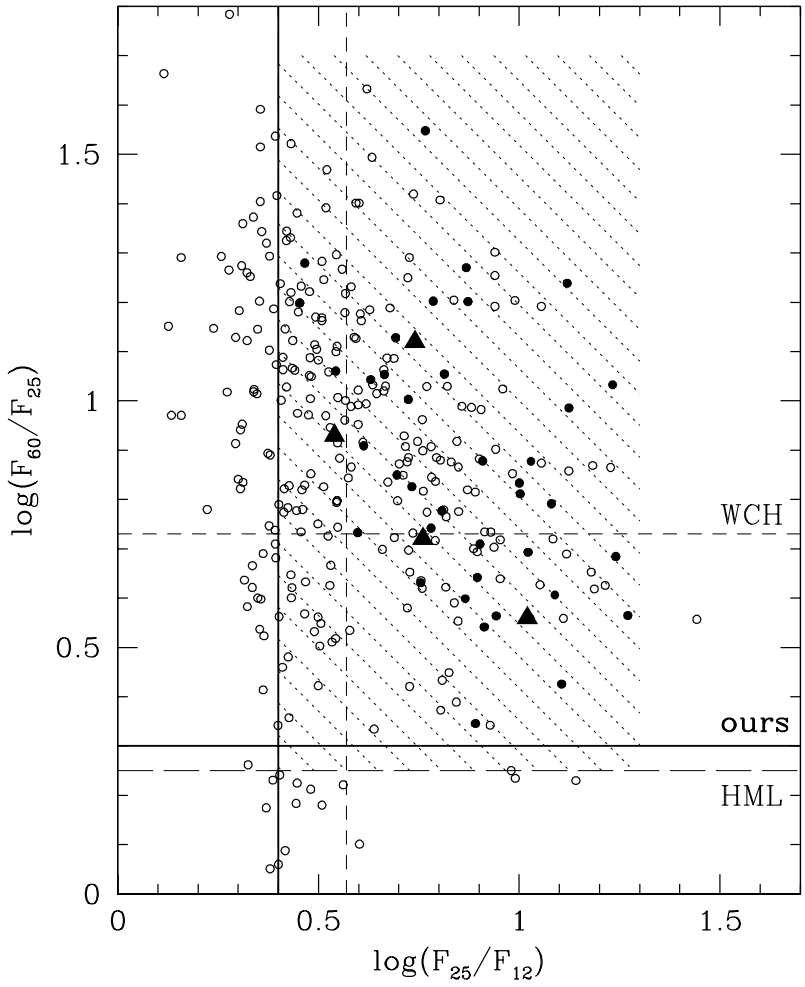

Figure 2.2 Infrared color-color diagram of IRAS sources. Sources are indicated as follows: cluster candidate (○), observed (●) and previously studied (▲) (e.g. Deharveng et al. 1997; Miralles et al. 1997; Salas and Cruz-González 1997, personal communication). Criteria including ours are also shown (WCH = Wood & Churchwell 1989; HML = Hughes & MacLeod 1989). The dashed box shows the intersection region from the criteria presented in Table 2.1.

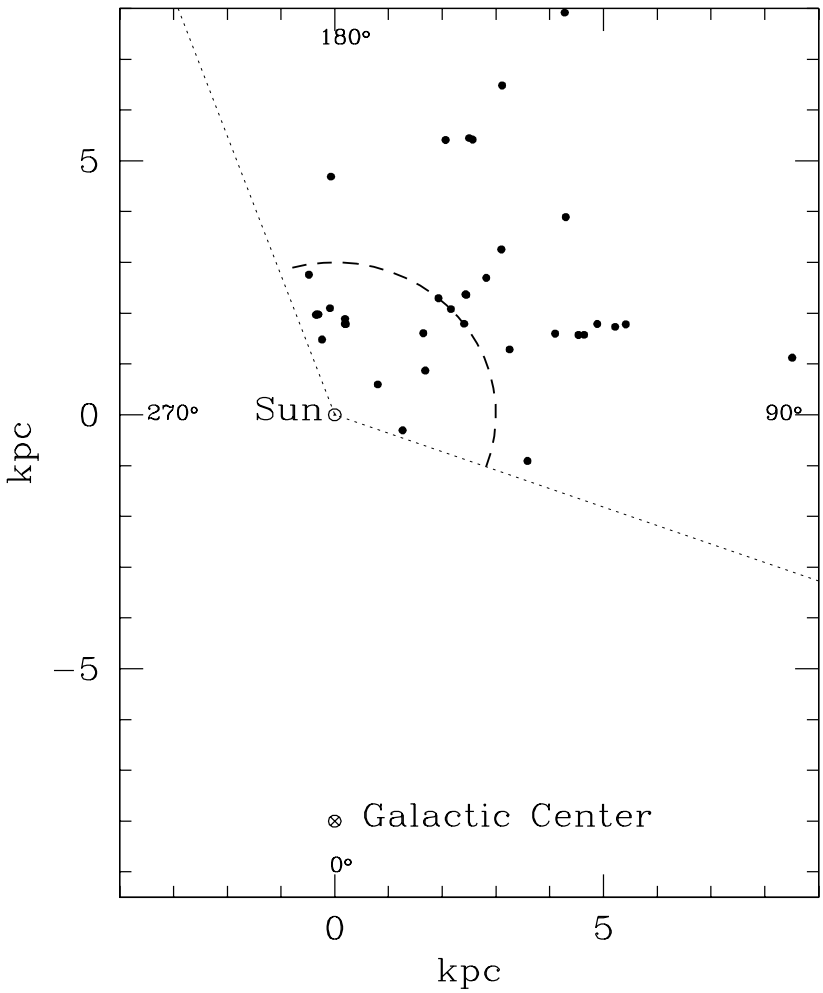

Figure 2.3 Distribution in the galactic plane of the 38 observed IRAS sources associated to YSCs. The dashed circle segment marks a distance of 3 kpc from the Sun. The dotted lines show the limits of the Perseus Arm region ($70° < \boldsymbol{l} < 200°$).

Table 2.2 PROPERTIES OF SELECTED IRAS SOURCES

YSC # (1)	IRAS source (2)	l (°) (3)	b (°) (4)	log F_{25}/F_{12} (5)	log F_{60}/F_{25} (6)	F_{100} (Jy) (7)	QN[q] (8)	H II (9)	D (kpc) (10)	L_{FIR}[r] (11)
1	01198+6136	126.66	-0.77	0.73	0.83	1717.0	3311	187	3.0[a]	11.7
2	01202+6133	126.71	-0.82	1.24	0.68	1717.0	3331	187	1.0[b]	2.7
3	02044+6031	132.16	-0.73	0.94	0.56	463.2	3333	189	5.8[c]	38.3
4	02219+6152	133.72	1.22	0.89	0.35	42110.0	3312	198	3.9[e]	876.6
5	02232+6138	133.94	1.06	1.12	1.24	10500.0	3333	198	3.0[d]	185.2
6	02236+6142	133.97	1.13	0.87	1.27	10500.0	3111	198	3.4[i,p]	98.3
7	02245+6115	134.24	0.75	0.45	1.20	1632.0	3231	198	3.4[i,p]	22.4
8	02252+6120	134.28	0.86	0.75	0.63	635.8	3311	198	2.3[h]	4.7
9	02461+6147	136.39	2.27	0.91	0.54	370.9	3332	196	4.5[e]	17.9
10	03035+5819	139.91	0.20	1.11	0.43	1297.0	3333	201	3.0[j]	30.2
11	04072+5100	151.62	-0.26	1.23	1.03	2723.0	2311	209	9.0[o,p]	181.5
12	04324+5106	154.35	2.61	1.02	0.69	642.4	3333	211	7.2[e]	86.8
13	04329+5045	154.65	2.43	0.60	0.73	833.7	3311	211	6.0[k]	22.2
14	04366+5022	155.33	2.60	1.27	0.56	467.1	3332	212	6.0[l]	24.8
15	04547+4753	159.14	3.26	0.90	0.64	365.1	3333	217	5.8[c]	32.9
16	05274+3345	174.20	-0.08	1.00	0.81	905.2	3333	237	1.9[c]	4.9
17	05281+3412	173.90	0.29	0.63	1.04	931.2	3333	237	1.8[m]	6.1
18	05358+3543	173.48	2.43	1.12	0.99	1310.0	3333	233	1.8[k]	6.4
19	05375+3536	173.77	2.67	0.72	1.00	1635.0	3331	235	1.8[k]	6.8
20	05490+2658	182.42	0.25	0.66	1.05	679.8	3333	242	2.1[k]	4.3
21	06006+3015	180.87	4.09	0.79	1.20	549.9	3312	241	4.7[k]	13.6
22	06055+2039	189.77	0.34	0.69	1.13	1715.0	3333	247	2.0[f]	10.8
23	06056+2131	189.03	0.78	0.70	0.85	2563.0	3322	247	1.5[h]	10.7
24	06058+2138	188.95	0.89	1.00	0.83	1666.0	3333	247	2.0[n]	10.8
25	06061+2151	188.80	1.03	1.08	0.79	1130.0	3333	247	2.0[n]	9.3
26	06063+2040	189.86	0.51	0.87	1.20	2045.0	2333	247	2.8[d]	23.6
27	06068+2030	190.05	0.53	0.47	1.28	1134.0	3333	247	2.0[n]	7.4

Table 2.2 Continued.

YSC # (1)	IRAS source (2)	l (°) (3)	b (°) (4)	log F_{25}/F_{12} (5)	log F_{60}/F_{25} (6)	F_{100} (Jy) (7)	QN[q] (8)	H II (9)	D (kpc) (10)	L_{FIR}[r] (11)
28	20198+3716	75.77	0.34	0.81	1.05	6965.0	3331	104	3.7[e]	181.3
29	20255+3712	76.38	-0.62	1.09	0.61	13130.0	3333	106	1.3[h]	49.0
30	21306+5540	97.52	3.18	1.03	0.88	958.0	3333	128	8.6[e]	135.5
31	22475+5939	108.20	0.58	0.78	0.74	1066.0	3333	146	5.7[e]	74.6
32	22542+5815	108.36	-1.06	0.54	1.06	861.0	3333	148	5.5[c]	41.8
33	22566+5828	108.75	-0.99	0.77	1.55	2228.0	3311	152	4.9[e]	73.0
34	22570+5912	109.10	-0.35	0.90	0.71	961.6	3333	153	4.8[c]	44.8
35	23030+5958	110.11	0.05	0.81	0.78	1833.0	3333	156	5.2[c]	110.8
36	23116+6111	111.54	0.78	0.87	0.60	14120.0	3333	158	3.5[g]	289.9
37	23138+5945	111.28	-0.66	0.91	0.88	2164.0	3333	159	4.4[e]	86.0
38	23545+6508	117.32	3.14	0.61	0.91	1059.0	3333	170	1.9[e]	7.3

[a] Clark 1991
[b] Fich & Blitz 1984
[c] Wouterloot & Brand 1989
[d] Kurtz et al. 1994
[e] Palagi et al. 1993
[f] Casoli et al. 1986
[g] Chan et al. 1996
[h] Wu et al. 1996
[i] Lahulla 1985
[j] Henning et al. 1992
[k] Snell et al. 1990
[l] Wouterloot et al. 1988
[m] Snell et al. 1988
[n] Carpenter et al. 1993
[o] Chan & Fich 1995
[p] Distance to Sharpless H II region
[q] IRAS/PSC quality numbers: 3 = good quality, 2 = moderate quality, 1 = upper limit
[r] In units of $10^3 L_\odot$.

Chapter 3

Observations and Data Reduction

3.1 Instrumental setup

We carried out a near-infrared survey of 50 candidate regions to search for young stellar clusters in the region of the Perseus Arm. Our aim was to obtain good quality photometric data in the JHK bands to study the young clusters stellar population.

The observations were obtained with the infrared camera CAMILA at the 2.1 m telescope in San Pedro Mártir, operated by the Observatorio Astronómico Nacional (OAN/SPM) in Baja California, México. A general description of the instrument is presented in Cruz-González et al. 1994, while detailed observing manuals of the instrument can be found in http://www.astrosen.unam.mx (Cruz-González et al. 1997 and Cruz-González, Salas & Ruiz 1996).

The f/4.5 camera setup of CAMILA was used, with a plate scale of 0.86 $''$/pix and field of view of 3.6 $'\times$ 3.6 $'$ for the NICMOS 3 (HgCdTe) 256×256 pixels detector. The filters central wavelength and bandwidth used are the following: broad-band K' (2.125 μm, $\Delta\lambda = 0.35$ μm, Mauna Kea K'), H (1.60 μm, $\Delta\lambda = 0.27$ μm), J (1.20 μm, $\Delta\lambda = 0.28$ μm); narrow-band H_2 v=1-0 S(1) (2.122 μm, $\Delta\lambda = 0.02$ μm), cK (2.26 μm, $\Delta\lambda = 0.06$), CO (2.295 μm, $\Delta\lambda = 0.02$), [FeII] (1.644 μm, $\Delta\lambda = 0.016$), Brγ (2.166 μm, $\Delta\lambda = 0.02$), CO (2.295 μm, $\Delta\lambda = 0.02$), [FeII] (1.644 μm, $\Delta\lambda = 0.016$).

3.2 Observing procedure

Images were obtained on five observing runs held in: 1996 November 2-5 (N/96); 1997 January 23-27 (E/97), June 25-30 (J/97) and December 7-12 (D/97); and 1998 January 5-8 (E/98). During the third observing run (J/97), the fourth

quadrant of CAMILA was blind, so we got "L" shape exposures. In the fourth observing run (D/97) the seeing was not very good, FWHM was ∼3-4 pix (2.5-3.4 arcsec). Even with these disadventages the data are considered useful for resolved stars. It is important to note that all the broad-band data were obtained under photometric conditions, since our goal is to obtain good quality stellar photometry.

For each YSC field a two step procedure was followed. First, short-time on-source and sky exposures of 24 s in the K-filter, called snap-shots, were done to select regions where an embedded clustering pattern was evident. Those regions with this characteristic were selected for longer exposures in the JHK filters. If we found evidence of nebulosities, jets or interesting extended structures, the sources were selected for a narrow-band study. H_2 has shown a potential to detect embedded Herbig-Haro like objects (e.g. Zinnecket et al. 1997).

The deep imaging product were sets of object and nearby sky frames taken with the same exposure times at adjacent positions to the object. Each set consists of 5 object and 4 sky images. The added object images were processed by subtracting a median-filtered image of the nearby sky frames. The resulting images were flattened using sets of low- and high-illumination sky flats obtained at sunset.

Table 3.1 sumarizes the observational data of the 38 regions studied in this work, as follows: (1) consecutive number as in Table 2.2, (2) and (3) equatorial IRAS source coordinates, (4) observing run, (5) filters, (6) integration time and (7) the point spread function (PSF) in each broad-band filter.

3.3 Composite color images

The final NIR images are presented in Appendix A. First, we include for comparison optical images of the 38 observed regions centered on the IRAS source covering a $3.6' \times 3.6$ field. Second, the individual JHK images were used to construct true color NIR composite images with J (blue), H (green) and K (red). Third, the 8 sources observed in H_2 (2.12 μm) and cK were used to construct RGB composite images with H (blue), H_2 (green) and cK (red), which show clearly the H_2 nebulosities. The images in Appendix A have been arranged in sets of images that contain on the even page optical images and on the odd page the NIR images. After these images, we include the color-composite images in H_2.

As can be seen, most of the sources are in regions of high extinction where very few stars are visible in the optical frames. In the NIR, all the regions show a large

Table 3.1 OBSERVATIONAL DATA

YSC #	α_{2000}	δ_{2000}	Observing run	Filters	Integration time (s) J / H / K	PSF J / H / K
(1)	(2)	(3)	(4)	(5)	(6)	(7)
1	1 23 07.49	61 52 02.38	E/97	J,H,K	600/600/900	2.1/1.8/2.1
2	1 23 32.30	61 48 48.75	N/96	J,H,K,H_2,cK[a]	600/480/1080	1.7/1.7/1.7
3	2 08 05.03	60 45 56.92	E/97	J,H,K	600/600/900	2.3/2.5/2.1
4	2 25 42.77	62 06 05.32	N/96	J,H,K,H_2,cK[a]	600/600/900	2.2/2.3/1.7
5	2 27 01.04	61 52 13.95	E/97	J,H,K,H_2,cK	600/600/900	2.9/2.2/1.9
6	2 27 25.38	61 55 29.91	E/97	J,H,K,H_2,cK	600/600/900	2.2/2.2/2.1
7	2 28 21.51	61 28 29.45	E/98	J,H,K	600/520/600	1.8/1.9/1.9
8	2 29 01.75	61 33 32.71	E/98	J,H,K	600/520/600	1.9/1.8/1.8
9	2 50 08.10	61 59 47.37	E/97,E/98	J,H,K,H_2,cK	600/600/900	2.3/2.2/2.2
10	3 07 25.60	58 30 52.53	D/97	J,H,K	600/520/600	3.1/2.5/2.3
11	4 11 04.66	51 08 01.95	D/97	J,H,K	600/520/600	3.4/2.5/2.3
12	4 36 19.69	51 12 44.69	N/96	J,H,K	600/600/870	1.8/1.9/1.9
13	4 36 48.51	50 52 00.70	E/98	J,H,K	600/520/600	2.0/1.9/2.0
14	4 40 26.11	50 28 24.86	N/96	J,H,K	900/600/900	2.6/2.1/2.1
15	4 58 29.65	47 58 27.66	E/97	J,H,K	600/600/900	1.8/2.1/2.5
16	5 30 45.61	33 47 51.68	D/97,E/98	J,H,K	600/520/600	3.1/2.5/2.5
17	5 31 26.59	34 14 57.75	N/96	J,H,K	900/600/840	1.9/1.8/1.8
18	5 39 10.38	35 45 19.27	E/97	J,H,K,H_2,cK[b]	600/600/900	2.3/2.2/2.3
19	5 40 52.51	35 38 23.85	N/96	J,H,K	900/600/900	2.3/1.9/1.9
20	5 52 12.92	26 59 32.87	E/98	J,H,K	600/520/600	1.9/1.8/1.8
21	6 03 54.09	30 14 54.96	E/98	J,H,K	600/520/600	1.8/1.8/1.9
22	6 08 32.81	20 39 16.15	E/97	J,H,K	450/450/900	2.4/2.2/2.3
23	6 08 40.96	21 31 00.60	E/97,E/98	J,H,K,H_2,cK	600/480/900	2.8/2.9/2.3
24	6 08 54.13	21 38 24.64	E/97	J,H,K,H_2,cK	600/480/720	2.3/2.1/2.3
25	6 09 07.80	21 50 38.66	D/97	J,H,K	600/520/600	3.0/2.9/3.0
26	6 09 21.91	20 39 27.57	E/97	J,H,K	600/600/900	2.1/2.2/2.1
27	6 09 51.70	20 30 04.39	E/98	J,H,K	600/520/480	2.6/2.4/2.4
28	20 21 41.15	37 25 53.46	J/97	J,H,K	880/600/720	1.8/1.8/1.8
29	20 27 26.48	37 22 47.92	J/97	J,H,K,H_2	880/600/900	2.2/2.1/2.1
30	21 32 11.50	55 53 23.87	D/97	J,H,K	600/520/600	3.1/2.9/2.3
31	22 49 29.41	59 54 56.88	N/96	J,H,K,H_2	900/600/900	2.2/2.3/2.5
32	22 56 16.96	58 31 13.53	N/96	J,H,K	920/600/900	1.8/1.9/1.9
33	22 58 46.33	58 44 50.50	N/96	J,H,K,H_2	900/600/900	2.1/2.0/2.0
34	22 59 06.44	59 28 27.90	D/97	J,H,K	600/520/600	3.3/2.7/2.3
35	23 05 10.57	60 14 40.62	J/97	J,H,K	880/600/900	1.8/1.8/1.8
36	23 13 45.57	61 28 17.78	J/97	J,H,K	880/600/900	1.8/1.8/1.8
37	23 16 04.73	60 01 59.99	J/97	J,H,K	720/600/880	1.8/1.8/1.8
38	23 57 05.18	65 25 10.89	E/97	J,H,K	600/600/900	2.4/2.5/2.3

[a]Also [FeII] and Brγ.
[b]Also CO.

number of stars associated to an embedded cluster. Also, these regions have at least one or several extremely red objects, usually associated to the stellar densest zones. In some cases, they also show red nebulosities characteristic of newborn star forming regions in which the gas has not yet been totally converted into stars and/or removed by stellar winds and jets.

The color molecular hydrogen images are able to enhance the regions where H_2 emission occurs and several of the nebulosities shown in green are Herbig-Haro candidates where shocks are responsible of the H_2 emission. This technique has been used to detect deeply embedded Herbig-Haro objects (e.g. in S255 IR, Miralles et al. 1997; in S187 IR, Salas et al. 1998; in S233 IR, Porras et al. 2000). We note that the regions S187 IR and S 233 IR correspond to YSC 2 and YSC 18, respectively, which have already been published. The analysis of the H_2 data of the remaining sources is really beyond the scope of this thesis and will be published later.

Finally, it should be mentioned that we recently began a program of observations of visible counterparts of these regions in the V, R, I and H_α filters. The idea is to construct the spectral energy distributions (SEDs) of the brightest stars to obtain their bolometric luminosity, and to compare color-diagrams and nebular gas morphology in the optical and IR. These observations are being carried out at the 2.1 m telescope in the Observatorio Astronómico Guillermo Haro (OAGH) in Cananea, Son., México. The photometric data in the visible needs several observing runs and the available data is insufficient for a fair analysis. We decided to wait until all the regions are observed in the visible and so the partial data is not considered in this thesis work.

3.4 IDL/DAOPHOT Routines

The reduction routines for the regions observed were developed in IDL with the goal of reducing all the fields in a systematic and uniform way. The same set of ordered routines were used for each observed field to guarantee a fair comparison between clusters.

Photometric data reduction made use of DAOPHOT package routines (Landsman 1996). Adaptations to these routines were required appropriate to star forming regions, where the presence of gas and dust makes difficult the construction of the Point-Spread Function (PSF).

The PSF is a model stellar-light profile in an observed frame. It is constructed by choosing stars without nearby neighbors, located far from crowded regions and outside nebulosities, to guarantee less contamination.

We followed the standard procedure of photometric data reduction in crowded fields (Stetson 1987). The routine names used in the reduction are presented in capital letters. First, we find stars (FIND) in the field above a threshold computed with average values of sky (SKY) across the frame. Then, we determine which of these stars are not contaminated with strong nebulosities by comparing photometry from the raw frame and a filtered one without the gas component. Stars close to nearby companions were also eliminated setting a minimum distance between stars. From the set of selected stars we construct the corresponding modelled PSF (GETPSF).

Once we get the PSF, it is compared with the observed PSF of all the stars in the raw frame in order to calculate the individual photometry and errors (NSTAR). This process has to be done for the three filters J, H and K. A supplementary routine (STAR_COREL) is used to cross-correlate the position of stars in the three frames and identify the same stars in all the bands.

In some cases, the reduction procedure was repeated after substracting stars (SUBSTAR) already found, this was done in order to find deemer stars, but these stars normally have not counterparts in all the bands and usually are detected in only one filter. Since we are interested in stars detected in the three bands, this step was eliminated, but is available.

In Appendix B we present more details on the IDL / DAOPHOT reduction process and include the programs listings since they may be useful for future work.

3.5 Output Parameters

The important quantities obtained from the photometric reduction process are: magnitudes, magnitude errors and relative positions of stars. The intrinsic error in the photometry is less than 7% and the higher values are mainly caused by the presence of the nebular component and/or close companions. We note that usually the H and K frames contain more stars that those found in J, due to the higher absorption of light by gas and dust at J.

We obtained individual JHK photometry of stars in the 38 young stellar cluster regions in the Perseus Arm. We found on average $\sim$150 stars in each observed frame, which results in NIR photometry of a total of 5781 stars.

It is important to note that the vast majority of the observed sources have not previously reported JHK photometry. Some sources are included in Hoddapp's catalog of K observations (Hoddapp 1994).

The resulting photometry will be used to study both the stellar population

associated to young stellar clusters (YSCs) and what is known as the extended population of stars surrounding clusters. We will show that with JHK photometry and distance information we are able to derive individual extinction and mass, as well as cluster extinction and age. Our goals are to construct the initial mass function (IMF) of each cluster and to study its behaviour in the Perseus Arm sample of YSCs.

3.6 Calibration

The flux calibration was obtained by observing UKIRT faint standard stars. The list of observed standard stars in each observing run is presented in Table 3.2, as well as the corresponding median value of magnitude zero points.

Table 3.2 CALIBRATION DATA

Observing run	UKIRT standard stars	$j_z \pm \Delta j_z$	$h_z \pm \Delta h_z$	$k_z \pm \Delta k_z$
N/96	7,11	20.31 ± 0.04	20.00 ± 0.01	19.76 ± 0.03
E/97	16,18,19,20	20.26 ± 0.04	19.96 ± 0.03	19.81 ± 0.03
J/97	25,28,30	19.99 ± 0.12	19.78 ± 0.03	19.50 ± 0.10
D/97	7,8,9,13,15,18	20.54 ± 0.02	20.14 ± 0.04	19.92 ± 0.01
E/98	4,7,8,11,13,18,19,20,24	20.38 ± 0.03	20.07 ± 0.03	19.84 ± 0.03

Instrumental magnitudes obtained with IDL / DAOPHOT routines, were transformed by the equations

$$\begin{aligned} j &= j_z + j_i - k_j(am_j - 1) \\ h &= h_z + h_i - k_h(am_h - 1) \\ k &= k_z + k_i - k_k(am_k - 1) \end{aligned} \tag{3.1}$$

where j_i, h_i, k_i are the measured instrumental magnitudes; k_j, k_h, k_k are the mean extinction coefficients in the air mass range [1,3] for the SPM Observatory site (Carrasco et al. 1991), am_j, am_h, am_k are the air mass values in the observations and j, h, k are the SPM stellar magnitudes. These magnitudes were transformed from the UKIRT system to the homogenized Glass-Johnson system, using the transformation equations of Bessell and Brett 1988.

Due to the large amount of data involved (6298 stars), the photometric data of each cluster is presented in Appendix C. Together with JHK magnitudes and errors, we also include values of individual extinction A_V and stellar mass M. The details on how these important quantities were obtained are presented in Chapters 5 and 6.

Chapter 4

Stellar Surface Density

4.1 Distance to YSCs

The distance to the IRAS sources, which are assumed associated with the YSC, is a basic parameter. The adopted values are not estimated by a single criterium and the uncertainty varies from region to region according to the estimation method. In Table 2.2 the adopted distance values to the IRAS source in our work were presented. In cases where a distance to the IRAS source is not available, we adopted the distance to the nearest Sharpless H II region. Until future large telescopes and missions to determine stellar parallaxes become available, which guarantee a direct and uniform distance estimation, we are restricted to distance values from the literature. If the distance to a source has an error of $\pm$ 1 kpc, this is translated to an error of $\pm$ 1 pc in the radius of the observed region.

The distribution of distances (see Fig. 4.1) shows two concentrations in distance, one at $\sim$2 kpc and the second, less prominent, at $\sim$6 kpc in agreement with the picture of the presence of two spiral arms in the outer part of the Galaxy: the Perseus Arm and the Outer Arm (see map in The Milky Way 1999).

The selected YSC sample has a mean distance value of 3.6 $\pm$ 1.8 kpc in an interval $1 < D < 9$ kpc. Due to the large distance span it would be interesting to compare the clusters at a single distance. We can use the observed NIR composite color images and scale them to a single distance of 3.5 kpc. The comparison of 12 YSCs, rich in stars, is shown in Fig. 4.2, where each cluster has been scaled to the same distance. The YSCs morphology and appearance is quite similar, all clusters are associated to a red nebulosity with star members, arranged in an almost circular distribution. The differences shown could be due to the distance estimation or to properties related to the evolving stage or star formation conditions of the cluster. It seems that the apparent sizes of these

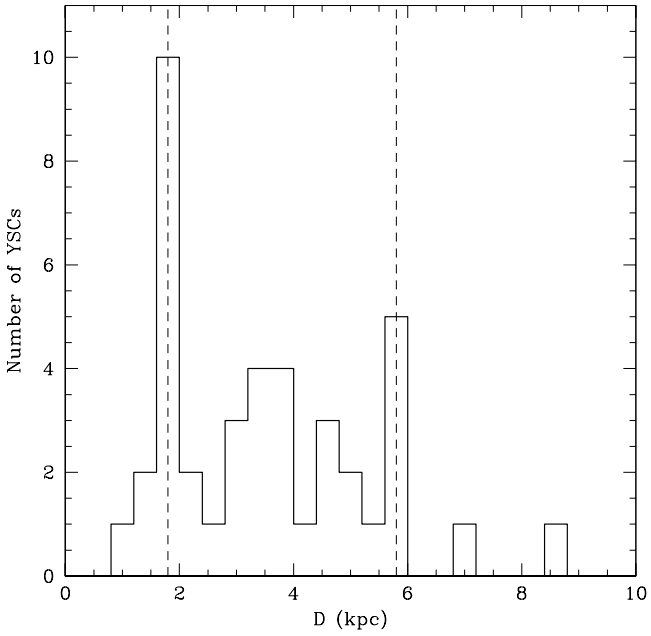

Figure 4.1 Histogram of the distance distribution values of a total of 38 YSCs presented in Table 4.1.

clusters are similar, with the exception of YSC 3 and YSC 26 that appear more extended than the rest.

4.2 Surface Density Profiles

In order to estimate the cluster radius we assume that the distribution of stars is spherical and concentrated in the center. The study of stellar richness in clusters is made considering H- and K-band star detections since these frames contain more detected stars.

By studying the density profiles of each cluster we are able to define the cluster radius, r_C, and to calculate the mean stellar surface density, $< \Sigma >$. We first estimate the location of the density peak of stars in a box of 25×25 pixels around the clustering zone revealed in the RGB images. Then we choose this density maxima as the cluster center and count stars in concentric annulus of 10 to 100 pixels in radii.

Density profiles for the 38 YSCs are shown in Fig. 4.3. A normalization to the

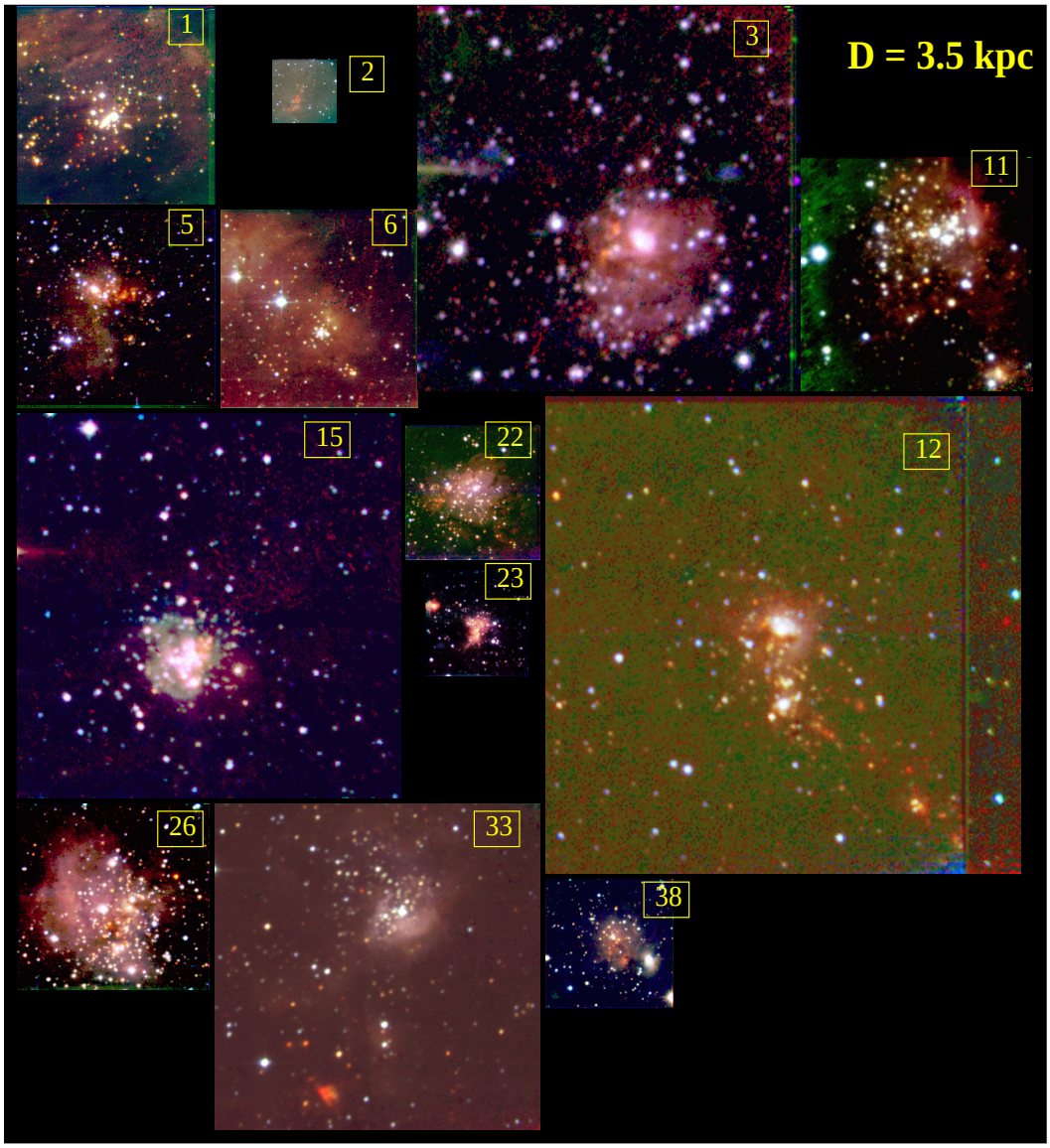

Figure 4.2 Thirteen YSCs, initially at different distances, shown as they would appear at a distance of 3.5 kpc away.

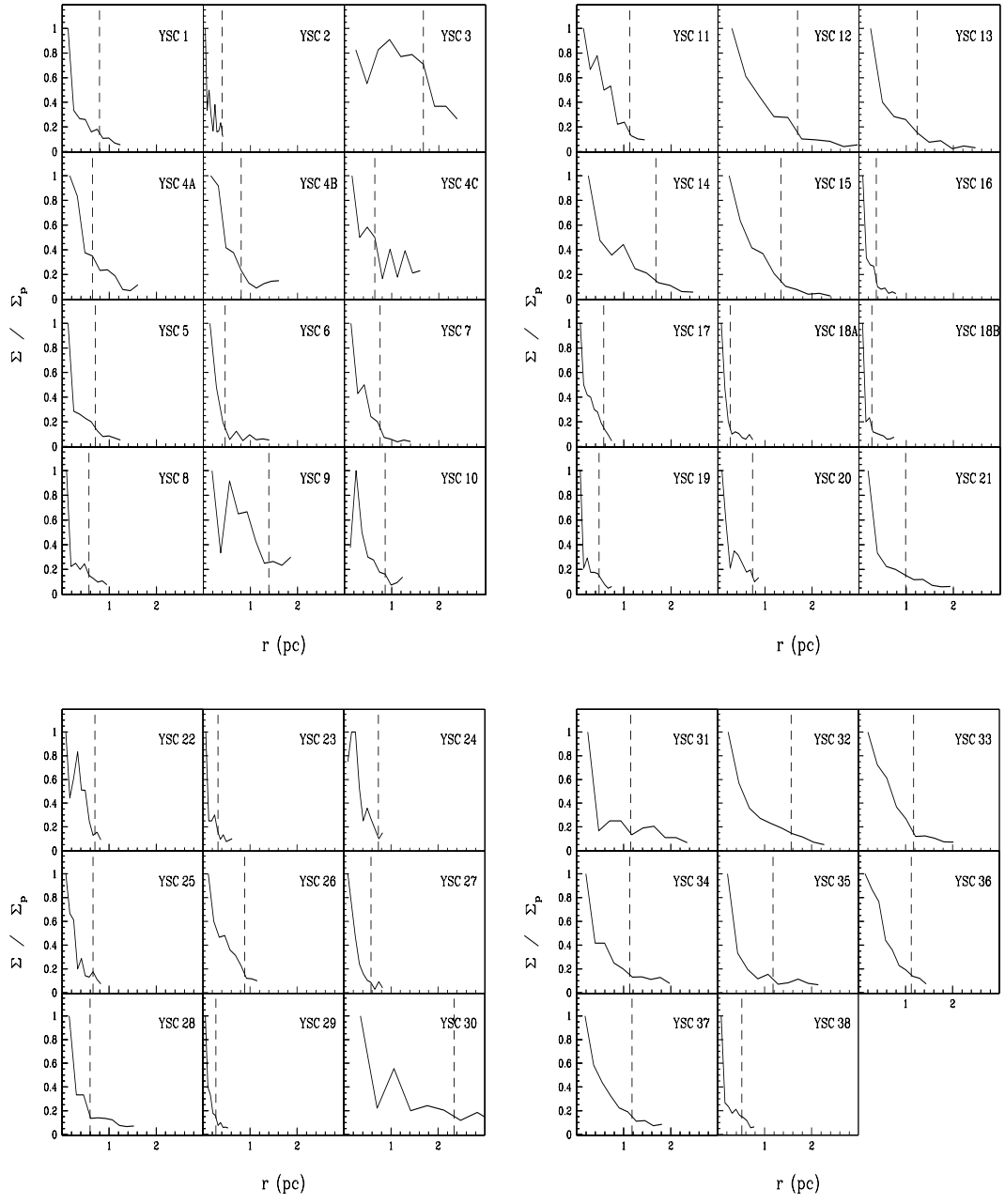

Figure 4.3 Stellar density profiles of clusters associated to IRAS sources. Each profile has been normalized to its peak value. Vertical dashed lines show the adopted cluster radii.

peak value has been applied and the radius is given in pc. We define the cluster radius, r_C, as the width of the surface density distribution at 3σ (~ 15 %) of the peak value (Σ_p).

Note that, in three cases, YSC 3, YSC 10 and YSC 24, the density profiles drop at the center, this may be due to a lack of resolution in the central group of stars and/or the presence of a gas component in this zone. YSC 3 and YSC 9 show an anomalous density profile and r_C has to be estimated in a different way. We assume a cluster radius by eye of 70 pixels and 75 pixels for YSC 3 and YSC 9, respectively. YSC 4 (W3) is not a single cluster but a set of three clusters (A, B and C), with their edges overlapping. In this case r_C is also estimated by eye for each density concentration. If it were considered as a single cluster the estimated radius would be 1.45 pc, with 138 members and Σ=21 pc^{-2}. Finally, YSC 18 contains two clusters (A and B) with no overlapping and the two density profiles are used to estimate r_C for each cluster; a detailed study of this region was presented in Porras et al. 2000.

In Table 4.1 we present the results of the stellar density analysis. For each cluster values of the radius r_C, number of stars inside the cluster radius N and mean surface density $< \Sigma > \equiv N/\pi r_C^2$ are given. We also include the presence of youthness tracers: young stellar object (YSO), molecular outflow and H_2O maser, obtained from the literature, together with presence of large infrared excess sources: protostar candidates (undetected in J and H-K$>$ 2.5) and highly reddened stars ($A_V > 20$ mag) obtained from our data and discussed in Chapter 6 below.

YSC 11 is an exception and we noticed that it stands out in r_C (2.89 for $D = 9.0$ kpc), which strongly suggest that its distance might be overestimated. Because distance is an important parameter in the analysis of clusters presented in this work, we decided to use the results of Fig. 4.2 to estimate a distance. These images show that the area covered by YSC 11 at 3.5 kpc is quite similar to that of the other clusters. Since this is also the mean distance of the sample and the 9 kpc distance corresponds to the HII region (S209) not the IRAS source, we adopt a 3.5 kpc distance value for this cluster. This would yield $r_C = 1.13$ pc for YSC 11. YSC 30 radius is also large, but in this case, a large distance to the cluster seems real.

We derived cluster radii values from 0.26 to 2.34 pc, with most clusters between 0.5 and 2 pc. The mean value is 0.89 $\pm$ 0.47 pc, which is consistent with previous measurements in studies of clustering associated to Ae/Be stars (e.g. Testi et al. 1998). The dispersion in the surface density is large (3 to 220 stars/pc^2), the mean value is 55 $\pm$ 52 stars/pc^2.

Most clusters show an r^{-2} behavior as expected. To compare all the clusters

we consider a normalization of the density profiles to the highest peak value (Σ_{p29} = 554.56 pc^{-2}) and plot all the clusters together, as is shown in Fig. 4.4. The dashed curve represents the best fit: $\Sigma/\Sigma_{p29} = A\, r^{-2} + B$, with $A = 0.0016 \pm 0.0005$ and $B = 0.0051 \pm 0.0042$.

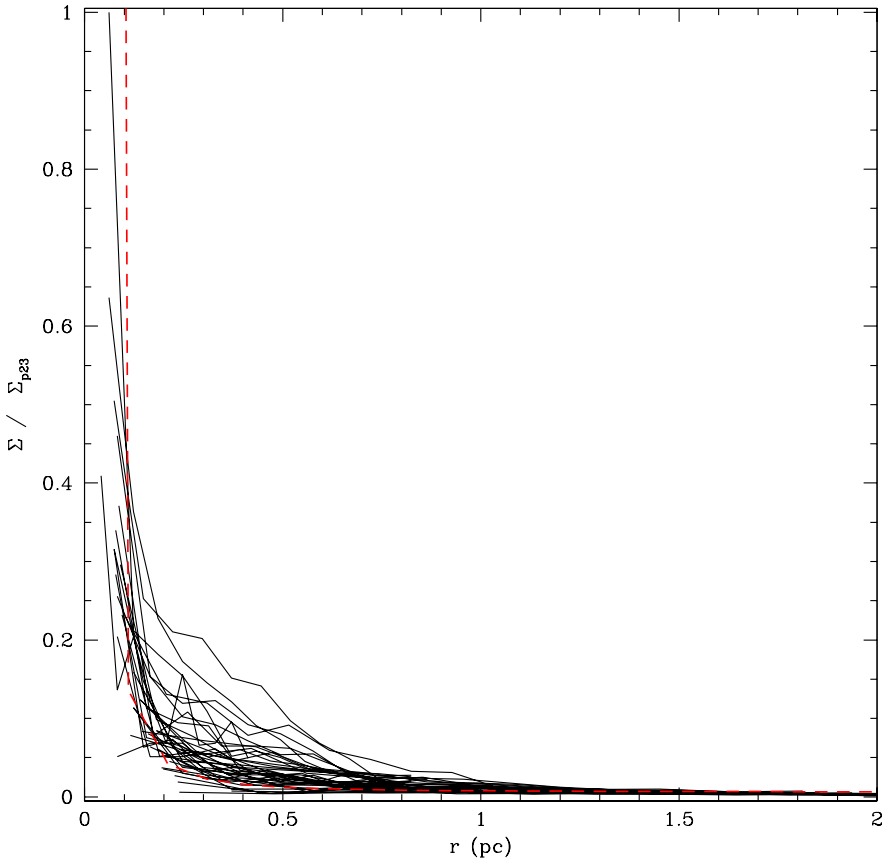

Figure 4.4 Stellar density profiles of 41 YSCs in Perseus Arm, normalized to the maximum peak Σ_{p29}. The dashed line is the best fit to the profiles.

Table 4.1 STELLAR DENSITY AND YOUTHNESS TRACERS

#	xc (pix)	yc (pix)	D (kpc)	r_C (pc)	N	$<\Sigma>$ (pc^{-2})	YSO[c]	CO outflow[d]	H_2O maser[e]	IR excess[g]
(1)	(2)	(3)	(4)	(5)	(6)	(7)	(8)	(9)	(10)	(11)
1	145	105	3.0	0.79	71	36.10				Y
2	125	85	1.0	0.40	86	182.62				Y
3	100	90	5.8	1.67	78	8.87				
4A[a]	70	185	3.9	0.64	37	28.50		Y	Y	Y
4B[a]	115	110	3.9	0.80	54	26.62				Y
4C[a]	180	175	3.9	0.64	22	16.94				Y
5	140	160	3.0	0.70	74	47.44		Y	Y	Y
6	125	100	3.4	0.46	27	40.20				
7	150	110	3.4	0.76	78	43.37				Y
8	155	155	2.3	0.57	72	70.87		Y		
9	140	130	4.5	1.39	89	14.65			Y	
10	155	125	3.0	0.87	58	24.65	Y	Y	Y	
11	120	150	3.5[f]	1.13[f]	106	26.66				
12	140	110	7.2	1.69	83	9.24		Y	Y	Y
13	145	125	6.0	1.24	88	18.33				
14	155	125	6.0	1.68	140	15.76				Y
15	155	90	5.8	1.34	138	24.52				Y
16	145	125	1.9	0.37	43	101.07		Y	Y	Y
17	85	110	1.8	0.57	226	220.52		Y		
18A[b]	100	90	1.8	0.26	22	103.90	Y			
18B[b]	150	140	1.8	0.27	20	84.52		Y	Y	Y
19	130	160	1.8	0.47	101	142.65		Y	Y	Y
20	130	110	2.1	0.74	130	76.48		Y		Y
21	170	140	4.7	0.99	69	22.51			Y	Y
22	150	105	2.0	0.70	146	94.69	Y	Y	Y	
23	100	105	1.5	0.32	35	107.83	Y	Y		
24	140	90	2.0	0.73	58	34.31	Y	Y	Y	Y
25	105	135	2.0	0.66	78	57.11	Y	Y	Y	
26	115	90	2.8	0.89	157	63.31		Y		Y
27	125	155	2.0	0.58	77	73.64		Y		

Table 4.1 Continued

#	xc	yc	D	r_C	N	$<\Sigma>$	YSO[c]	CO	H_2O	IR
	(pix)	(pix)	(kpc)	(pc)		(pc^{-2})		outflow[d]	maser[e]	excess[g]
(1)	(2)	(3)	(4)	(5)	(6)	(7)	(8)	(9)	(10)	(11)
28	160	105	3.7	0.59	42	37.81			Y	Y
29	150	100	1.3	0.27	42	179.10	Y	Y	Y	Y
30	100	105	8.6	2.34	52	3.03			Y	
31	140	95	5.7	1.15	30	7.21	Y		Y	
32	185	135	5.5	1.56	129	16.79				
33	120	185	4.9	1.17	97	22.51	Y		Y	Y
34	155	130	4.8	1.13	47	11.77				
35	150	75	5.2	1.18	44	10.08	Y			
36	170	65	3.5	1.13	157	43.08	Y	Y	Y	Y
37	115	155	4.4	1.18	141	32.31	Y		Y	
38	125	150	1.9	0.52	69	82.25	Y			Y

[a] Three sub-clusters in W3 IRS5 region.
[b] Double cluster near S233 H II region.
[c] Chan et al. 1996 and references therein.
[d] Wu et al. 1996 and references therein.
[e] Palagi et al. 1993, Migenes et al. 1999.
[f] Adopted distance and derived cluster radius, see §4.2.
[f] This work.

4.3 Stellar Concentration in YSCs

The parameter known as the cluster concentration is defined for globular clusters as $c = \log (r_t / r_s)$, where r_t is the tidal radius at which the surface brightness flattens and r_s is the radius at which the surface brightness is half of the peak value (Cruz 1998). The mean value for a sample of 117 globular clusters is $c_{GC} = 1.36 \pm 0.43$ (see Fig. 1.5b in Cruz 1998), in agreement with the modelled value of $r_t / r_c \sim 30$ (King 1962).

Similar parameters can be estimated for YSCs. We assume our estimations of the cluster radius r_C, as the tidal radius r_t and estimated r_s from the observed stellar density profiles. Our sample concentration mean value is $c_{YSC} = 0.51 \pm 0.24$. The distribution histogram of parameter c for YSCs is presented in Fig. 4.5, which shows that YSCs are less concentrated than globular clusters, by a factor of ~ 3.

4.4 YSC Characteristics

Now we are in the possibility to define what we really consider as a young stellar cluster (YSC). From our results the following properties should be fulfilled:

1. The associated IRAS source satisfies our selection criteria (see Chapter 1).
2. It should have at least 20 stars.
3. To be young they should be embedded and contain star formation tracers such as YSOs, molecular cores, outflows, masers, infrared excess stars and nebulosity at K.
4. The expected cluster parameters values are a diameter of 1.6 pc with a concentration $c_{YSC} \simeq 0.5$.

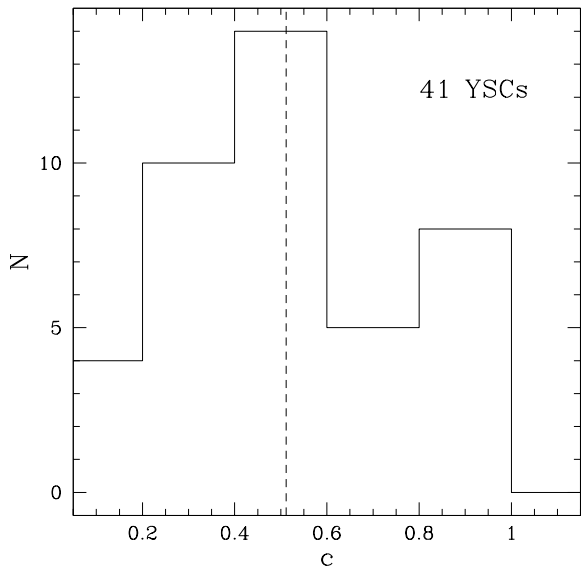

Figure 4.5 Histogram of the concentration parameter in YSCs. The mean value of 0.51 $\pm$ 0.24 is shown with a dashed vertical line.

Chapter 5

Infrared Photometry Results

5.1 Color-color Diagrams

Since the 60's and specially throughout the 70's (e. g. Grasdalen et al. 1973, Strom et al. 1975, Vrba et al. 1975) the J-H / H-K diagrams have been used as diagnostic diagrams to study the embedded young stellar population in a particular region. In Fig. 5.1 four zones are shown to distinguish different stellar populations based on the location of stars in this diagram (e.g. Meyer 1996; Hillenbrand et al. 1995; Carpenter et al. 1993). First, they include the main sequence (MS) and giant branch (GB) taken from Koorneef 1983 and Bessel & Brett 1988 and transformed into the Glass-Johnson system. The standard reddening law (Bessel & Brett 1988) is represented as a vector for $\vec{A}_V$=10 mag.

Region **A** corresponds to the reddened zero age main sequence stars along the extinction vector A_V. It may contain reddened early and old type stars as well as some weak T-Tauri stars (WTTS).

Region **B** is populated by reddened classical T-Tauri stars (CTTS), above the CTTS loci (extended to H-K=1.5 mag) described by Meyer 1996 and Hillenbrand et al. 1995, i.e. those low-mass stars that are in the process of accreting material and with a charateristic dust disk that produces their infrared excess.

Region **C** is populated by stars with IR-excess due to a more complicated geometry than a disk which includes Herbig Ae/Be stars and protostar candidates.

Finally, region **D** is the loci theoretically determined by Smith 1995 for J- and C-shocks associated to intense components of Herbig-Haro objects (HH).

The potential information that emerges from J-H vs. H-K diagrams is very rich. With the construction of this diagram we are able to distinguish stellar populations, i.e. the content of reddened MS stars and lower mass CTTS+Ae/Be as well as the presence (or lack) of stars with strong IR excess, i.e. stars with

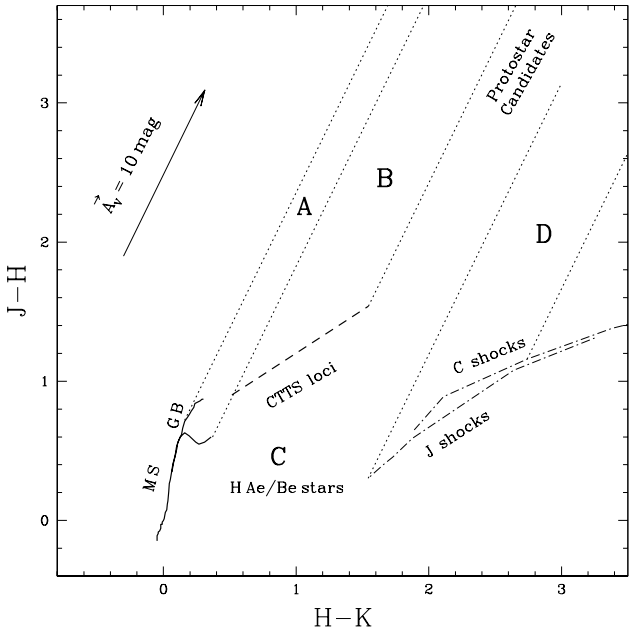

Figure 5.1 Important zones in a J-H vs. H-K diagram to be considered in the diagnosis of a YSC.

extreme values of $A_V \gtrsim 20$. Also, it shows the distribution of the extinction in the cluster. It allows to calculate individual extinction values to reddened stars in region **B** by their distance to the CTTS loci. Nevertheless, this is not possible for stars in region **A** due to the shape of the MS curve and it is necessary to use the J vs. J-H diagram for reddened MS and WTT stars. Additionally, protostar candidates can be selected for thermal infrared studies, as well as YSCs with shocks for a detailed study of molecular gas emission and kinematics.

As an example, we present this diagram for YSC 2 in Fig. 5.2. This cluster illustrates the presence of 92 stars and their location in the four zones described above. Region **A** contains 31 MS + WTTS, **B** and **C** contain 17 CTTS+Ae/Be and 1 candidate of HH knot in region **D**.

With the photometric data in JHK we constructed color-color diagrams for the YSC sample. The complete J-H / H-K diagrams of each cluster is presented in the YSC catalog (Appendix D).

For comparison in Fig. 5.3 J-H / H-K diagrams of 12 YSCs are presented. Note that in these diagrams some of the clusters present a wide spread in A_V while others are very crowded around a single value, which gives information of

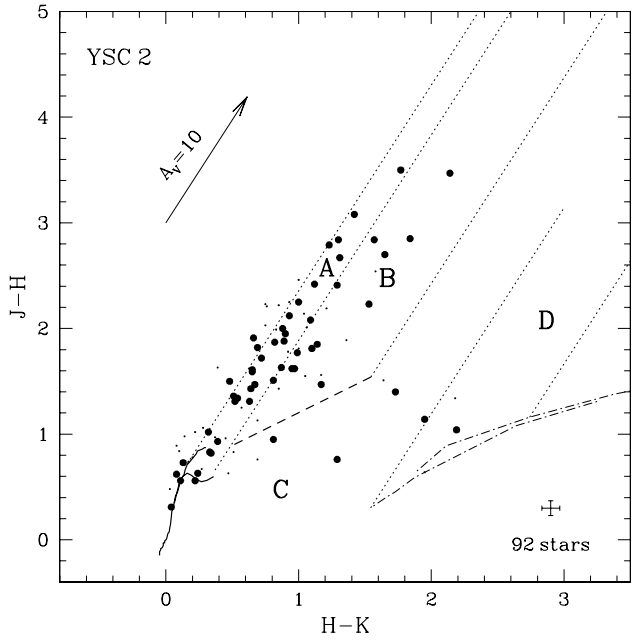

Figure 5.2 Example of J-H vs. H-K diagram from YSC 2 which has objects in the four zones (see text).

the location of the stars inside the molecular gas cloud. In a detailed study of YSC 18 (Porras et al. 2000) we can distinguish two groups of stars at different extinction values which could indicate a distance difference, i.e. one is more deeply embedded than the other one, or an age difference, i.e. the redder cluster would be younger.

The stellar population of the YSCs is presented in Table 5.1. The population of stars in each field can be roughly divided into **cluster members** and **field stars**, which are members of the extended population of sources around the cluster. Table 5.1, shows the number of stars in regions **A**, **B/C** and **D** corresponding to reddened MS stars, CTT+Ae/Be stars and HH knots candidates, respectively.

Sources that lie in the theoretical region of HH-like knots predicted by Smith 1995 (Cols. (7) and (10)) are present in 20% of the YSCs (2 (S187IR), 4B (W3), 12, 15, 18A (S233IR), 29, 31 and 35). These sources are usually strong deeply embedded HH knots. Detailed H_2 observations of S187IR are reported in Salas et al. 1998 and Salas et al. 2000, where the curved jet morphology and velocity field are studied. While the S233IR H_2 study is presented in Porras et al. 2000.

Whenever a cluster shows sources in zone **D** it strongly suggests the presence of a deeply embedded HH outflow.

In the observed fields **foreground stars** are considered to have colors J-H < 1, H-K < 0.4 and extinction $A_V < 1.8$ mag. Their numbers are presented in Col. (3). These stars are excluded from the IMF study.

Stars outside and to the left of zone **A** have anomalous colors which in most cases correspond to a close unresolved pair of stars (see Col. (4)). These sources represent ($\sim 1\%$) and are also excluded from our IMF study. Higher spatial resolution photometry is needed for these pairs.

Also, as we found from RGB images there are some very red ($A_V > 20$ mag) sources that appear along the CTTS locus and are interpreted as embedded YSOs (Col. (11)). We note that some of the clusters are richer in red objects (YSC 4B, 5, 7 and 20). Finally, we also include the number of stars without J-counterpart in the cluster, $N_{H,K}$ (Col. (12)). The latter are also excluded from the IMF study.

With the data from Table 5.1 we find that for cluster stars about 59% show more MS than CTTS+Ae/Be stars, 29% show a balance between the two populations and the remaining 12% are more abundant in CTTS+Ae/Be. Furthermore, we have calculated the percentage of CTTS + Ae/Be stars to the total (MS + CTTS+Ae/Be) for cluster and field stars. Then, we can compare the proportions between cluster and field lower mass populations. Of the whole sample, 39% show a similar percentage of CTTS+Ae/Be stars both in cluster and in field regions. In 42% of the clusters these stars are more abundant in the cluster region. The remaining 19% show a larger percentage of CTTS+Ae/Be stars in the field. We think that these results may be indicative of a different star formation history in the YSCs, and a full discussion will be presented below (§6.5).

The "field" stars or distributed population, in excess of expected field galactic contamination is evident from our study. The existence of a "distributed" versus "clustered" population in molecular clouds is a controversial issue being currently investigated in different regions (e.g. Carpenter 2000).

5.2 Completeness Limit and Luminosity Functions

Luminosity functions (LF) are histograms that show the distribution of light in stars at an specific wavelength in absolute magnitudes. They give information of the content of bright stars and show a cut in the lower-end, due to instrumental limitations. A review on LF for YSCs is presented in Lada et al. 1998.

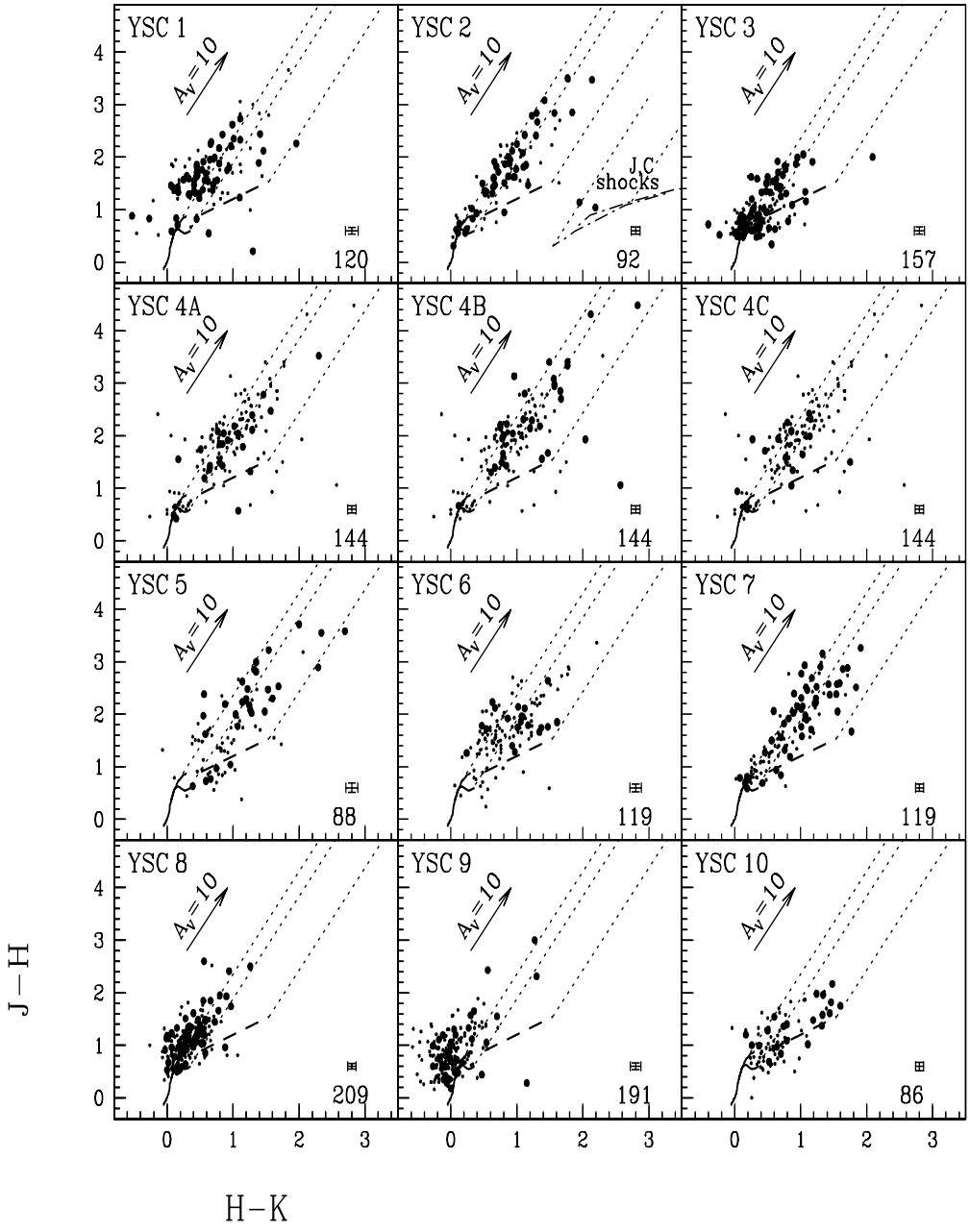

Figure 5.3 Example of color-color diagrams of 12 YSCs. Big dots correspond to cluster stars while small dots to field or non cluster stars.

Table 5.1 YSC POPULATION

# YSC	N_T	Foreground	Not resolved	Cluster			Field			IR excess	$N_{H,K}$
				A	**B/C**	**D**	**A**	**B/C**	**D**		
(1)	(2)	(3)	(4)	(5)	(6)	(7)	(8)	(9)	(10)	(11)	(12)
1	120	0	2	50	7	0	49	12	0	2	13
2	92	0	8	31	17	1	21	11	3	3	26
3	157	0	18	50	16	0	50	23	0	0	7
4A	144	0	8	15	11	0	72	36	1	1	10
4B	144	0	8	19	14	1	68	33	0	8	20
4C	144	0	7	11	5	0	77	42	1	2	6
5	88	0	0	13	20	0	17	38	0	9	41
6	119	0	1	8	13	0	54	43	0	0	6
7	119	0	2	26	24	0	48	19	0	8	28
8	209	0	24	56	3	0	116	10	0	0	7
9	184	6	60	51	2	0	67	2	1	1	11
10	86	1	5	11	26	0	19	24	0	0	21
11	119	1	5	17	55	0	16	25	0	0	32
12	134	1	1	41	12	0	59	19	1	3	29
13	186	1	7	35	35	0	67	41	0	0	16
14	180	3	15	83	6	0	69	4	0	1	46
15	152	1	7	46	20	0	49	25	4	1	70
16	120	1	32	13	15	0	40	19	0	1	12
17	353	1	59	113	71	0	79	30	0	0	9
18A	101	2	7	15	5	0	40	31	1	0	1
18B	101	2	7	6	4	0	49	33	0	1	10
19	185	0	8	62	19	0	80	16	0	3	17
20	145	0	6	49	37	0	37	16	0	10	40
21	217	4	10	52	5	0	142	4	0	1	10
22	133	0	5	75	29	0	17	6	0	5	39
23	97	5	6	21	3	0	56	6	0	0	10
24	74	0	9	19	18	0	15	13	0	1	17
25	97	2	8	37	14	0	23	14	0	2	23
26	221	0	17	46	81	0	31	46	0	1	20
27	108	0	13	34	30	0	15	15	0	0	12
28	164	0	10	16	14	0	92	32	0	2	12
29	105	2	8	17	13	1	35	29	0	1	10
30	146	0	3	27	18	0	70	28	0	0	5
31	161	4	14	19	3	0	94	26	1	0	4
32	255	1	7	52	55	0	89	51	0	0	13
33	201	1	19	59	18	0	84	19	1	1	13
34	112	1	16	21	7	0	54	13	0	0	16
35	125	0	19	9	25	1	27	42	1	0	8
36	194	2	9	59	53	0	47	24	0	2	23
37	199	22	43	59	11	0	46	18	0	0	37
38	138	0	6	35	12	0	50	35	0	3	20

It is important to estimate the completeness in magnitude of our observations, i.e. the limiting magnitudes. There are two magnitude limits that can be considered: the photometric limit and the differential completeness limit.

The photometric limit is estimated as the maximum magnitude obtained under certain photometric error. For an error of 0.3 in our NIR photometry, we reach instrumental photometric limits of 19.5, 19.0 and 18.0 for J, H and K, respectively.

The differential completness limit is obtained as the magnitude at wich ∼99% of stars artificially added (via ADDSTAR[a]) are recovered within a magnitude bin (Carpenter et al. 1997). This limit is usually smaller than the photometric limit. For all the clusters average values are 18.2 ± 0.6, 17.6 ± 0.7 and 16.8 ± 0.6 for J, H and K filters, respectively. We prefer to be conservative and use differential completeness limits. Magnitude limits are very important because they will be translated to a completeness limit in mass for cluster stars (see Chapter 6).

Table 5.2 lists the differential completeness limit values for each YSC in the JHK filters. It was found that in regions with strong nebulosity, the differential completeness limit decrease by $\sim$ 2 mag in H and K bands. This effect is not detected in J-band, because the nebulosity contribution at J is less evident.

With the adopted distances (see Table 4.1) we construct for each YSC the luminosity function histograms JLF, HLF and KLF. These histograms are presented in frames 5, 6 and 7 in the Appendix D catalog, which summarizes the main information of our work in each cluster.

As an example, in Fig. 5.4 we present luminosity histograms for YSC 19 to YSC 22. The histograms correspond to cluster stars without restrictions (dotted histograms) and taking into account the mass completeness limits described in §6.1.1 (solid). A comparison of these histograms gives an idea of the number of cluster stars missed on the IMF study presented in Chapter 6 in each YSC.

5.3 Age

The most reliable method to estimate the stellar age in a nearby embedded cluster is the combined study of photometric and spectroscopic data (e.g. Herbig 1998; Luhman et al. 1998) reviewed in Meyer et al. 2000. Because our sources are located at distance $D > 1$ kpc they are weak for a spectroscopic study and it would require several observing runs in a large telescope. So, an age estimate is not possible by the usual process.

[a]ADDSTAR procedure was buildt doing only some modifications to the SUBSTAR procedure.

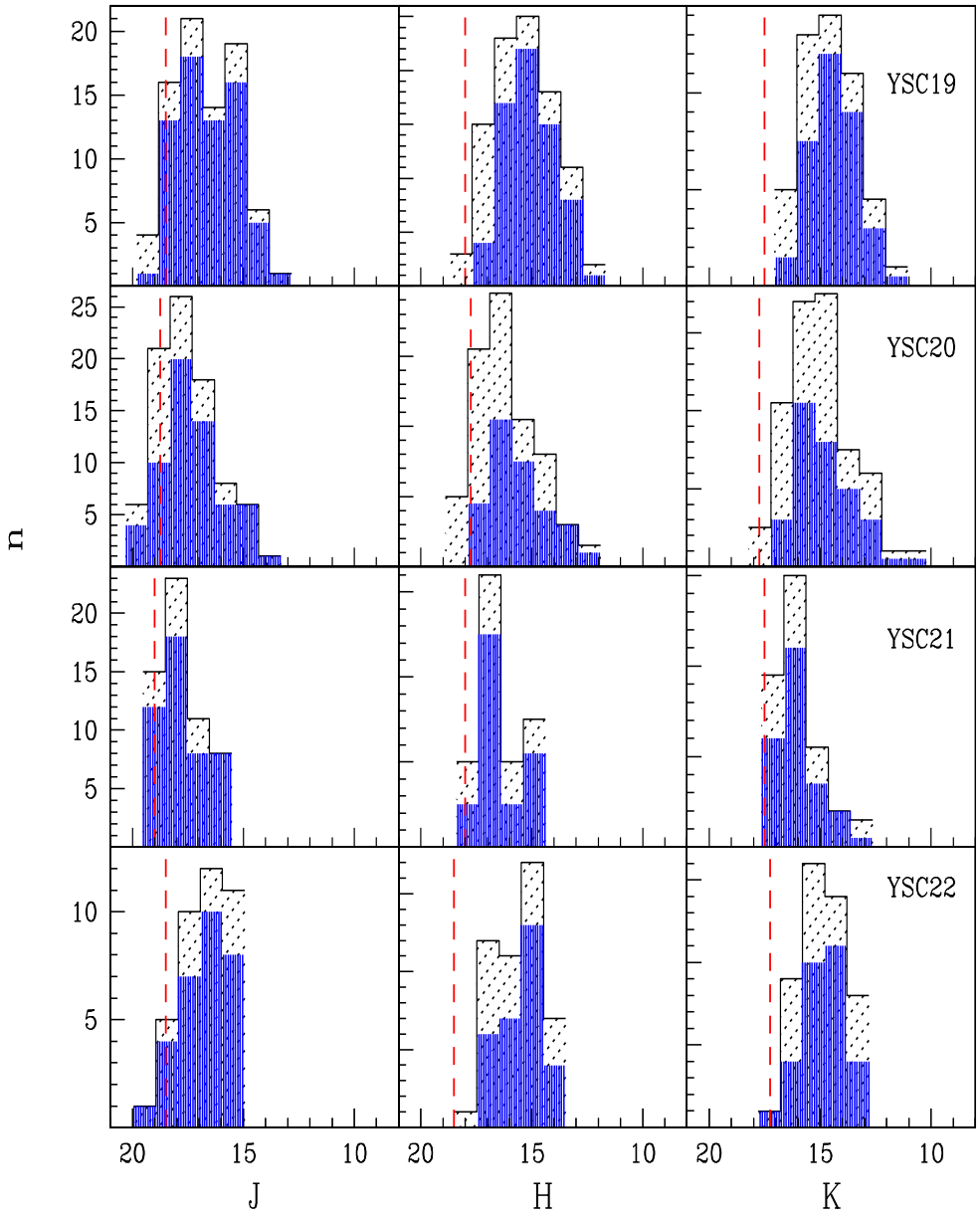

Figure 5.4 Luminosity function histograms (JLF, HLF and KLF) of four YSCs. The dotted histograms correspond to the cluster population, while solid ones to the population complete in mass (c.f. §7.1.1). The dashed vertical lines show the differential completness limits listed in Table 5.2.

Table 5.2 DIFFERENTIAL COMPLETENESS LIMIT IN JHK BANDS

YSC # (1)	J_{lim} (2)	H_{lim} (3)	K_{lim} (4)
1	19.0	18.5	16.0
2	18.5	18.8	17.3
3	18.5	17.8	17.0
4	18.0	16.0	15.0
5	18.5	18.5	17.0
6	18.8	18.3	16.5
7	18.8	18.0	17.8
8	18.8	17.8	17.0
9	18.5	18.0	17.5
10	17.5	16.8	16.8
11	17.3	17.0	16.8
12	18.5	18.0	17.3
13	18.3	17.5	17.3
14	17.5	16.5	16.8
15	18.8	18.0	16.5
16	17.3	17.5	17.0
17	17.5	17.3	17.3
18	19.3	18.5	17.0
19	18.5	18.0	17.5
20	18.8	17.8	17.8
21	19.0	18.0	17.5
22	18.5	18.5	17.3
23	17.8	16.8	16.5
24	18.3	17.8	16.5
25	17.3	17.3	16.5
26	18.5	18.0	17.0
27	17.5	16.5	16.5
28	18.0	16.8	16.3
29	17.5	16.0	15.3
30	17.0	16.8	16.8
31	18.3	17.0	17.0
32	18.0	17.5	16.8
33	18.3	17.0	16.5
34	17.3	17.3	17.0
35	18.8	18.3	17.0
36	18.0	17.3	16.5
37	18.5	17.5	16.0
38	18.5	17.8	17.0

We present in this thesis a purely photometric method to calculate the average age of a YSC, first published in Porras et al. 2000. This method is based on a comparison between observed and theoretical luminosity function (LF) histograms. The models presented by Zinnecker et al. 1993 and Strom et al. 1993 (SSM), for K-band and J-band absolute luminosity functions respectively, provide the necessary KLF and JLF theoretical histograms.

Since the J-filter provides a more reliable estimate of the true photospheric emission for stars with IR excess, we prefer to use JLF instead of KLF for the age determination. The SSM model is based on the assumption of coeval star formation, uses the pre-main sequence isochrones by D'Antona & Mazzitelli 1994 and assumes the IMF of Miller & Scalo 1979. They trace six different evolutionary

histograms at ages of 0.3, 0.7, 1, 3, 7 and 10 Myr.

To calculate YSC ages we propose the following method:

1. We use an interval in luminosity ranging from 0.75 to 7.75 mag, with 26 bins of 0.25 mag for each histogram.

2. Histograms treated as vectors can be used to construct a matrix $\widehat{M}$, where each column contains the theoretical JLF at each age. The dimension of $\widehat{M}$ is then 26×6.

3. It is possible to recover any JLF vector simply by

$$\overrightarrow{JLF} = \widehat{M}\ \overrightarrow{\delta}$$

   where $\overrightarrow{JLF}$ is the J-luminosity function and $\overrightarrow{\delta}$ is defined as a Delta function of ages (e.g. $\overrightarrow{\delta}$ = [0,0,0,1,0,0] will reproduce the JLF at 3 Myr).

4. On the other hand $\widehat{M}$, considered as an influence matrix, can be used to estimate an age vector $\overrightarrow{E}$, for the observed JLF ($\overrightarrow{JLF}_{obs}$) in each cluster, by means of the transformation:

$$\overrightarrow{E} = \widehat{M}^{-1}\ \overrightarrow{JLF}_{obs}.$$

5. The elements in $\overrightarrow{E}$ give the distribution of stars in all ages and the age estimate can be obtained with the maximum value. We fit a parabola to the maximum value and two adjacent points to estimate the age of the cluster. This maximum is the most probable age of the bulk stellar population. We note that the distributions have to be normalized to the number of stars in the region.

The results obtained by this procedure are presented in the Catalog of Appendix D. In frame 8 of this catalog a plot of $\overrightarrow{E}$ for each YSC is presented. In Fig. 5.5 we present examples of the age vectors obtained for some YSCs.

We also estimated the age for the extended population or local field stars. The estimated ages of YSCs and corresponding local field stars are presented in Table 5.3. We note that the estimated ages for clusters yield a mean value of 2.42 ± 1.20 in an interval from 1.1 to 5.5 Myr, while field stars are older and have a mean age of 2.84 ± 2.81 in an interval from 1.2 to 18.1 Myr. Both values are consistent with the expected lifetime of a GMC (10^{6-7} Myr). It is interesting to note that, in general, local field stars (distributed population) are older than cluster members, as expected, but they are also young. In some cases (7 YSCs, according to the

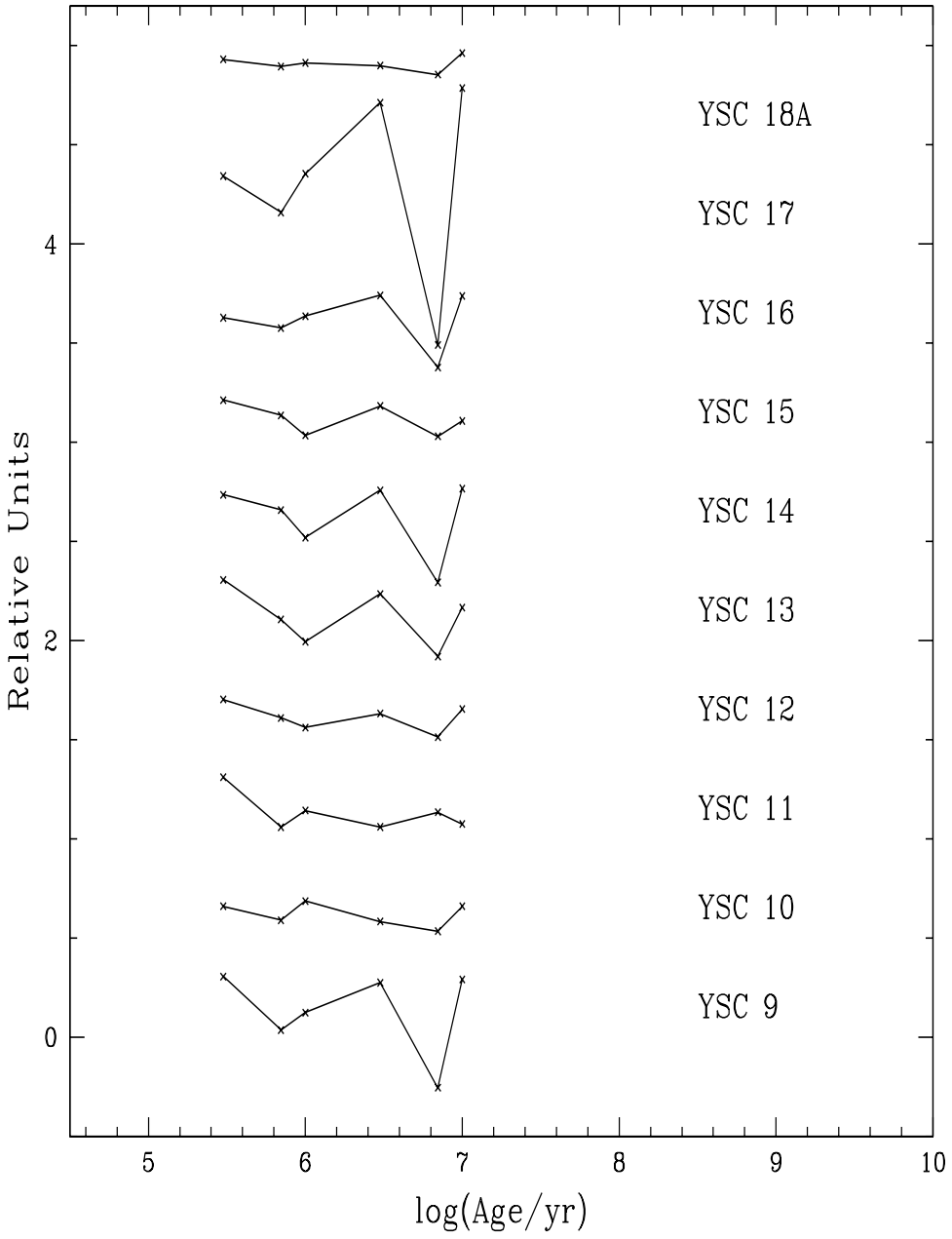

Figure 5.5 Example of age plots from ten YSCs .

associated isochrone) the obtained field ages result smaller, which is unexpected. Whether this is a true characteristic remains open until a less crude method of age estimation is developed.

Fig. 5.6 shows a plot of age vs. cluster radius, compared to the predicted time scale for star formation (crossing time for turbulent motions) according to the size of the region obtained from Elmegreen et al. 2000, $t_{SF} \propto s^{0.5}$. Excluding the 5 clusters which lie in the upper region, we find $t_{YSC} \propto s^{0.2\pm0.1}$, slightly flatter than the expected prediction. Moreover, different symbols are used to show the presence of youthness tracers (c.f. Table 4.1). Apparently, there is not a clear correlation between these tracers and the age or cluster radius.

5.3.1 Isochrones

In this section we discuss the construction of isochrones plotted in the observational J/J-H and K/H-K diagrams (see § 6.3), which are an essential tool for the determination of stellar masses. The isochrones are obtained from pre-main sequence evolutionary tracks by D'Antona & Mazzitelli 1994, assuming Alexander opacities and the Canuto & Mazzitelli convection model. For $2.5 < M < 20$ $M_\odot$ we used the tracks presented by Hillenbrand et al. 1995.

For each stellar mass M, the corresponding luminosity L and effective temperature T_e are obtained. From L we derive M_{bol} =4.74 - 2.5 $log\ (L/L_\odot)$ (Bessell et al. 1998). From T_e the bolometric correction is obtained via a polinomial function presented by Flower 1996. These quantities allow us to calculate the visual absolute magnitude $M_V = M_{bol} - BC$. Also from T_e, the colors V-J and J-H for dwarfs are obtained from Bessell & Brett 1988, using the T_e values of Tokunaga 2000. Finally, the absolute magnitude J is calculated via $J = M_V - (V - J)$, i.e. in general,

$$J = 4.74 - 2.5\,log\ (L/L_\odot) - BC(T_e) - (V - J) \qquad (5.1)$$

Isochrones at ages 0.1, 0.3, 1, 3, 10, 30 and 100 Myr are available from D'Antona & Mazzitelli 1994 models and are plotted in Fig. 5.7. They will be used to associate a mass value to dereddened stars in the J/J-H diagram (see Chapter 6). Isochrones for each YSC were selected according to the closer value of cluster age. The corresponding isochrone age values are presented in Col. (3) of Table 5.3.

The corresponding isochrone for each cluster are also included in the YSC Catalog in Appendix D, and are shown both in the J/J-H and K/H-K diagrams (frames 2 and 4, respectively).

Table 5.3 ESTIMATED AGE AND ISOCHRONES OF YSC'S

# YSC (1)	YSC Age (Myr) (2)	I_{YSC} (Myr) (3)	Field Age (Myr) (4)	I_{field} (Myr) (5)
1	2.2	3.0	2.0	3.0
2	2.0	3.0	9.2	10.0
3	2.1	3.0	1.6	1.0
4A	1.1	1.0	1.9	1.0
4B	1.7	1.0	1.9	1.0
4C	5.5	10.0	1.9	1.0
5	2.5	3.0	2.2	3.0
6	2.2	3.0	2.2	3.0
7	2.8	3.0	2.4	3.0
8	2.4	3.0	2.1	3.0
9	2.1	3.0	2.1	3.0
10	1.4	1.0	2.0	3.0
11	1.4	1.0	2.1	3.0
12	2.3	3.0	2.7	3.0
13	2.5	3.0	2.0	3.0
14	2.3	3.0	2.7	3.0
15	2.6	3.0	2.3	3.0
16	2.1	3.0	2.1	3.0
17	2.1	3.0	2.0	3.0
18A	1.5	1.0	1.4	1.0
18B	1.5	1.0	1.2	1.0
19	1.5	1.0	2.0	3.0
20	2.4	3.0	5.4	10.0
21	1.4	1.0	1.4	1.0
22	1.9	1.0	2.0	3.0
23	5.3	10.0	2.2	3.0
24	1.4	1.0	2.0	3.0
25	2.0	3.0	1.8	1.0
26	2.1	3.0	2.1	3.0
27	1.7	1.0	1.5	1.0
28	5.3	10.0	2.4	3.0
29	1.5	1.0	2.6	3.0
30	2.4	3.0	4.3	3.0
31	2.7	3.0	2.3	3.0
32	1.7	1.0	18.1	10.0
33	2.6	3.0	2.8	3.0
34	2.0	3.0	1.8	1.0
35	5.5	10.0	2.4	3.0
36	2.0	1.0	1.7	1.0
37	5.5	10.0	5.2	10.0
38	2.0	3.0	2.4	3.0

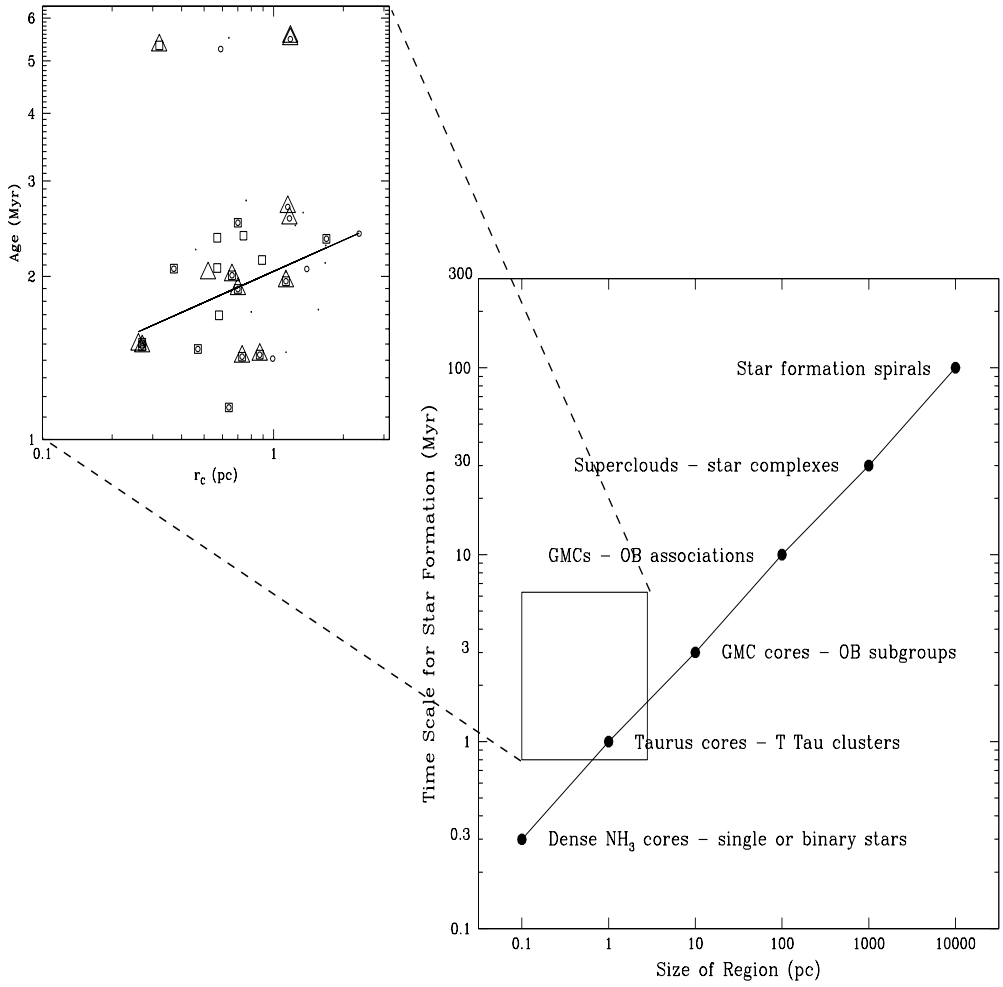

Figure 5.6 Age vs. YSC radius in our sample, compared to Fig. 3 from Elmegreen et al. 2000. Symbols correspond to the presence of YSO (△), CO outflow (□), H_2O maser (○) and clusters without youthness tracers (.).

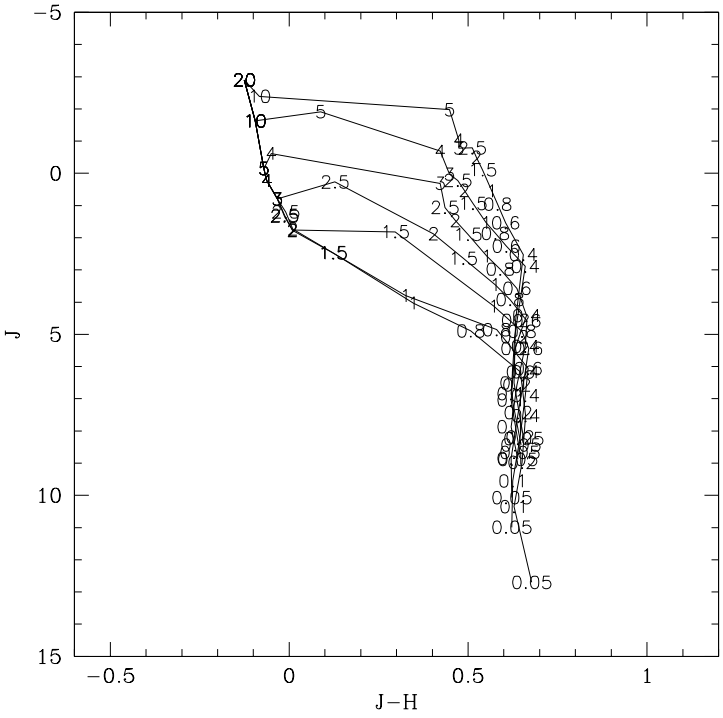

Figure 5.7 Isochrones at ages 0.1, 0.3, 1, 3, 10, 30 and 100 Myr with mass scale in $M_{\odot}$. Upper isochrone corresponds to the smallest age while the lower one corresponds to the ZAMS.

5.4 Color-Magnitude Diagrams

To complete our view of stellar NIR photometry in YSCs we use two color-magnitude diagrams: J vs. J-H and K vs. H-K.

J vs. J-H diagram is useful to estimate individual stellar extinction and mass of reddened MS stars. It also helps to find a mass limit, M_{lim} at which we can consider that the cluster is complete (see section 6.1.1).

K vs. H-K diagram includes stars shown in the J / J-H and also stars without a J-counterpart. So it is then useful to determine the additional number of stars that are deeply embedded in the region (c.f. Col (12) in Table 5.1), both inside the cluster and in the field.

The color-magnitude diagrams of all the clusters are shown in Appendix D, presented as frames 2 and 4 for each cluster. Fig. 5.8 shows examples of a group of twelve of these color-magnitude diagrams. As we expected, most of the stars

lie in the region of low mass stars; only very few correspond to a more massive star. These massive stars appear to be deeply embedded in some clusters (A_V up to ∼30 mag, e.g. YSC 20) and their relative position to the cluster center will be discussed on Chapter 6.

As was seen from color-color diagrams, in some cases it seems to be present a bimodal distribution along the reddening vector, i.e. two groups of stars at a different extinction, this probably indicates the presence of two, instead of one, clusters inside the radius r_C (as S233IR presented in Porras et al. 2000). The most remarkable example is YSC 6, which is also a distant source. Our photometric technique allows to get values even for those far away sources with good accuracy.

If the distance to a cluster is underestimated, the whole set of stars will be shifted downwards in J vs. J-H diagram, and upwards if it is overestimated. An error of ± 1kpc in distance will correspond to an error of ∼ ± 1 spectral type for intermediate mass stars (A0 - F0), it will be smaller for early type stars (O, B), and larger for late type stars (G-M).

5.5 Extinction

The computation of the extinction to individual stars depends on its location in the J-H/H-K diagram. Thus, we use two methods: one applicable to stars along the reddened MS, region **A** in Fig. 5.1 and the second for stars along the reddened CTT and Ae/Be stars loci (Meyer 1996), region **B**.

The extinction of sources in region **A**, was estimated from the J/J-H diagrams, taking each star along the A_V vector direction to the zero age main sequence (ZAMS) as a first approximation. This process is made for both, cluster and field stars. As Carpenter et al. 1997 point out, region **A** can be populated also by weak emission T Tauris (WTTS). So filter-J rather than K in K/H-K diagrams is better to avoid the IR excess contribution to the A_V estimate.

Furthermore, a refined estimation of the individual extinction was done by dereddening stars in region **A** to the corresponding isochrone at the cluster and field ages estimated in §5.3.

Extinction of sources in region **B** are dereddened directly in the J-H/H-K diagram, based on their distance to the CTTS line along the A_V vector.

The average $< A_V >$ value for each cluster is presented in Col. (2) of Table 6.1 included in next Chapter. We note that these values include both reddened MS and CTT stars and that we have excluded stars of very high extinction ($A_V >$ 20 mag), because these anomalous objects have an intrinsic reddening which is likely produced by a protostellar disk. In general, all clusters show mean A_V

values greater than $\sim$4 magnitudes and about 20 % of the YSC sample have mean A_V >10 mag.

Due to the uncertainty in distance to YSCs, we calculate that the effect on A_V for twice the distance is that the mean value, $< A_V >$, increases by $\sim$8 %.

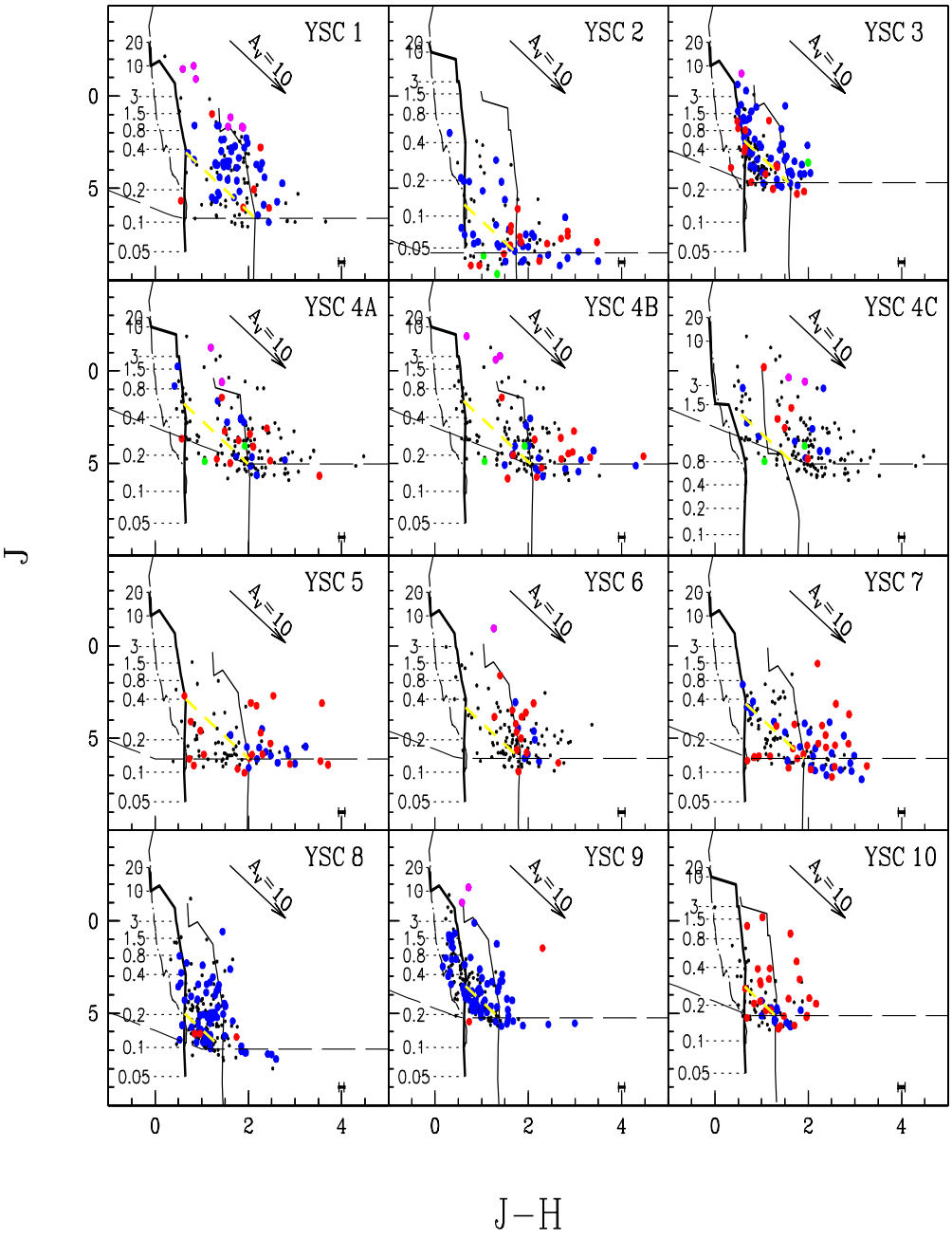

Figure 5.8 Sample of color-magnitud diagrams in J / J-H. Dots are the same as in Fig. 5.3. The isochrones shown correspond to ZAMS (dashed curve), cluster age (darker curve) and cluster age shifted to the right by the mean value of extinction (light curve).

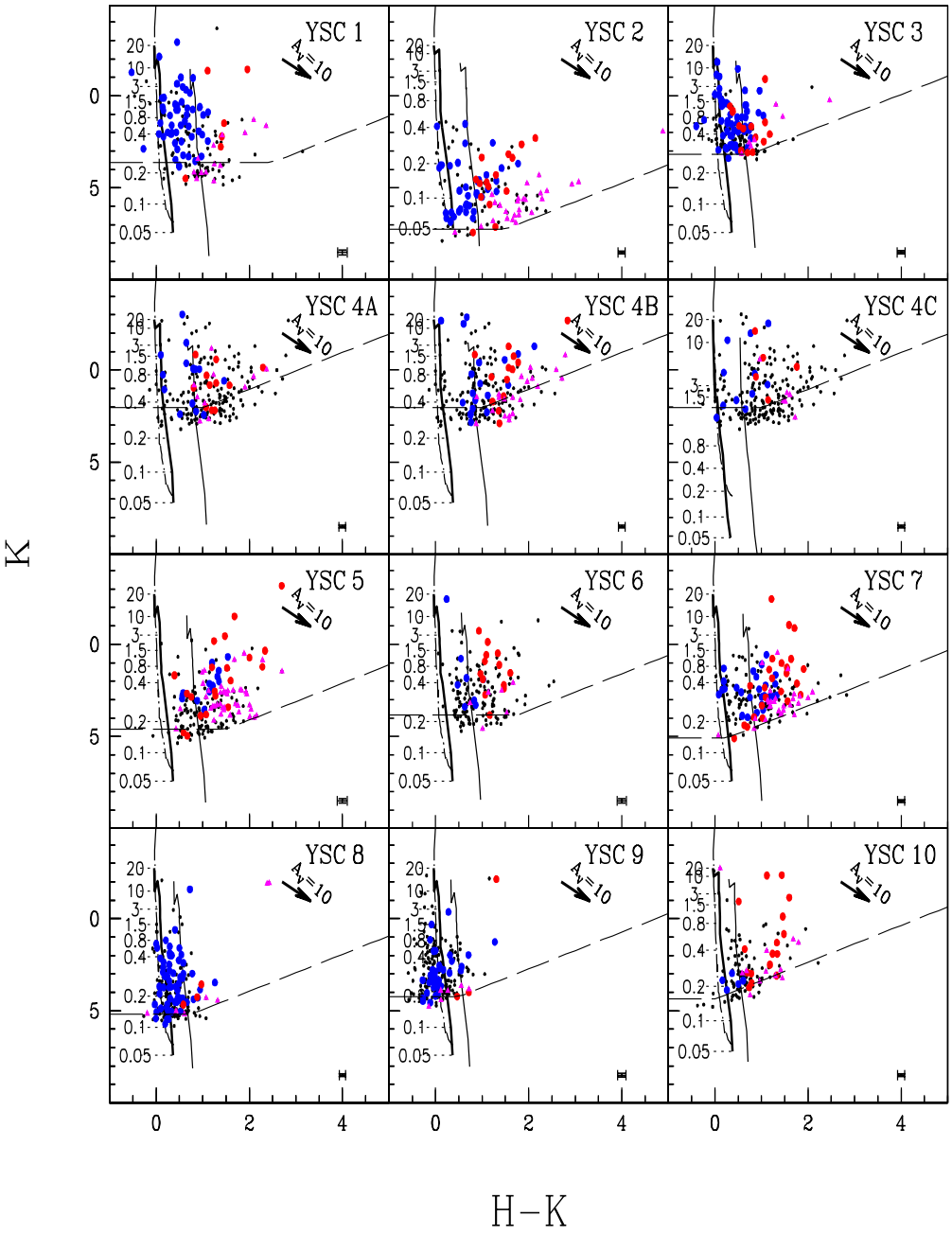

Figure 5.9 Sample of color-magnitud diagrams in K / H-K. Dots and curves are the same as in Fig. 5.8 but small triangles show the stellar population without J counterpart in each cluster.

Chapter 6

Mass of Cluster Stars and IMF

6.1 Mass

Following previous work by Meyer 1996 and Carpenter et al. 1993, we derive stellar masses by a three step procedure. First, we identify the reddened MS and CTTS+Ae/Be stars located in the J-H/H-K diagram (regions **A**, **B** and **C** shown in color-color diagram of Fig. 5.1).

Second, the mass of MS reddened stars can be obtained from the J/J-H diagram by de-reddening them to the previously estimated isochrone (see Table 5.3). For each star, the mass value is obtained from the scale along the corresponding isochrone by moving paralel to the A_V vector from its original position to the isochrone. As an example, we present YSC 8 J/J-H diagram in Fig. 6.1

Third, in the case of reddened CTT and Ae/Be stars, we use the Carpenter et al. 1993 empirical relations:

$$\log M = -0.25\ M_H + 0.44$$
$$\log M = -0.24\ M_K + 0.24,$$

where M_H and M_K are the uncorrected for extinction H- and K-band magnitudes. These relations result from masses of stars in the Taurus molecular cloud. We are then assuming that the Perseus cluster CTT and Ae/Be stars are similar than in Taurus. A similar study such as that of Carpenter et al., for other nearby ($\lesssim$500 pc) star forming regions –where masses can be estimated via spectroscopic observations– is needed, in order to study the possible changes to these relations due to the intrinsic cluster characteristics.

We note that an error in A_V of 10 mag would yield an underestimation of the mass of 0.24 dex.

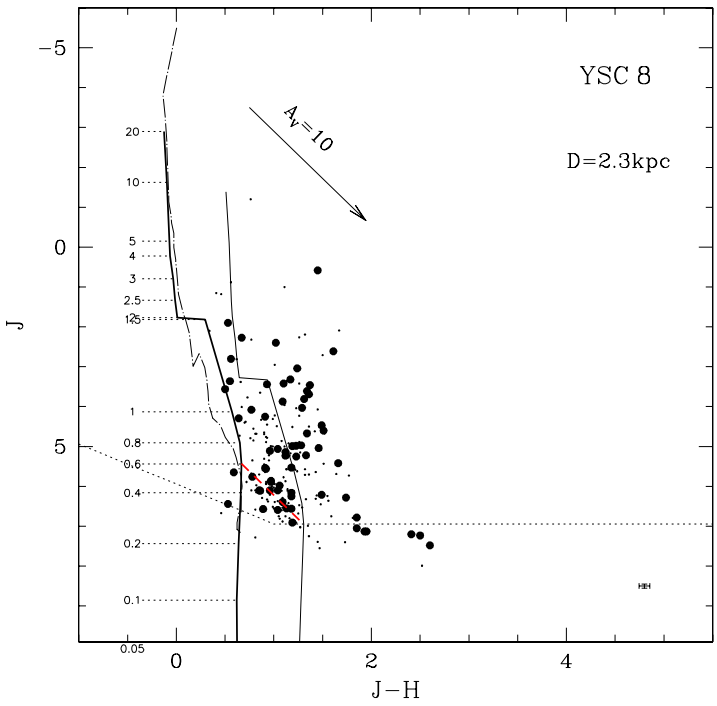

Figure 6.1 J vs. J-H diagram of YSC 8.

With this method we obtained the mass values for all stars with JHK magnitudes in our sample of young clusters. These individual masses are listed in the last column of the data tables presented in Appendix C.

6.1.1 Mass Completeness Limit

In order to do a realistic comparison of cluster mass distributions, it is important to consider only unbiased data. Photometric limitations and extinction in each cloud lead to a stellar mass, M_{lim}, which defines the mass limit at which a sample of stars in a cluster is considered as complete.

To clarify the M_{lim} determination let us consider Fig. 6.2. If the isochrone in the J / J-H diagram is shifted along the extinction vector to any value such that a significant fraction of the cluster stars are included, it intersects the differential completeness limit at the point P. We choose the mean value $< A_V > + 1\sigma$. The projection of P back to the original isochrone along the A_V vector yields the value of M_{lim}. In the example shown is considered a YSC at D=3.5 kpc,

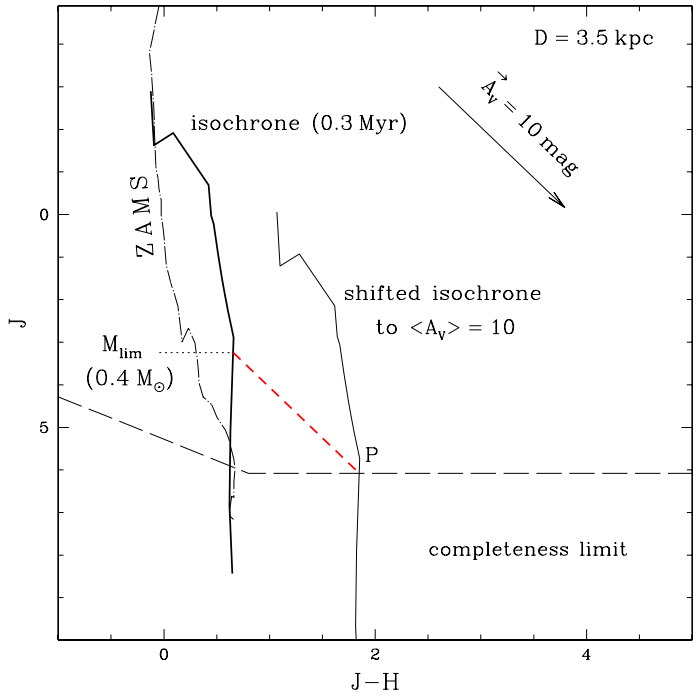

Figure 6.2 J vs. J-H diagram that shows the limiting mass value at which a YSC is considered complete. In this example, a YSC at a distance of 3.5 kpc and age of 0.3 Myr is complete down to 0.4 $M_\odot$.

$< A_V >$=10 mag and age of 0.3 Myr, which yields M_{lim} =0.4 $M_\odot$. Thus, all the stars contained inside the area above the broken line constitute the unbiased sample of the stellar population. These are the only stars that will be considered in the construction of the IMF histograms.

Using the mean extinction values listed in Table 6.1, we can estimate the completeness in mass for each cluster. These M_{lim} values are listed in Col. (3) and the number of cluster stars in the complete sample are given in Col. (4). As can be seen, M_{lim} values range from 0.2 to 1.8 $M_\odot$. Since the number of stars in YSC 18B is only 7, we decided to remove it from the subsequent analysis.

The M_{lim} distribution is plotted in Fig. 6.3. It clearly shows two peaks, one at 1.2 $M_\odot$ and another less prominent at 0.6 $M_\odot$. In other words, there are 14 YSCs that are complete down to a $M_{lim} \sim 0.6\ M_\odot$ and 29 YSCs are complete down to 1.2 $M_\odot$. So in order to compare all the clusters the mass limit would be $M_{lim} \sim 2\ M_\odot$.

Table 6.1 PARAMETERS DEFINING YSCs COMPLETE IN MASS

YSC # (1)	$< A_V >$ (mag) (2)	M_{lim} ($M_\odot$) (3)	N_{CC} (4)	M_T ($M_\odot$) (5)	Γ bin 0.25 (6)	$C^{0.6}$ (7)
1	12.15 ± 4.888	1.029	45	298.2 (7)	0.18 ± 0.24	—
2	8.907 ± 4.518	0.300	34	18.2 (0)	-0.93 ± 0.54	0.60
3	7.611 ± 4.589	1.224	47	162.0 (1)	-1.14 ± 0.17	—
4A	10.26 ± 5.072	1.082	21	115.0 (2)	-0.16 ± 0.37	—
4B	11.74 ± 5.183	1.223	20	97.5 (3)	-0.13 ± 0.63	—
4C	8.76 ± 5.813	1.683	11	65.5 (2)	-0.03 ± 0.25	—
5	9.134 ± 5.541	0.921	19	14.8 (0)	0.00 ± 0.70	—
6	9.149 ± 5.213	0.929	16	34.9 (1)	-0.43 ± 0.15	—
7	9.444 ± 5.542	0.954	34	39.7 (0)	-1.06 ± 0.65	—
8	6.764 ± 4.123	0.489	47	53.9 (0)	-1.45 ± 0.51	1.23
9	6.777 ± 3.932	0.985	44	141.7 (2)	-0.70 ± 0.19	—
10	3.903 ± 2.839	0.497	29	31.8 (0)	-0.83 ± 0.39	0.86
11	3.783 ± 2.556	0.640	57	61.3 (0)	-1.69 ± 0.13	—
12	9.97 ± 5.121	1.569	40	172.2 (2)	-0.75 ± 0.09	—
13	5.563 ± 4.095	1.146	57	129.7 (1)	-1.10 ± 0.15	—
14	8.503 ± 3.794	1.626	71	319.6 (2)	-1.22 ± 0.14	—
15	7.88 ± 4.939	1.171	51	153.9 (0)	-0.30 ± 0.50	—
16	4.179 ± 3.076	0.578	23	13.8 (0)	-1.40 ± 0.29	1.33
17	3.663 ± 2.687	0.448	159	117.5 (0)	-1.26 ± 0.31	0.75
18A	7.843 ± 4.901	0.181	16	19.7 (0)	-1.07 ± 0.29	1.33
18B	15.59 ± 3.263	0.609	7	8.2 (0)	—	—
19	7.582 ± 4.095	0.272	68	56.9 (0)	-1.70 ± 0.34	1.70
20	8.22 ± 4.598	0.543	63	51.4 (0)	-1.50 ± 0.52	0.87
21	7.293 ± 3.406	0.602	47	58.3 (0)	-1.05 ± 0.61	0.55
22	7.954 ± 4.363	0.561	84	83.5 (0)	-1.68 ± 0.65	1.82
23	10.02 ± 5.036	1.132	18	25.9 (0)	1.47 ± 0.72	—
24	5.129 ± 3.266	0.229	25	18.1 (0)	-0.81 ± 0.56	0.80
25	8.091 ± 4.608	0.943	36	29.7 (0)	-1.70 ± -0.80	—
26	5.643 ± 4.53	0.580	96	84.6 (0)	-1.37 ± 0.28	0.86
27	4.486 ± 2.908	0.340	54	54.8 (1)	-0.71 ± 0.24	0.89
28	8.52 ± 4.952	1.615	22	89.8 (1)	-0.83 ± 0.17	—
29	4.989 ± 3.558	0.195	25	16.1 (0)	-0.80 ± 0.46	1.00
30	6.231 ± 3.043	1.819	36	139.4 (2)	-1.28 ± 0.18	—
31	9.25 ± 4.226	1.429	17	92.8 (3)	-0.60 ± -0.26	—
32	4.728 ± 3.438	0.807	87	144.0 (1)	-1.33 ± 0.20	—
33	7.965 ± 4.095	1.219	61	254.1 (3)	-1.04 ± 0.45	—
34	6.984 ± 3.497	1.424	23	96.7 (1)	-0.68 ± 0.30	—
35	4.951 ± 3.589	1.229	23	41.8 (0)	-1.20 ± 0.70	—
36	6.303 ± 4.748	0.628	80	106.3 (1)	-0.90 ± 0.39	—
37	5.715 ± 3.136	1.269	53	135.0 (2)	-1.13 ± 0.22	—
38	10.75 ± 5.241	0.759	35	64.2 (1)	-0.67 ± 0.17	—

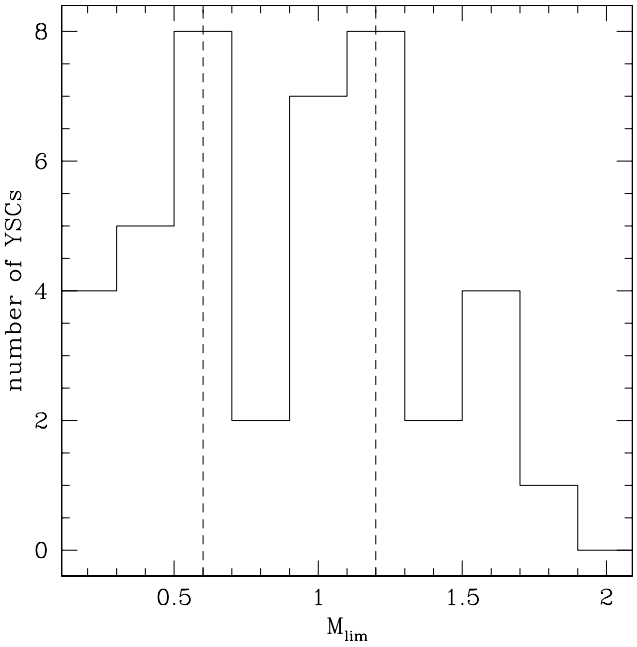

Figure 6.3 Distribution of M_{lim} values which shows that two conspicuous peaks at 0.6 and 1.2 $M_{\odot}$.

6.1.2 Cluster Total Mass

We have calculated the cluster total mass M_T by adding the derived stellar masses including only objects in the complete sample:

$$M_T = \sum_{i=1}^{N_{CC}} M_i, \tag{6.1}$$

where M_i are the individual masses and N_{CC} is the number of stars considered in each cluster. Derived M_T values are presented in column (6) of Table 6.1. They cover a wide range of masses, from 8 to 320 $M_{\odot}$. The average value is 90.6±73.9 and 14 YSCs have $M_T > 100$ $M_{\odot}$. Furthermore, the number of massive stars in the cluster is listed in parentesis to check their contribution to the total mass, indeed 12/14 of the massive clusters contain massive stars.

6.2 IMF

The distribution of stellar masses formed within a molecular cloud. i.e. the initial mass function (IMF) is a fundamental astrophysical problem that has been the subject of studies for more than 50 years (see historical references in Elmegreen et al. 2000).

In this thesis the commonly used power-law notation for the IMF to characterize the mass in a certain mass interval is used. The IMF index value is defined as

$$\Gamma = \frac{d\, log\Phi(logM)}{d\, logM}, \tag{6.2}$$

where $\Phi(\log M)$ is the number of stars per unit logarithmic mass interval.

In this notation, Salpeter's value is Γ_{Sal} = -1.35 in a mass range of 1 to 10 $M_\odot$ for the solar neighborhood. This value has been adopted in open clusters, in galactic and extragalactic star formation regions and is even used as an standard input in population synthesis models (e.g. Bruzual 1994). Therefore, any clue to variations in this function is crucial for our understanding of the initial stages of stellar evolution.

The slope value calculated by Salpeter, was later studied for the full range of stellar masses by Miller & Scalo 1979. They obtained a function with three values of Γ: -0.4, -1.5 and -2.3 for the low-mass range ($M \leq 1\ M_\odot$), intermediate-mass range (1 - 10 $M_\odot$) and high-mass range ($M > 10\ M_\odot$), respectively. This last value was changed to -1.2 after the review made by Scalo 1986.

Kroupa et al. 1993 study of stars with masses between 0.08 and 100 $M_\odot$ shows that the IMF can be approximated with Γ: 0.3 to -0.85 for $0.08 < M < 0.5\ M_\odot$, -1.2 for $0.5 \leq M \leq 1\ M_\odot$ and -1.7 for $M > 1\ M_\odot$.

The IMF calculations of star clusters both in our Galaxy and in the Magellanic Clouds are in general consistent with the local IMF, and the slope values above one solar mass generally scatter around the Salpeter's value (see Fig. 1.1). In order to be consistent in selecting an IMF for galactic evolutionary studies, Scalo 1998 suggest the three-segment power law form

$$\begin{array}{rlll} \Gamma & = & -0.2 \pm 0.3 & 0.1 - 1\ M_\odot \\ & & -1.7 \pm 0.5 & 1 - 10\ M_\odot \\ & & -1.3 \pm 0.5 & 10 - 100\ M_\odot \end{array} \tag{6.3}$$

where the $\pm$ symbols can be interpreted as a measure of the empirical uncertainties and/or the real IMF variations.

Because no evidence of the dependence of the IMF with any property of the clusters studied has been found, there exist a wide acceptance that the IMF is universal, at least in the local universe (Meyer et al. 2000; Larson 1999).

6.2.1 IMF estimation in YSCs

Deeply embedded young clusters have unique attributes which make them useful for studies of the IMF (Meyer et al. 2000):

- Because of their youth, evolutionary corrections needed from present day distribution of stellar masses into IMF are minimized.
- Youth precludes wandering of cluster members far from their birthsites due to peculiar motions.
- Small area encompassed by dense rich clusters minimizes contamination by foreground stars.
- Cloud core extinction minimizes contamination by background stars.
- Greater sensitivity to substellar mass objects than in older open clusters.

We have now the possibility of deriving the IMF in the young stellar clusters studied in this thesis. Our aim is to compare our results with the widely used Salpeter or Miller & Scalo IMFs (Salpeter 1955, Miller & Scalo 1979) and to recent studies of other young clusters.

In practice, the construction of IMF histograms and slope values have difficulties due to the lack of stars in some mass bins, the small number in others, and their consecuent large error bars. Thus, a compromise with the mass bin size has to be done when trying to construct IMF histograms.

To calculate the IMF index for each cluster, we did a linear least-squares fit in different mass intervals, using values of mass above M_{lim}, given in Table 6.1. Thus, the slope values were calculated from M = 0.6 $M_\odot$ for 14 YSCs ($\Gamma_{0.6}$), from M = 1.2 $M_\odot$ for 14 YSCs ($\Gamma_{1.2}$) and from M = 2 $M_\odot$ for the remaining 12 clusters ($\Gamma_{2.0}$). In order to select the most convenient bin size we also calculated the IMF index for different mass bins: 0.1, 0.15, 0.2, 0.25, 0.3, 0.35, 0.4, 0.45 and 0.5. Fig. 6.4 shows the bin-size vs. mean values of Γ (Γ_1, Γ_2, Γ_3) for the three fitting intervals. Error bars correspond to the mean value of fitting errors. We decided that a good compromise was to choose the 0.25 bin size for the IMF histograms and indices presented in this work. The resulting IMF indices for a 0.25 bin in $\log M$ are listed in Col. (6) of Table 6.1.

We did a weighted mean fit to the points in Fig. 6.4 and obtained for the three mass intervals:

$< \Gamma_1 >$ = -1.11 ± 0.23 $< \Gamma_2 >$ = -0.90 ± 0.15 $< \Gamma_3 >$ = -0.86 ± 0.23.

These fits are presented as a broken horizontal line. Therefore, we chose a mean value of Γ_{YSC} = -0.96 ± 0.14 along the whole mass spectrum, consistent with the three estimations. The error is the standard deviation in the mean gamma values.

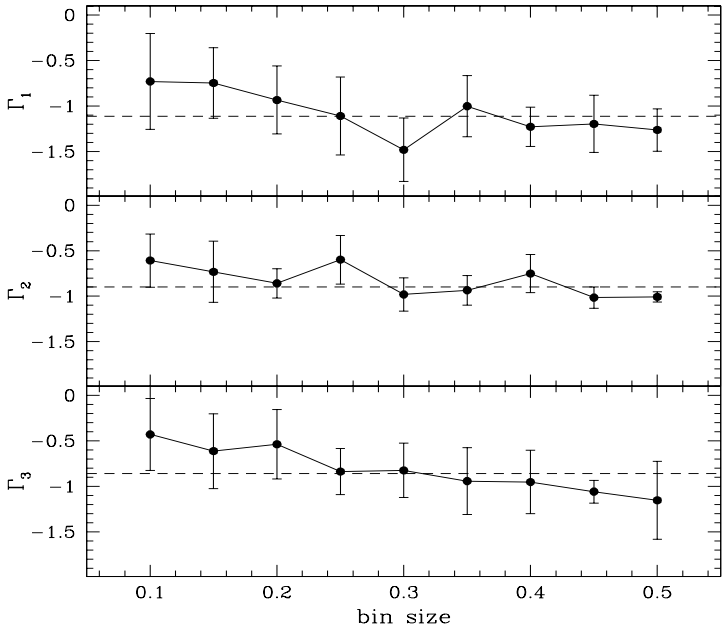

Figure 6.4 Variations of Γ values according with the bin-size used. Upper graph corresponds to histograms fits from 0.6 to 20 $M_\odot$ (Γ_1), middle graph, from 1.2 to 20 $M_\odot$ (Γ_2), and lower plot from 2 to 20 $M_\odot$ (Γ_3). Error bars represent the average sigma values of the fits.

We decided to construct mass histograms in a log-log representation. The complete sample of IMF histograms is shown in Fig. 6.5 to Fig. 6.8, where darker histograms correspond to the 14 YSCs selected as the most complete in the low-mass regime, $M_{lim} < 0.6$ $M_\odot$.

The resulting IMF histogram for each YSC is presented in frame 9 of the Catalog in Appendix D.

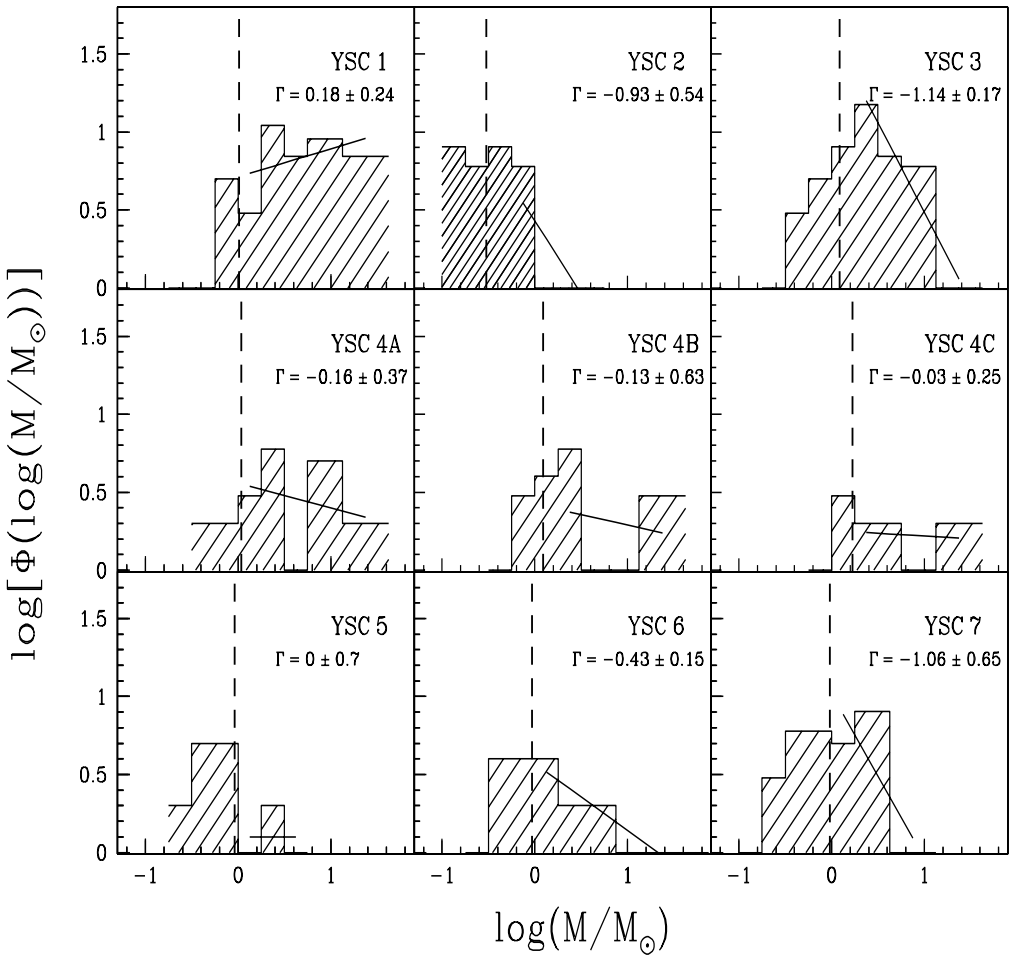

Figure 6.5 Sample of IMF histograms with a bin value of 0.25 in $\log M$. Dashed lines correspond to the M_{lim} values listed in Table 6.1, while Γ values correspond to fits (shown as a continuous line) as they appear in Table 6.1. Darker histograms correspond to clusters with M_{lim} <0.6 $M_\odot$.

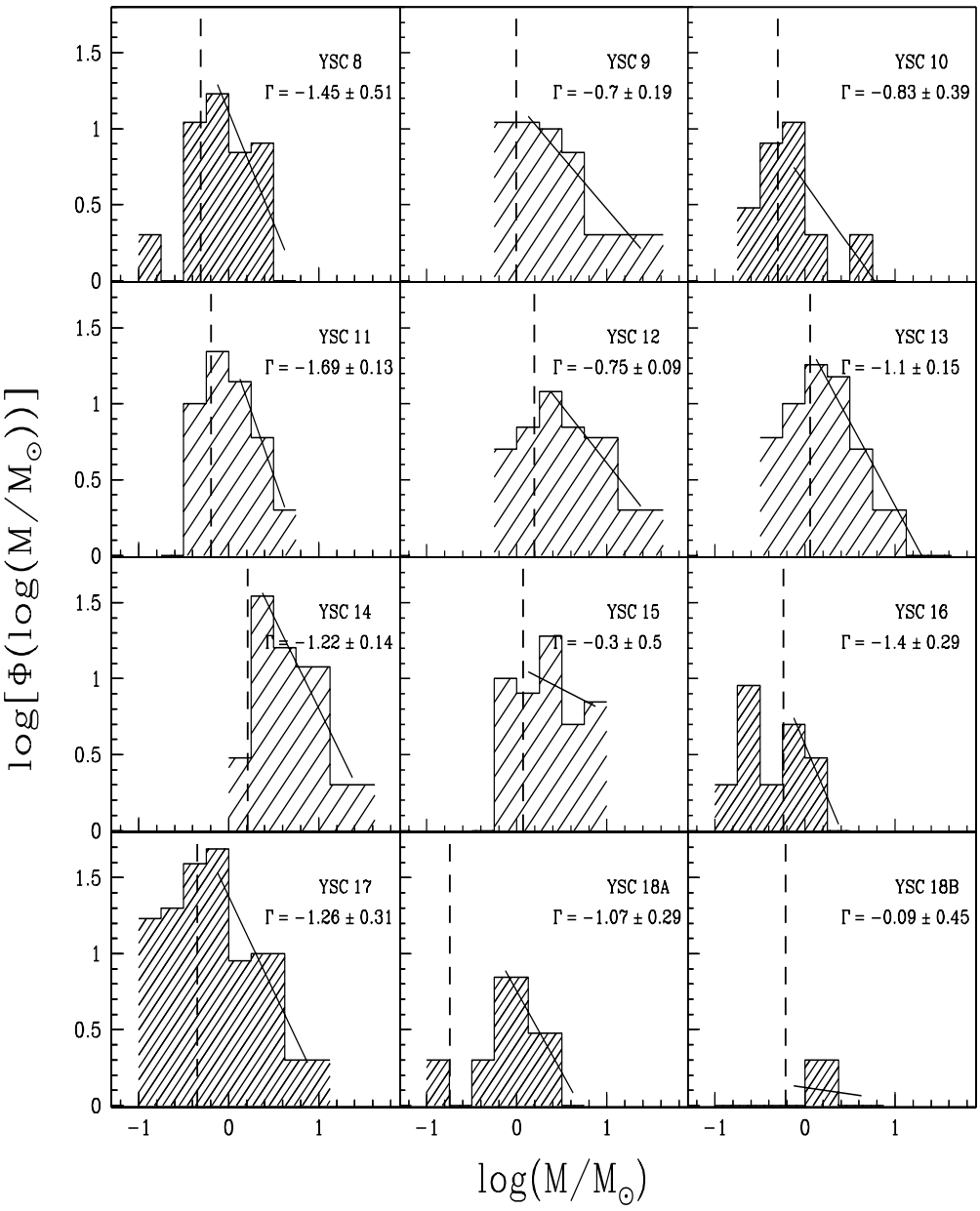

Figure 6.6 Same as Fig. 6.5.

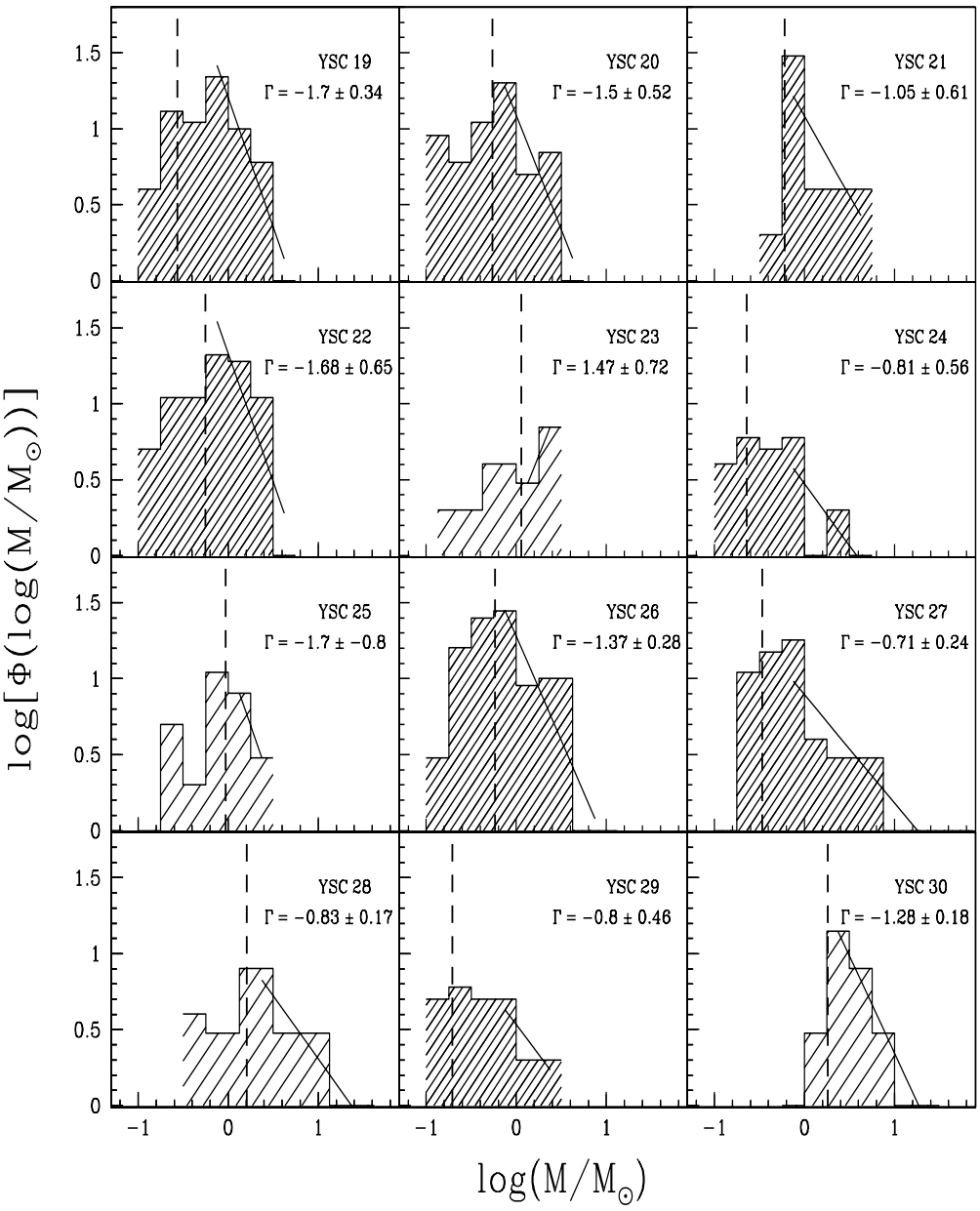

Figure 6.7 Same as Fig. 6.5.

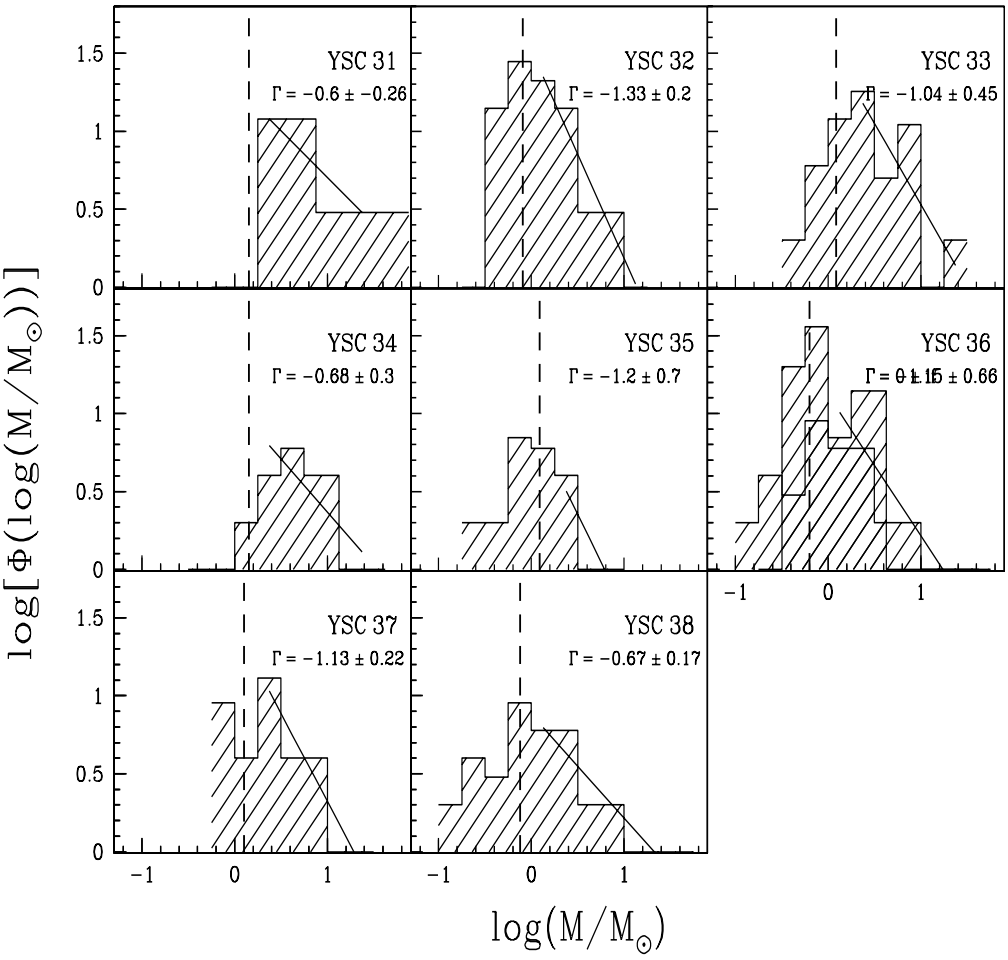

Figure 6.8 Same as Fig. 6.5.

6.2.2 Mass ratios

Alternatively, as has been suggested by Meyer et al. 2000, a rather useful diagnostic parameter in YSCs is the ratio of intermediate-to-low-mass stars

$$R \; = \; N(1-10\ M_{\odot})/N(0.1-1\ M_{\odot}), \tag{6.4}$$

which has the advantages that it minimizes the number of bins to only two, as well as the uncertainties in this ratio.

Following this idea, we define the ratio

$$C = N(1.2-20\ M_{\odot})/N(0.6-1.2\ M_{\odot}) \tag{6.5}$$

based in the minimum and maximum mass values that we obtained in our YSC sample.

We can calculate this ratio only for the 14 YSCs complete in these mass intervals. The resulting values are listed in the last column of Table 6.1 and plotted in Fig. 6.9. The mean value obtained for the 14 YSCs is $C^{0.6}$=1.04±0.39. The horizontal lines presented in this figure from top to bottom, represent the ratio for: our mean value $C^{0.6}$, the expected value for our IMF $C^{0.6}_{-0.96}$=0.99, $C^{0.6}_{Sc}$=0.64±0.04 for a Scalo 1998 IMF range, $C^{0.6}_{Sal}$=0.63 appropiate for a Salpeter IMF and $C^{0.6}_{Kr}$=0.50 for a Kroupa IMF. These values were estimated via the integration of $dN/dM = M^{-\gamma}$, where γ was selected for each IMF in the corresponding mass intervals and $\Gamma = \gamma + 1$.

Fig. 6.9 shows that most clusters lie well above the expected values for the different IMFs. Only two clusters have a C value close to Salpeter's ratio and it seems that the clusters separate in two groups according to $C^{0.6} > 1.2$. As expected the mean value is consistent with our IMF $C^{0.6}_{-0.96}$.

The IMFs obtained by Scalo 1998 (equation 6.3) and Kroupa et al. 1993 (see §6.2) do not present a single IMF index in the whole mass regime. The difference in the $C^{0.6}$ values might be produced by this brake in the low-mass regime.

To check this possibility, we look for Γ and M_{brake} values that would produce a $C^{0.6}$=1.04, when combined with a power law of -0.96 for larger masses ($M > M_{brake}$). The resulting slopes vs. brake point values are shown in Fig. 6.10. In this plot, we note that for low-masses ($M < 1\ M_{\odot}$) there is a minimum value of $\Gamma \sim$ -0.75 at $M_{brake} \sim 1 \pm 0.07\ M_{\odot}$ for which the condition $C^{0.6}$=1.04 holds. This would imply that a power-law of the type

$$\begin{aligned} \Gamma \; = \; & -0.75 \pm 0.10 \qquad M < 1 M_{\odot} \\ & -0.96 \pm 0.14 \qquad M > 1 M_{\odot} \end{aligned} \tag{6.6}$$

would be consistent. Also for values of Γ=0 the brake occurs at 0.65 $M_\odot$ and positive values are obtained for masses close to 0.6 $M_\odot$.

Alternatively, if we assume a composite IMF with Scalo's and Kroupa's low-mass slope and our YSC slope for masses larger than 1 $M_\odot$, we obtain: $C^{0.6}_{Sc,-0.96}$ = 1.16±0.07 and $C^{0.6}_{Kr,-0.96}$=0.94, which are both in agreement with our mean value of 1.04. The dispersion in Scalo's value is due to the range of values in his IMF.

On the low-mass end we have only 6 YSCs (2, 18A, 19, 24, 27 and 29) that are complete down to 0.3 $M_\odot$. We can define again $C^{0.3} = N(1.2 - 20\ M_\odot)/N(0.3 - 1.2\ M_\odot)$ to present them in Fig 6.11. The mean value is $C^{0.3}$=0.34 and is close to the expected Scalo value $C^{0.3}_{Sc}$=0.29±0.05 (also in Fig 6.11). In this case $C^{0.3}$ = $C^{0.3}_{-0.96}$ = 0.34. The expected mass ratios for Salpeter's and Kroupa's IMF lie quite close to the observed points, which suggests that these IMFs might indeed be the YSCs IMF. Finally, it is interesting to note that Meyer et al. 2000 mass ratios, R, for nearby clusters (Fig. 6.12) are between 0.1 and 0.45, which implies a closer agreement with our $C^{0.3}$ value than with our $C^{0.6}$ value. Thus, it is of crucial importance to reach the very low-mass regime with more sensitivity and spatial resolution. These considerations suggest that in the low-mass regime, we can assume the Scalo value.

However, for the high-mass regime our uncertainties grow because theoretical PMS isochrones are unknown above ∼20 $M_\odot$ and it is possible that the estimated masses of some stars might be larger than this value. For this region Scalo 1998 suggests another slope value (see equation (6.3), but we are unable to test this high-mass regime in the YSCs. We tried to define another C value ($N(10 - 20\ M_\odot)/N(1.2 - 10\ M_\odot)$) appropiate for this mass range, but unfortunately clusters with high-mass stars turned out to have a rather large M_{lim} and this prevented us from getting any result.

Our results suggest that young stellar clusters have an IMF:

$$\begin{aligned} \Gamma \;=\; & -0.20 && \text{for } 0.3 < M < 0.6 M_\odot \\ & -0.75 \pm 0.10 && \text{for } 0.6 < M < 1 M_\odot \\ & -0.96 \pm 0.14 && \text{for } M > 1 M_\odot \end{aligned} \tag{6.7}$$

where the first value comes from the study of 6 YSCs, the second of 14 YSCs and the final one from the most complete sample of IMF indices of 40 YSCs.

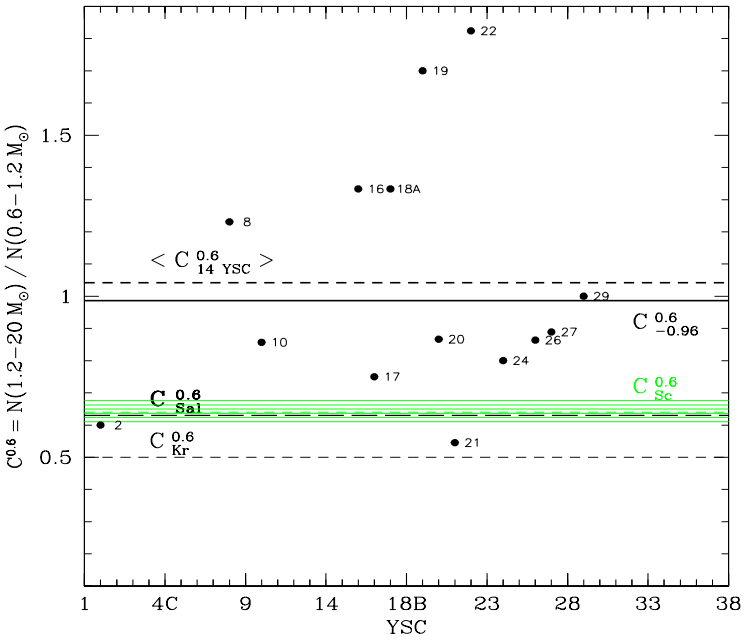

Figure 6.9 Values of intermediate-to-low-mass stars ratios C for 14 YSCs complete down to 0.6 $M_{\odot}$.

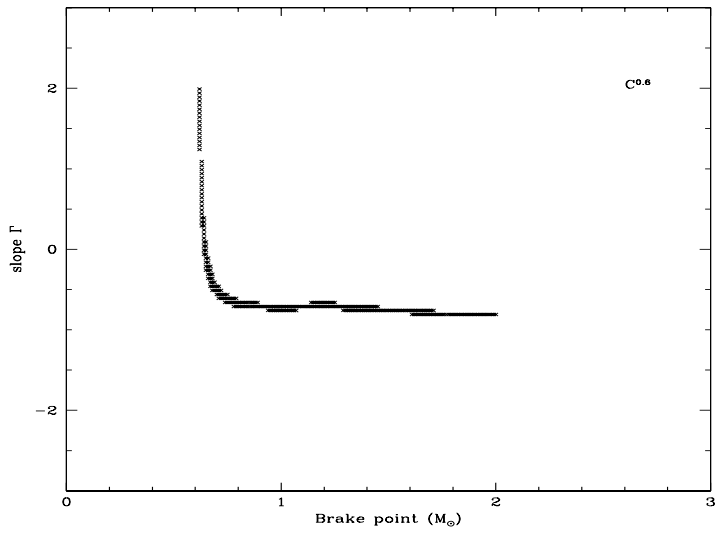

Figure 6.10 Values of Γ vs. possible brake points ($M_{\odot}$) in the IMF.

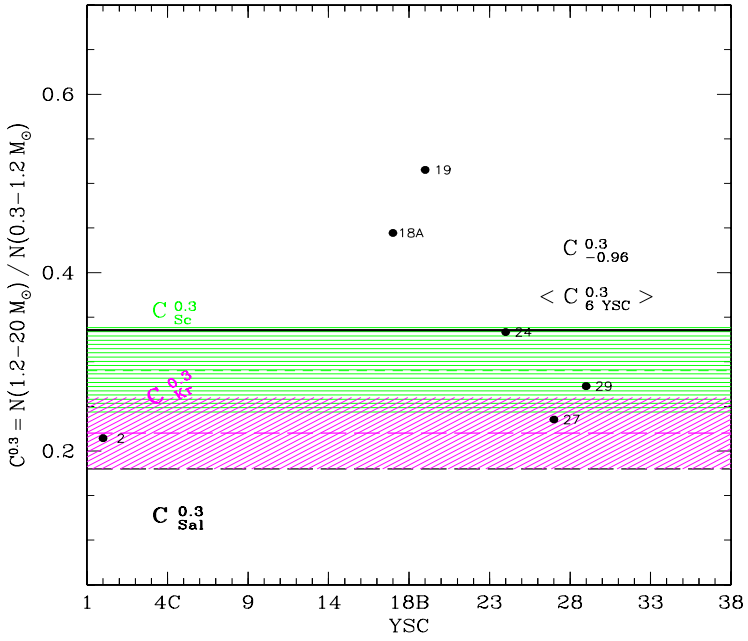

Figure 6.11 Values of intermediate-to-low-mass stars ratios C for 7 YSCs complete down to 0.3 $M_\odot$.

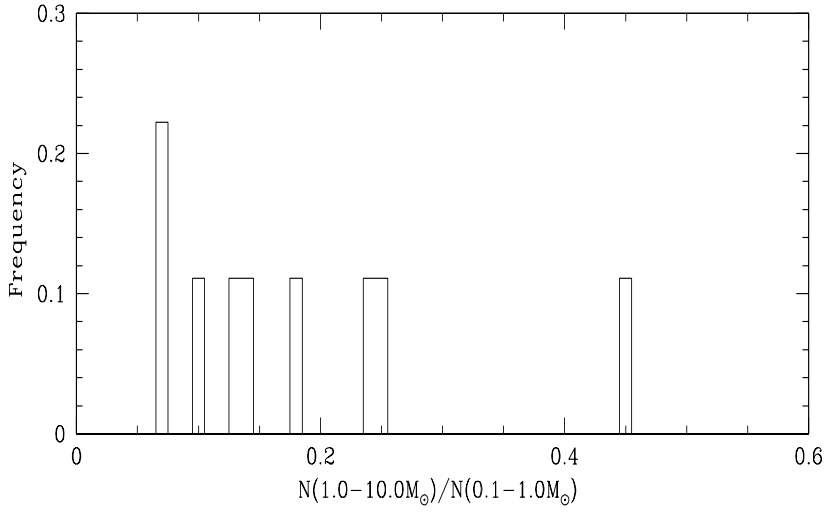

Figure 6.12 Values of R for nearby clusters. Fig. 3 in Meyer et al. 2000.

6.2.3 "Average" cluster

The large number of stars with derived masses in the YSCs studied in this thesis give us a statistically significant sample to construct an single IMF from all of them. We thus decided to construct from our data an "average" cluster which contains the average value, bin by bin, of the overall cluster sample. The number of stars per bin in this average cluster is defined as:

$$N_i = \frac{1}{N_c} \sum_{j=1}^{41} N_c N_j \tag{6.8}$$

where i=mass bin, j=cluster number, N_c=number of complete clusters at bin i.

The resulting "average" cluster is presented in Fig. 6.13 constructed with the averaged values bin by bin of 0.3 in log M, where two histograms are plotted: 1) the 40 clusters (continuous line) with $\Gamma_{all} = -1.01 \pm 0.09$, and 2) the 14 YSCs complete below 0.6 $M_{\odot}$ (broken line) with $\Gamma = -1.84 \pm 0.09$. As is expected, because the number of averaged bins in the low-mass regime is lower and dependent on M_{lim}, these bins tend to increase their values and produce a steeper slope (c.f. equation (6.8)). Finally, the continous line represents the three-segment power law given in equation (6.7), which is our final IMF for young stellar clusters.

6.3 Spatial Distribution of Mass

Once the individual stellar masses are known, it is possible to locate them and study their spatial distribution inside the cluster area. We decided to consider only those stars included in the mass complete sample because our mass values are more reliable and they were used on the IMF estimation. Our results are presented in four figures, Fig. 6.14, Fig. 6.15, Fig. 6.16 and Fig. 6.17. Symbols are as follows: massive stars (M>10 $M_{\odot}$) are blue stars, intermediate-mass (1<M$\leq$10 $M_{\odot}$) yellow dots, low-mass (M$\leq$1 $M_{\odot}$) as red dots, the remaining stars which include field and non-complete cluster stars are black dots.

From these distributions we observe the following:

- 20 YSCs contain massive stars (1, 3 4A, 4B, 4C, 6, 9, 12, 13, 14, 27, 28, 30, 31, 32, 33, 34, 36, 37, 38), which corresponds to 49% of the sample. In most cases they are located in the central region of the cluster, although in some cases they lie near the border. The cluster with more massive stars is YSC 1.

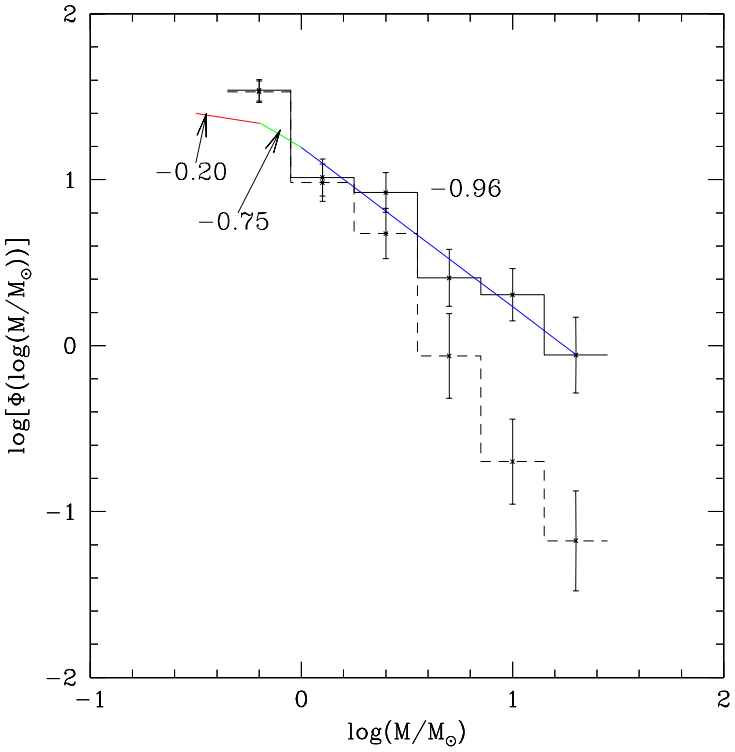

Figure 6.13 IMF histogram of the "average" cluster constructed with the averaged values bin by bin of 0.3 in log M of all the 40 clusters (continuous line) and of the 14 YSCs complete below 0.6 $M_{\odot}$ (broken line). The continous line shows the three-segment power law given in equation (6.7).

- A balanced population of massive, intermediate and low-mass stars is found in 10 clusters (24%): 4A, 4B, 4C, 6, 13, 27, 28, 32, 36, 38.
- The remaining clusters with massive stars (22%) are dominant in intermediate-mass stars and present very few or none low-mass stars.
- The clusters without massive stars show three cases: 11 (27%) have a balanced distribution of intermediate and low-mass stars (7, 8, 9, 11, 18A, 18B, 19, 20, 21, 22, 25, 26); 7 (17%) are dominant in low-mass stars (2, 5, 10, 16, 17, 24, 29); and only 3 (7%) are dominant in intermediate-mass stars (15, 23, 35).
- From the population of stars that is dominant, we conclude that 31% of the young clusters show more intermediate-mass stars while 17% show more

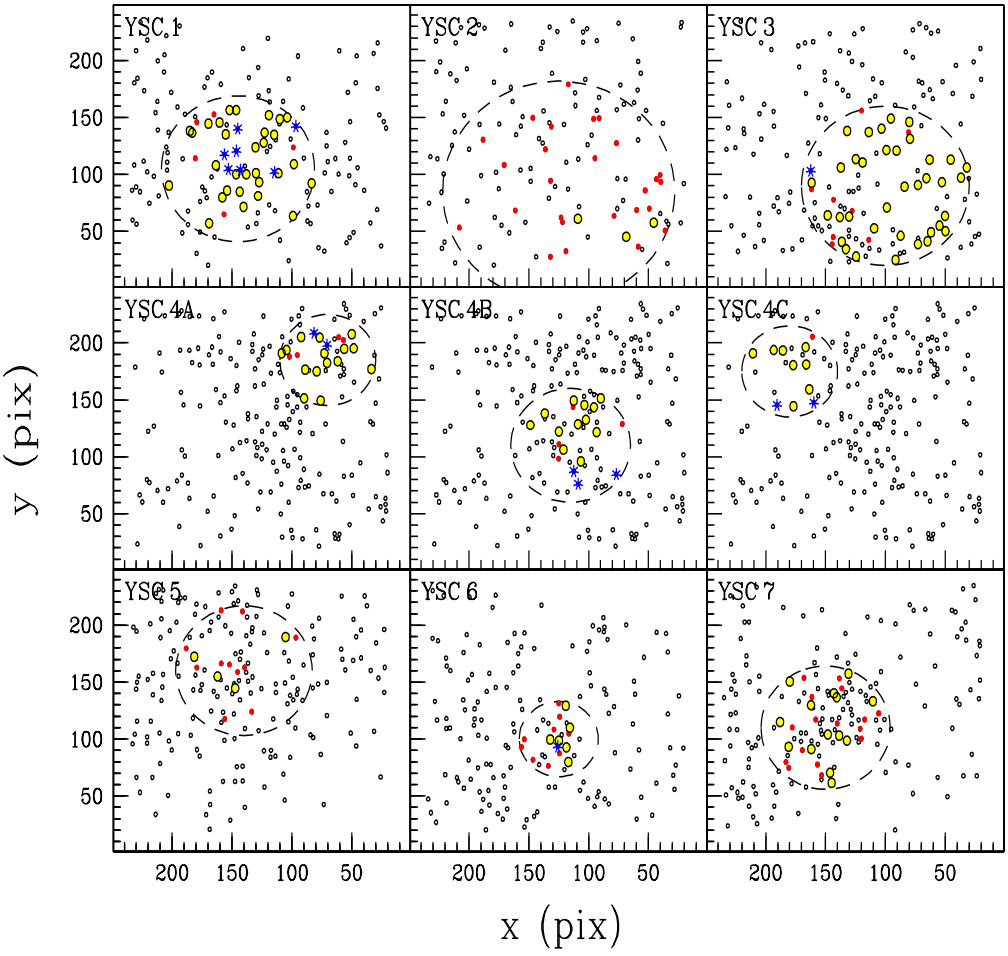

Figure 6.14 Sample of spatial distributions of mass. Dashed lines correspond to the cluster radius. Red dots correspond to low-mass ($M < 1M_{\odot}$), yellow circles to intermediate-mass ($1M_{\odot} < M < 10M_{\odot}$), and blue asteriscs correspond to massive stars ($M > 10M_{\odot}$).

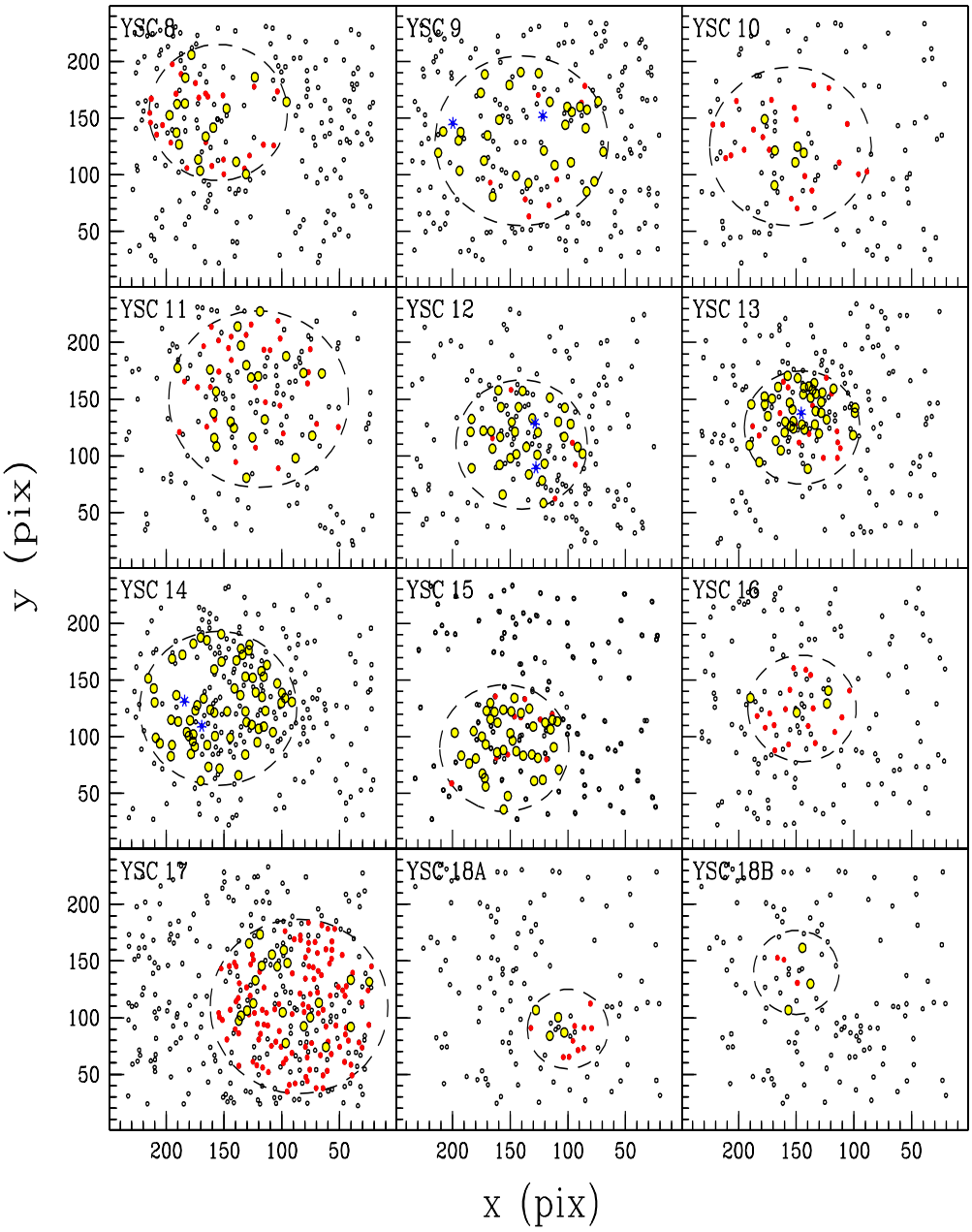

Figure 6.15 Same as Fig. 6.14.

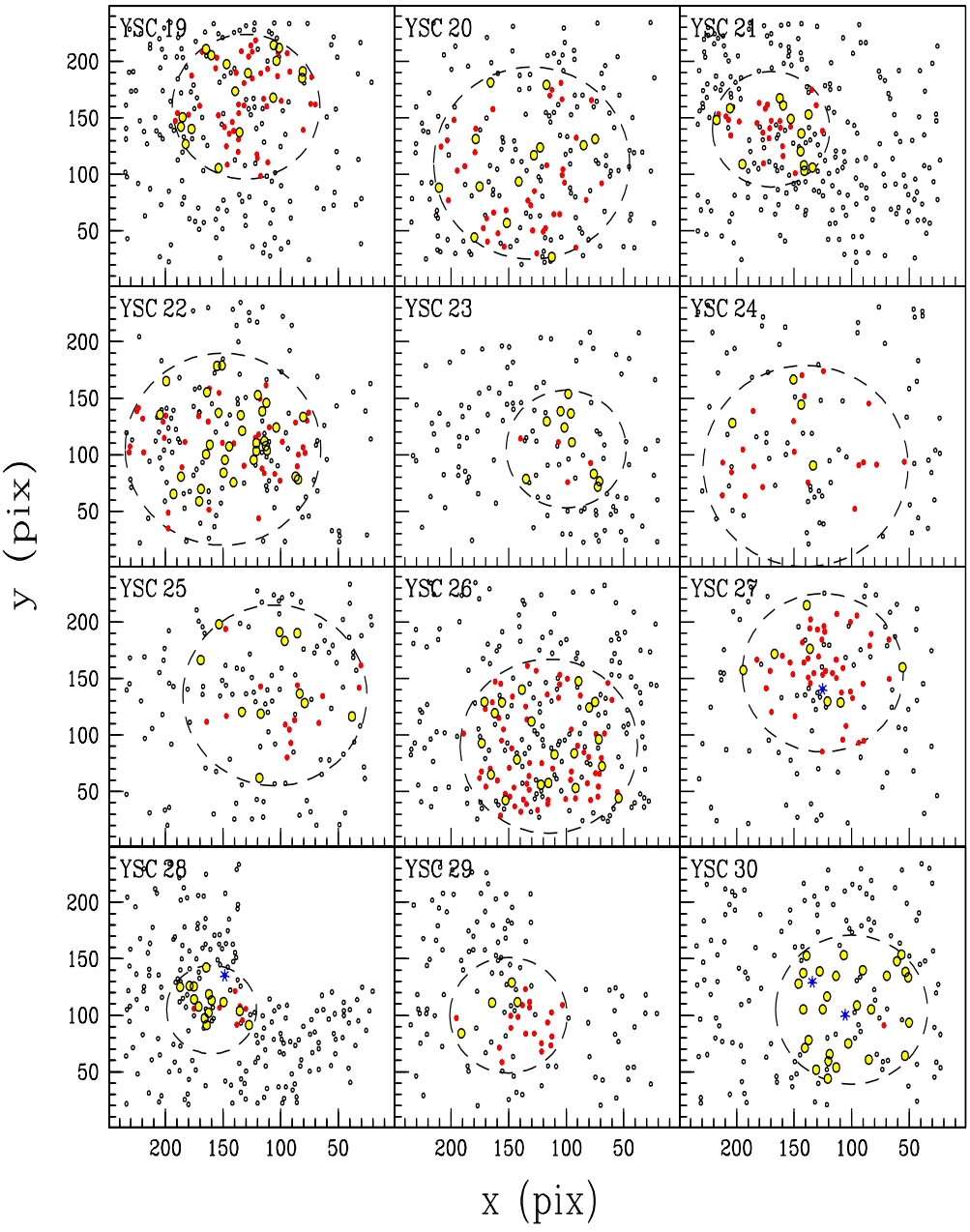

Figure 6.16 Same as Fig. 6.14.

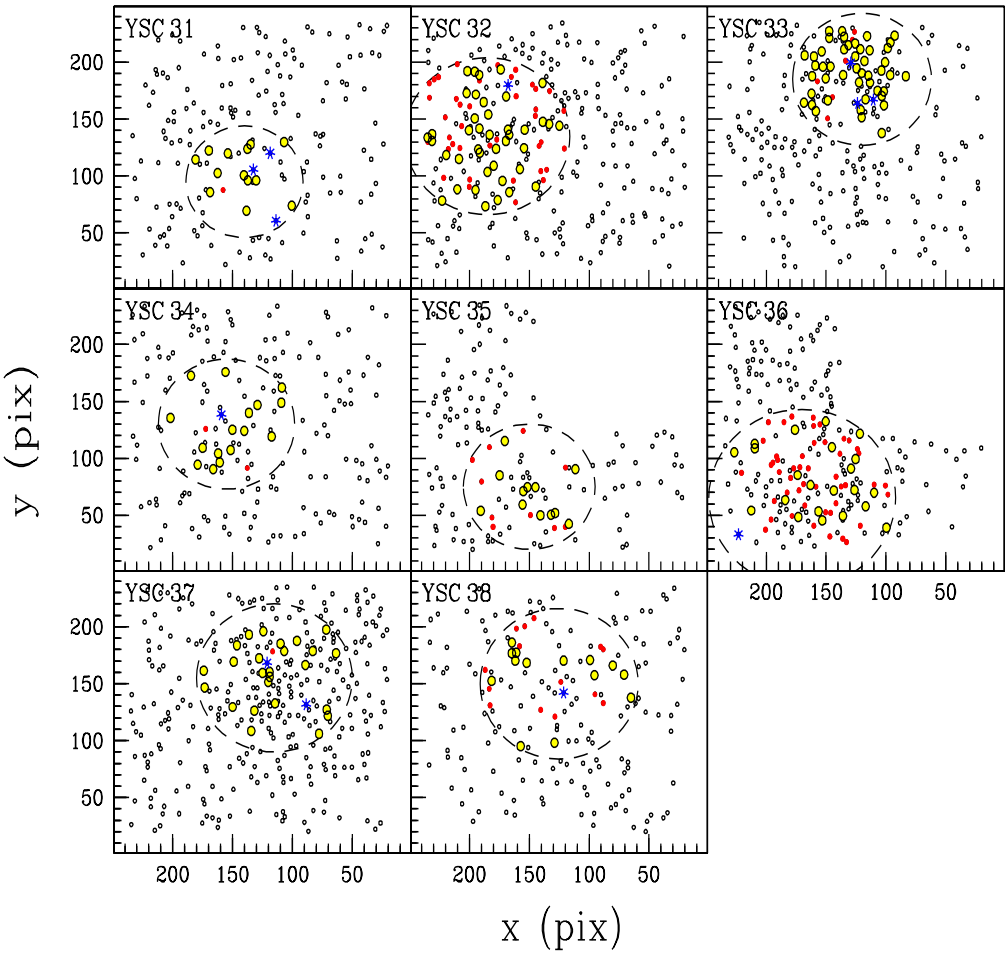

Figure 6.17 Same as Fig. 6.14.

low-mass stars.

- 53% of the embedded clusters show a more balanced and uniformly distributed intermediate and low-mass stellar population.

The role of star formation processes and the interplay between the initial conditions of the parent cloud and the newborn stars formed, in the determination of stellar masses is an extremely complex problem. Our observational results in deeply embedded clusters show that three different mass compositions are possible: regions with an even balance of low and intermediate-mass stars, regions where intermediate-mass stars are dominant and regions where low-mass stars are dominant.

From the young stellar cluster sample in the Perseus Arm we find that the first scenario is most probable, since half of the embedded clusters show similar numbers of low and intermediate-mass stars distributed more or less uniformly in the cluster area.

6.4 Mass Segregation

The important problem of mass segregation is discussed by Stahler et al. 2000. It is present when the average stellar mass in a YSC increases towards the cluster center, which is also the densest region.

To check for mass segregation in our sample of YSCs, let us define the quantities m_1, m_2 and m_3 for each cluster. m_1 is the average mass value inside the region with a radius $r_1 = r_C/3$; m_2 is the average mass value of stars inside the annulus beetwen r_1 and $r_2 = 2r_C/3$; and finally, m_3 is the average mass value of stars inside the annulus beetwen r_2 and r_C.

Our results are presented in Fig. 6.18 and we expect that if segregation occurs $m_1 > m_2 > m_3$. Clear mass segregation is observed in 18 young clusters (44% of the sample).

6.5 Comparison of Cluster Parameters

At this stage we have derived the following cluster parameters: radius (r_C), surface density (Σ), number of members in the mass complete sample (N_{CC}), age, average extinction ($< A_V >$), IMF index (Γ), completeness mass limit M_{lim} and total mass (M_T). We looked for possible correlations between these parameters and we found the following:

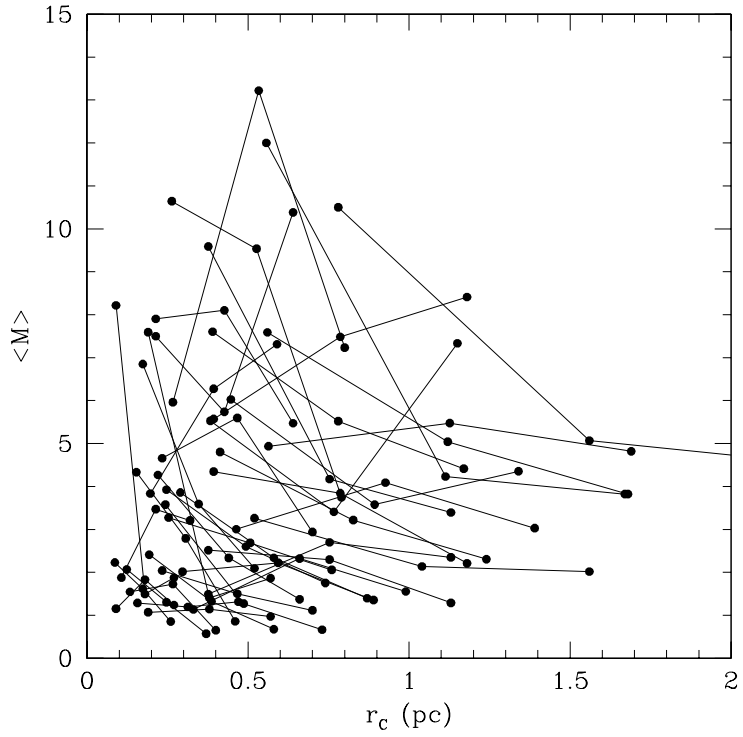

Figure 6.18 Average mass value in the regions inside a radius $r_1 = r_C/3$; inside the annulus beetwen r_1 and $r_2 = 2r_C/3$; and inside the annulus beetwen r_2 and the cluster radius r_C.

- There is a bimodal correlation of clusters in N_{CC} vs. M_{tot} (see Fig. 6.19a). Clusters with more than one massive star (open circles) separate from the rest of the clusters (filled circles). The slopes in the linear correlations found are 3.19±0.72 (r=0.77) and 0.88±0.11 (r=0.86). This strongly suggest two types of clusters, massive and low-mass. For the same number of formed stars the massive one has a total cluster mass about three times that in the low-mass case. We will use this distinction in the analysis of other correlations.

- The total mass M_T is probably correlated with the cluster radius r_C for the low-mass clusters, we obtained in this case a slope of 98.0±14.3 (r= 0.81), excluding YSC 17 which shows an odd behaviour. The massive clusters do not show this correlation (see Fig. 6.19b).

- The surface density Σ and M_T (see Fig. 6.19c) show a similar polinomial function as the one reported in §5.2 for Σ and r_C. Massive clusters are confined to low values of Σ (see Fig. 6.19d) below 50 stars/pc^2.

- The cluster radius r_C is probably correlated with N_{CC} (see Fig. 6.19e) for the low-mass clusters, we obtained in this case a slope of 60.5±10.9 (r= 0.74), excluding YSC 17 which shows an odd behaviour. The massive clusters do not show this correlation and their radii interval are usually larger than in low-mass clusters.

- There is no correlation between the mean extinction value $< A_V >$ and the number of stars in a cluster, N_{CC}, neither for massive nor for low-mass clusters. In both cases we have the same range in $< A_V >$ which possibly indicates that the sample is not biased (see Fig. 6.19f).

- The cluster age does not correlate with any other parameter.

- The IMF index which is the calculated value for each cluster shows:

  - The centroid for massive clusters at $\Gamma \sim$-0.5 and for low-mass clusters at $\Gamma \sim$-0.89.
  - A possible correlation with the cluster radius r_C (see Fig. 6.20a) for the massive clusters, we obtained in this case a slope of -0.66±0.16 (r= 0.79). The low-mass clusters show no indication of a correlation. The cluster radius is larger for massive clusters.

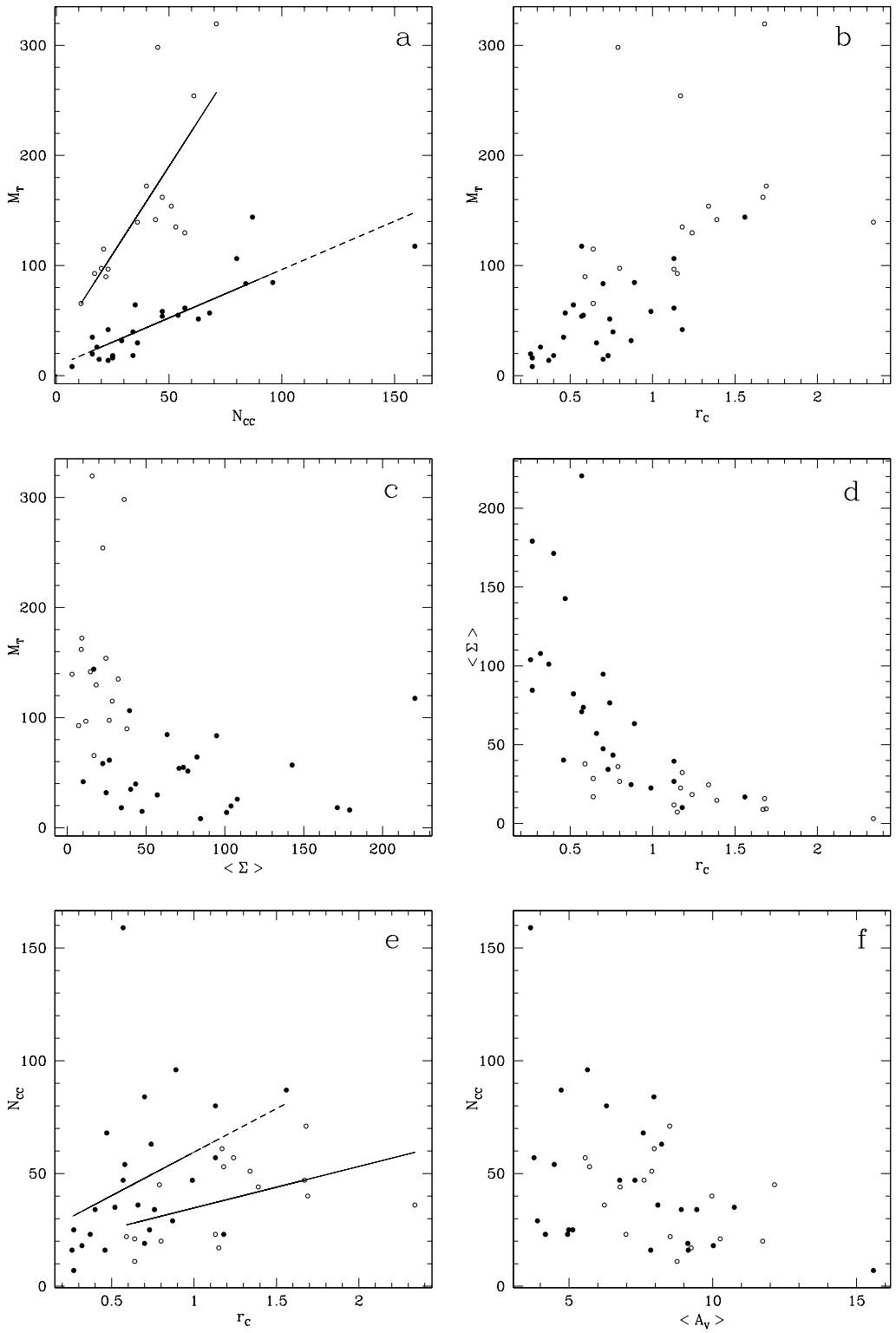

Figure 6.19 Comparison of cluster parameters: (a) N_{CC} vs. M_{tot}, (b) M_T vs. r_C, (c) Σ vs. M_T, (d) Σ vs. r_C, (e) r_C vs. N_{CC} and (f) $< A_V >$ vs. N_{CC}. Symbols correspond to massive clusters ($\circ$) and low-mass clusters ($\bullet$).

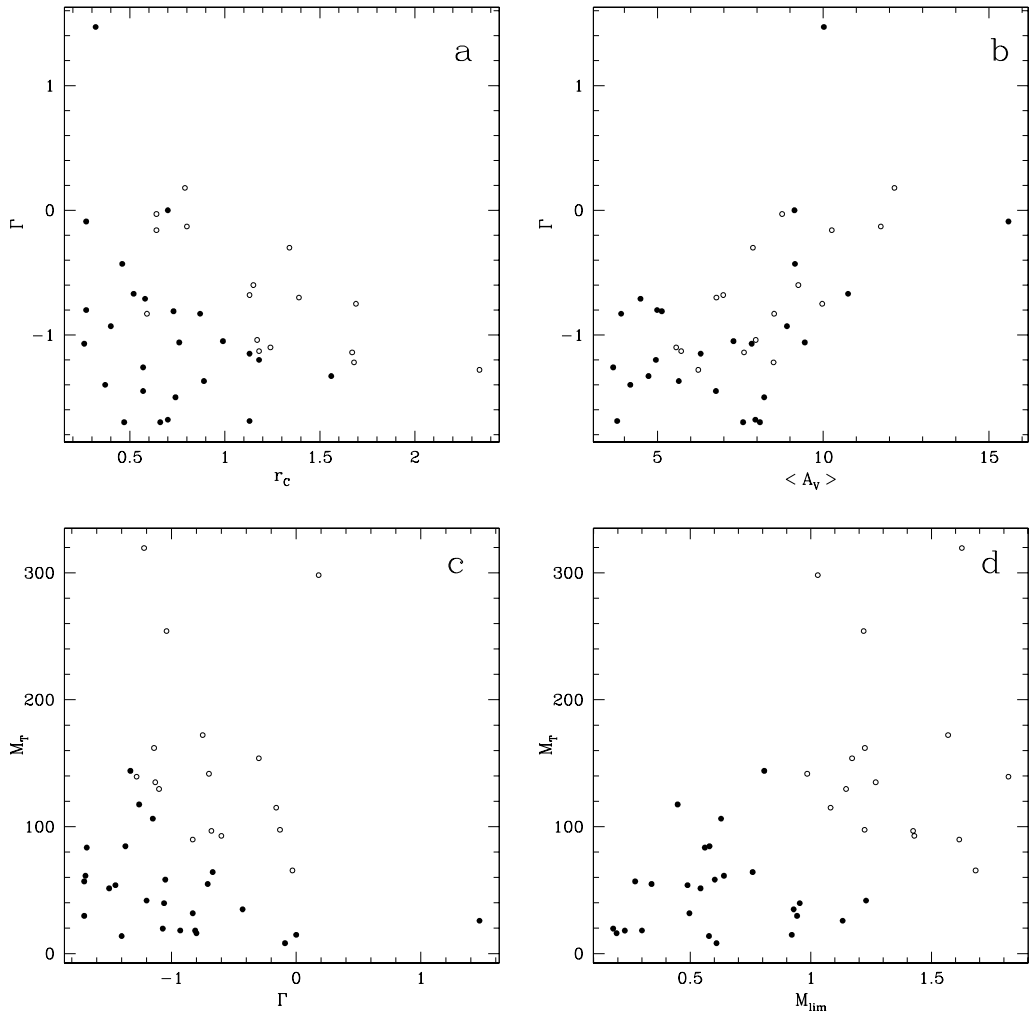

Figure 6.20 Comparison of IMF indices with (a) r_C, (b) $< A_V >$ and (c) M_T. Comparison of M_{lim} and M_T in frame (d). Symbols correspond to massive clusters ($\circ$) and low-mass clusters ($\bullet$).

  - A possible correlation with extinction $< A_V >$ (see Fig. 6.20b) for the massive clusters, yields a slope of 0.15±0.04 (r= 0.74). The low-mass clusters show no indication of a correlation.
  - No correlation with Σ, but the separation of the two types of clusters is evident.
  - No correlation with total mass M_T, but a separation of the two types is also evident (see Fig. 6.20c). The typical massive cluster has Γ ∼-0.5 and 125 stars while the low-mass cluster has Γ ∼-0.89 and 40 stars.

- The total mass M_T and the mass limit M_{lim} presented in Fig. 6.20d shows a clear separation of massive and less massive clusters. The completeness mass limit in massive clusters does not go below 1 $M_\odot$, which possibly explains why less massive clusters produce a steeper average IMF index (see also Fig. 6.13).

Chapter 7

Summary and Conclusions

The main goal in this thesis was to study the IMF in a sample of 38 embedded star formation regions along the Perseus Arm. Selection criteria were established to search in the near-infrared for YSCs associated to IRAS sources ($2 \times 10^3 < L_{FIR} < 9 \times 10^3$ L$_\odot$) and nearby Sharpless H II regions. A survey of the 38 star forming regions was done in the J, H and K photometric bands, which provides information on 6298 stars. The intrinsic error achieved in the photometry was less than 7%. Images, IDL programs and photometry data tables are presented in Appendix A, B and C, respectively.

In the regions observed 41 young stellar clusters were found. We propose that an embedded YSC must fulfill the following properties: 1) Candidate sources are near a small-diameter (d $\lesssim$ 6 pc) Sharpless H II region. 2) Sources are associated to an IRAS point source with a spectral energy distribution such that fluxes 1 Jy $\lesssim F_{12\mu m} < F_{25\mu m} < F_{60\mu m} < F_{100\mu m}$, the flux in the 12, 25 and 60 μm bands satisfy the ratios $log(F_{60\mu m}/F_{25\mu m}) \gtrsim 0.3$ and $log(F_{25\mu m}/F_{12\mu m}) \gtrsim 0.4$, and the flux $F_{100\mu m} \gtrsim 1000\ Jy$. 3) They should be deeply embedded and contain star formation tracers such as YSOs, molecular cores, outflows, masers, infrared excess stars and nebulosity at K. 4) Should contain at least 20 stars.

With distances obtained from the literature (mean value 3.6$\pm$1.8 kpc) and the observed spatial distribution of stars, we obtain cluster parameters such as surface density, cluster radius and average concentration parameter. Our results are: 3$< \Sigma <$220 stars/pc^2, with a mean value of 55$\pm$52 stars/pc^2. 0.26$< r_c <$2.34 pc, with most clusters between 0.5 and 2 pc, and a mean value of 0.89$\pm$0.47 pc. c_{YSC}=0.51$\pm$0.24, which means that their stellar concentration is $\sim$3 times smaller than globular clusters.

We develop a method to estimate ages based on a comparison between observed and theoretical luminosity function (LF) histograms. The model of Strom

et al. 1993 is used as theoretical JLF. It is based on the assumption of coeval star formation, uses the pre-main sequence isochrones by D'Antona & Mazzitelli 1994 and assumes the IMF of Miller & Scalo 1979. They trace six different evolutionary histograms at ages of 0.3, 0.7, 1, 3, 7 and 10 Myr. Ages are obtained from the observed JLF using $\overrightarrow{E} = \widehat{M}^{-1}\ \overrightarrow{JLF}_{obs}$. The elements in $\overrightarrow{E}$ give the distribution of stars in all ages and the age estimate can be obtained with the maximum value, which is the most probable age of the bulk stellar population. The estimated ages for clusters yield a mean value of 2.42 $\pm$ 1.20 Myr in an interval from 1.1 to 5.5 Myr. While the distributed population around a cluster are older, with a mean age of 2.84 $\pm$ 2.81 Myr in an interval from 1.2 to 18.1 Myr. It is interesting to point out that the distributed population is also young. Both values are consistent with the expected lifetime of a GMC (10^{6-7} yr).

The construction of isochrones plotted in the observational J/J-H and K/H-K diagrams are an essential tool for the determination of stellar masses. The isochrones are obtained from pre-main sequence evolutionary tracks by D'Antona & Mazzitelli 1994, assuming Alexander opacities and the Canuto & Mazzitelli convection model. For 2.5 $< M <$ 20 $M_\odot$ we used the tracks presented by Hillenbrand et al. 1995. For each stellar mass M, the corresponding luminosity L and effective temperature T_e are obtained to derive the absolute magnitude $J = 4.74 - 2.5\,log\ (L/L_\odot) - BC(T_e) - (V - J)$, where the first three terms correspond to M_V and the colors V-J and J-H for dwarfs are obtained from Bessell & Brett 1988, using the T_e values of Tokunaga 2000. In a similar way isochrones are obtained for absolute magnitude K. Since isochrones at ages 0.1, 0.3, 1, 3, 10, 30 and 100 Myr are available from D'Antona & Mazzitelli 1994 models, the isochrone for each YSC are selected according to the closer value of the cluster age.

The computation of the extinction to individual stars depends on its location in the J-H/H-K diagram. For stars along the reddened MS the J/J-H diagram was used taking each star along the A_V vector direction to the corresponding isochrone. This process is made for both, cluster and field stars. While for reddened CTT and Ae/Be stars they are dereddened directly based on their distance to the CTTS line (Meyer 1996). All clusters show average values greater than $\sim$4 magnitudes and about 20% of the YSC sample have $< A_V > > 10$ mag.

We develop a method to derive individual stellar masses by a three step procedure: 1) we identify the reddened MS and CTTS+Ae/Be stars located in the J-H/H-K diagram. 2) The mass of MS reddened stars can be obtained from the J/J-H diagram by de-reddening them to the previously estimated isochrone. For each star, the mass value is obtained from the scale along the corresponding isochrone by moving paralel to the A_V vector from its original position to

the isochrone. 3) In the case of reddened CTT and Ae/Be stars, we use the $\log M = -0.25\ M_H + 0.44$ and $\log M = -0.24\ M_K + 0.24$, where M_H and M_K are the uncorrected for extinction H- and K-band magnitudes (Carpenter et al. 1993). These relations result from masses of stars in the Taurus molecular cloud and we implicitly assume that the Perseus cluster CTT and Ae/Be stars are similar.

In order to do a realistic comparison between cluster mass distributions, it is important to consider only unbiased data. Photometric limitations and extinction in each cloud lead to a stellar mass, M_{lim}, which defines the limit at which a sample of stars in a cluster is considered complete. The M_{lim} values range from 0.2 to 1.8 $M_\odot$. From their distribution we find that there are 14 YSCs that are complete down to a $M_{lim} \sim 0.6\ M_\odot$, 29 (15+14) YSCs are complete down to 1.2 $M_\odot$ and 40 (11+15+14) are complete down to $M_{lim} \sim 2\ M_\odot$.

Stellar masses are obtained to construct the mass distributions that yield the cluster IMF. The construction of IMF histograms and IMF index values have difficulties due to the lack of stars in some mass bins, the small number in others, and their consecuent large error bars. Thus, a compromise with the mass bin size is required. Using a log-log representation we did a linear least-square fit using values of mass above the mass completeness limit M_{lim}, the IMF indexes for a 0.25 bin in log M were calculated from 0.6 $M_\odot$ for 14 YSCs (Γ_1), from 1.2 $M_\odot$ for 15 YSCs (Γ_2) and from 2 $M_\odot$ for the remaining 11 clusters (Γ_3).

As suggested by Meyer et al. 2000, a rather useful diagnostic is the ratio of intermediate-to-low-mass stars ($R = N(1-10\ M_\odot)/N(0.1-1\ M_\odot)$) since it minimizes the number of bins to only two as well as its uncertainties. Following this idea, we define the ratio $C^{0.6} = N(1.2-20\ M_\odot)/N(0.6-1.2\ M_\odot)$, based in the minimum and maximum mass values obtained in our YSC sample. We can calculate $C^{0.6}$ only for the 14 YSCs complete in these mass intervals and compare the mean value $C^{0.6}$ =1.04±0.39 to appropiate values for a Salpeter 1955, Scalo 1998 and Kroupa 1993 IMFs, i.e. $C^{0.6}_{Sal}$= 0.63, $C^{0.6}_{Sc}$= 0.64±0.04 and $C^{0.6}_{Kr}$= 0.50, respectively. Only two embedded clusters are in agreement to $C^{0.6}_{Sal}$ and the remaining clusters show values above the $C^{0.6}_{Sal}$ line. Possibly two subgroups of clusters with a similar behaviour are evident according to $C^{0.6}$ >1.2. So, this simple test rules out a Salpeter, Scalo or Kroupa IMF for the 14 YSCs complete down to 0.6 $M_\odot$. The difference between these expected values and the mean $C^{0.6}$ for the 14 YSCs might be due to a break in the slope in the low-mass regime. This possibility implies a two segment power-law:

$$\begin{aligned} \Gamma &= -0.75 \quad \text{for } M < 1M_\odot \\ &\quad -0.96 \quad \text{for } M > 1M_\odot \end{aligned} \tag{7.1}$$

In a similar form, we define the ratio $C^{0.3}$ for only 6 YSCs complete down to 0.3 $M_\odot$. In this case, the mean value $C^{0.3}$ =0.34 is consistent to the expected Scalo value $C^{0.3}_{Sc}$ =0.29±0.05, while Salpeter and Kroupa values are also close. In general, the $C^{0.3}$ values for the 6 YSCs are in close agreement with the mass ratios R for nearby clusters given by Meyer et al. 2000, indicating that reaching the very low-mass end is quite important. These considerations suggest that in the low-mass regime, we can assume the Scalo value:

$$\Gamma \;=\; -0.20 \qquad\qquad \text{for } 0.3 < M < 0.6 M_\odot \tag{7.2}$$

On the other hand, the possible break in the high-mass regime for YSCs still remains as an open question until theoretical isochrones above ∼20 $M_\odot$ are available and AO observations of the cores of YSCs are carried out.

Mass segregation is present when the average stellar mass in a YSC increases towards the cluster center, which is also the densest region (Stahler et al. 2000). Our check for mass segregation in our sample of YSCs is based on the calculated values m_1, the average mass value inside the region with a radius $r_1 = r_C/3$; m_2, the average mass value of stars inside the ring section between r_1 and $r_2 = 2r_C/3$; and, m_3, the average mass value of stars inside the annulus beetwen r_2 and r_C. If mass segregation occurs then $m_1 > m_2 > m_3$. Clear mass segregation is found in 44% of the cluster sample.

The spatial distribution of stellar masses inside the cluster area show that 46% of the sample contain massive stars and that three different mass compositions are possible: regions with an even balance of low and intermediate mass stars, regions where intermediate mass stars are dominant and regions where low mass stars are dominant.

We looked for possible correlations between the cluster parameters: radius (r_C), surface density (Σ), number of members in the mass complete sample (N_{CC}), age, average extinction ($< A_V >$), IMF index (Γ), completeness mass limit M_{lim} and total mass (M_T). We found the following: a) The star formation processes involved are able to create two types of clusters with different cluster mass: massive and low-mass. For the same number of formed stars the massive one has a total cluster mass about three times that in the low-mass case. b) The low-mass clusters show possible correlations in r_C with total mass M_T and N_{CC}. c) The resulting surface density Σ in massive clusters has lower values than the low-mass cases. d) The total mass M_T and the mass limit M_{lim} shows a clear separation of massive and less massive clusters. The completeness mass limit in massive clusters does not go below 1 $M_\odot$, which possibly explains why less massive clusters produce a steeper average IMF index.

The IMF index for each cluster shows:

- The centroid for massive clusters at Γ $\sim$-0.5 and for low-mass clusters at Γ $\sim$-0.89.
- A possible correlation with the cluster radius r_C for the massive clusters, with a slope of -0.66$\pm$0.16 (r= 0.79). The low-mass clusters show no indication of correlation. The cluster radius is larger for massive clusters.
- A possible correlation with extinction $< A_V >$ for the massive clusters yields a slope of 0.15$\pm$0.04 (r= 0.74). The low-mass clusters show no indication of correlation.
- No correlation with Σ, but the separation of the two types of clusters is evident.
- No correlation with total mass M_T, but a separation of the two types is also evident . The typical massive cluster has Γ $\sim$-0.5 and 125 stars, while the low-mass cluster has Γ $\sim$-0.89 and 40 stars.

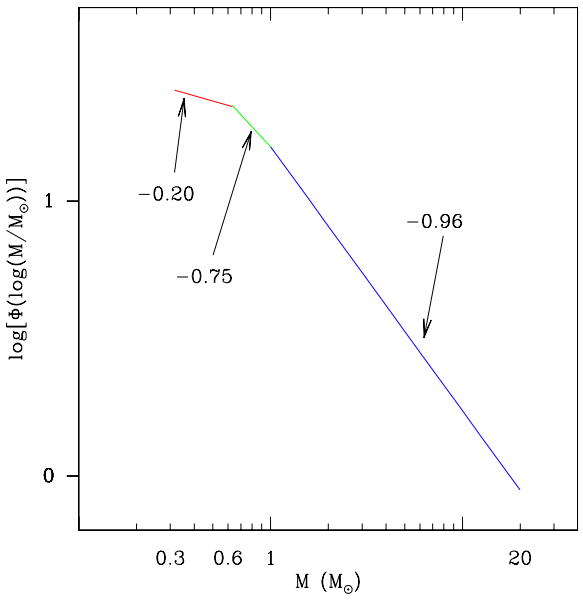

Figure 7.1 The IMF of young stellar clusters in the Perseus Arm.

In summary, our study of the Initial Mass Function (IMF) in a sample of 40 young stellar clusters (YSCs) in the Perseus Arm reveals the following main results:

- ⋆ In general, the mass distributions are not Salpeter type.
- ⋆ Evidence is found to support a change of slope in the low-mass end, as has been previously found by other authors.
- ⋆ Young stellar clusters have an IMF composed of three segments:

$$\begin{aligned} \Gamma \;=\; & -0.20 && \text{for } 0.3 < M < 0.6 M_{\odot} \\ & -0.75 \pm 0.10 && \text{for } 0.6 < M < 1 M_{\odot} \\ & -0.96 \pm 0.14 && \text{for } M > 1 M_{\odot} \end{aligned} \tag{7.3}$$

  where the first value, from Scalo 1998, is suggested from the study of 6 YSCs, the second arises from 14 YSCs and the final one from the most complete sample of IMF indices of 40 YSCs.

- ⋆ The spatial mass distributions of YSCs show two types of clusters, massive and less massive. The less massive clusters present an IMF that is steeper than the IMF of the massive ones.

With our work we have shown that young stellar clusters offer an excellent and advantageous laboratory to study the IMF. Future work in this line of investigation is greatly encouraged.

Bibliography

Beichman , C. A., Myers, P. C., Emerson, J. P., Harris, S. Mathieu, R., Benson, P. J., Jennings, R. E., 1986, ApJ, 307, 337.

Bessell, M. S., Brett, J. M., 1988, PASP, 100, 1134.

Bessell, M.S., Castelli, F., Plez, B. 1998, A&A, 333, 231.

Braz, M. A., Gregorio Hetem, J. C., Scalise, E. Jr., Monteiro Do Vale, J. L., Gaylard, M., 1989, A&AS, 77, 465.

Bruzual, G., 1994, Stellar population synthesis models at low and high redshift. In: Proceedings of the XI Canary Islands Winter School of Astrophysics on Galaxies at High Redshift, eds I. Perez-Fournon, M. Balcells, and F. Sanchez.

Buie, M., 1999, IDL Library. In: http://www.lowell.edu/users/buie/idl.

Carpenter, J. M., 2000, AJ, 120, 3139-3161

Carpenter, J. M., Meyer, M. R., Dougados, C., Strom, S. E., & Hillenbrand, L. A. 1997, AJ, 114, 198

Carpenter, J.M., Snell, R.L., Schloerb, F.P., Skrutskie, M.F., 1993, ApJ, 407, 657.

Carrasco, L., Recillas-Cruz, E., García-Barreto, A., Cruz-González, I., Serrano, A., 1991, PASP, 103, 987.

Casoli, F., Combes, F., Dupraz, C., Gerin, M., Boulanger, F., 1986, A&A, 169, 281.

Chan, G., Fich, M., 1995, AJ, 109, 2611.

Chan, S. J., Henning, T., 1996. A Catalogue of Massive Young Stellar Objects: A Description. In: The Role of Dust in the Formation of Stars, Proceedings of the ESO Workshop Held at Garching, Germany, 11 - 14 September 1995. H. U. Käufl & R. Siebenmorgen, eds. Springer-Verlag Berlin Heidelberg New York. Also ESO Astrophysics Symposia (European Southern Observatory), p.105.

Chan, S. J., Henning, T., Schreyer, K., 1996, A&AS, 115, 285.

Clark, F. O., 1991, ApJS, 75, 611.

Clarke, C. J., 1998. Star Formation Theories and the IMF. In: The Stellar Initial Mass Function (38th Herstmonceux Conference), eds. G. Gilmore and D. Howell, ASP Conference Series, Vol. 142, p. 189.

Clarke, C. J., Bonnell, I. A., Hillenbrand, L. A., 2000. The Formation of Stellar Clusters. In: Protostars and Planets IV, Tucson: University of Arizona Press; eds. Mannings, V., Boss, A.P., Russell, S. S., p. 151.

Cruz, F. 1998, Ph. D. Thesis, Instituto de Astronomía-Facultad de Ciencias, UNAM.

Cruz-González, I. et al., 1994, Proc. SPIE, 2198, 774.

Cruz-González, I., Salas, L., Ruiz, E., Valdez, J., Lazo, F., Cobos, F., 1997, Manuales de Usuario del IAUNAM MU-97.

Cruz-González, I., Salas, L., Ruiz, E. 1996, Manuales de Usuario del IAUNAM MU-96-02.

Deharveng, L., Zavagno, A., Cruz-González, I., Salas, L., Caplan, J., Carrasco, L., 1997, A&A, 317, 459.

D'Antona, F., Mazzitelli, I., 1994, ApJS, 90, 467.

Elmegreen, B.G., 1999. The IMF and its Evolution. In: "The evolution of Galaxies on Cosmological Timescales," eds. J.E. Beckman and T.J. Mahoney, ASP Conference Series, San Francisco, in press.

Elmegreen, B.G., Efremov, Y.; Pudritz, R. E.; Zinnecker, H., 2000, Observations and Theory of Star Cluster Formation. In: In: Protostars and Planets IV, Tucson: University of Arizona Press; eds. Mannings, V., Boss, A.P., Russell, S. S., p. 179.

Emerson, J.P., 1987. IRAS and star formation in dark clouds. In: Star forming regions; Proceedings of the Symposium, Tokyo, Japan, Nov. 11-15, 1985. Dordrecht, D. Reidel Publishing Co., p. 19.

Evans, N.J., II, 1999, Annual Review of Astronomy and Astrophysics, 37, 311.

Fich, M., Blitz, L., 1984, ApJ, 279, 125.

Flower, P. J., 1996, ApJ, 469, 355.

Garay, G., Lizano, S., 1999, PASP, 111, 1049.

Gilmore, G., Howell, D., 1998. Editors of The Stellar Initial Mass Function (38th Herstmonceux Conference), ASP Conference Series, Vol. 142.

Grasdalen, G. L., Strom, K. M., Strom, S. E. 1973, ApJ, 184, L53.

Henning, T., Cesaroni, R., Walmsley, M., Pfau, W., 1992, A&AS, 93, 525.

Herbig, G.H. 1998, ApJ, 497, 736.

Hillenbrand, L. A., 1995, Ph.D. Thesis, Univ. of Massachusetts.

Hillenbrand, L. A., 1997, AJ, 113, 1733.

Hillenbrand, L. A., Meyer, M. R., Strom, S. E., Skrutskie, M. F., 1995, AJ, 109, 280.

Hoddapp, K. W., 1994, ApJS, 94, 615.

Hughes, V. A., MacLeod, G. C. 1989, AJ, 97, 786

King, I., 1962, AJ, 67, 471.

Koornneef, J., 1983, A&A, 128, 84.

Kroupa, P.; Tout, C. A.;Gilmore, G., 1990, MNRAS, 244,76.

Kroupa, P., Tout, C. A., Gilmore, G., 1993, MNRAS, 262, 545.

Kurtz, S.; Churchwell, E.; Wood, D. O. S., 1994, ApJS, 91, 659.

Lada, E., Lada, C., Muench, A., 1998, Infrared Luminosity Functions of Embedded Clusters. In: The Stellar Initial Mass Function (38th Herstmonceux Conference) edited by Gary Gilmore and Debbie Howell. ASP Conference Series, Vol. 142, p. 107.

Lahulla, J.F., 1985, A&AS, 61, 537.

Landsman, W. B., 1993. Astronomical Data Analysis Software and Systems II, A.S.P. Conference Series, Vol. 52, 1993, R. J. Hanisch, R. J. V. Brissenden, and Jeannette Barnes, eds., p. 246. "The IDL Astronomy User's Library".

Landsman, W. B., 1996, IDL Astronomy User's Library. In: http: //idlastro.gsfc.nasa.gov.

Larson, R. B., 1985, MNRAS, 214, 379.

Larson, R. B., 1998, MNRAS, 301, 569.

Larson, R. B., 1999. The Stellar Initial Mass Function. In: Star Formation 1999, Proceedings of Star Formation 1999, held in Nagoya, Japan, June 21 - 25, 1999, Ed. T. Nakamoto, Nobeyama Radio Observatory, p. 336-340.

Luhman, K. L., Rieke, G. H., Lada, C. J., Lada, E. A., 1998, ApJ, 507, 347.

Meyer, M.R., 1996, Ph.D. Thesis, University of Massachusetts.

Meyer, M. R., Adams, F. C., Hillenbrand, L. A., Carpenter, J. M., Larson, R. B., 2000. The Stellar Initial Mass function: Constraints from Young Clusters and Theoretical Perspectives. In: Protostars and Planets IV, Tucson: University of Arizona Press; eds. Mannings, V., Boss, A.P., Russell, S. S., p. 121.

Migenes, V.; Horiuchi, S.; Slysh, V. I.; Val'tts, I. E.; Golubev, V. V.; Edwards, P. G.; Fomalont, E. B.; Okayasu, R.; Diamond, P. J.; Umemoto, T.; Shibata, K. M.; Inoue, M., 1999, ApJS, 123, 487.

Miller, G.E., Scalo, J.M., 1979, ApJS, 41, 513.

Miralles, M.P., Salas, L., Cruz-González, I., Kurtz, S., 1997, ApJ, 488, 749.

Palagi, F., Cesaroni, R., Comoretto, G., Felli, M., Natale, V., 1993, A&A, 101, 153.

Palla, F.; Brand, J.; Comoretto, G.; Felli, M.; Cesaroni, R., 1991, A&A, 246, 249..

Porras, A., Cruz-González, I. & Salas, L., 2000, A&A, 361, 660.

Salas, L., Cruz-González, I. & Porras, A., 1998, ApJ, 500, 853.

Salas, L., Cruz-González, I. & Rosado, M., 2000, RevMexAA, 36, 113.

Salpeter, E. E., 1955, ApJ, 121, 161.

Scalo, J. M. 1986, Fundamentals of Cosmic Physics, vol. 11, May 1986, p. 1-278.

Scalo, J. M. 1998. The IMF Revisited: A Case for Variation. In: The Stellar Initial Mass Function (38th Herstmonceux Conference), eds. G. Gilmore and D. Howell, ASP Conference Series, Vol. 142, p. 201.

Sharpless, S., 1959, ApJS, 4, 257.

Smith, M. D., 1995, A&A, 296, 789.

Snell, R. L.; Huang, Y.-L.; Dickman, R. L.; Claussen, M. J., 1988, ApJ, 325, 853.

Snell, R.L., Dickman, R.L., Huang, Y.-L., 1990, ApJ, 352, 139.

Stahler, S. W.; Palla, F.; Ho, P. T. P., 2000. The Formation of Massive Stars. In: Protostars and Planets IV, Tucson: University of Arizona Press; eds. Mannings, V., Boss, A.P., Russell, S. S., p. 327.

Stetson, P. B., 1987, PASP, 99, 191.

Strom, K. M., Strom, S. E., Carrasco, L., Vrba, F. J., 1975, ApJ, 196, 489.

Strom, K.M., Strom, S.E., Merrill, M., 1993, ApJ, 412, 233.

Testi, L., Palla, F. & Natta A., 1998, A&AS, 133, 81.

Testi, L., Palla, F. & Natta A., 1999, A&A, 342, 515.

The Milky Way Map included in Supplement to National Geographic Society, Washington, D.C., October, 1999.

Tokunaga, A.T., 2000, Infrared Astronomy. In: Allen's Astrophysical Quantities, Cox, A.N. (ed.), (New York: Springer-Verlag), p. 143.

Vrba, F. J., Strom, K. M., Strom, S. E., Grasdalen, G. L., 1975, ApJ, 197, 77.

Williams, J. P.; Blitz, L.; McKee, C. F., 2000. The Structure and Evolution of Molecular Clouds: from Clumps to Cores to the IMF. In: Protostars and Planets IV, Tucson: University of Arizona Press; eds. Mannings, V., Boss, A.P., Russell, S. S., p. 97.

Wouterloot, J. G. A., Brand, J., 1989, A&AS, 80, 149.

Wouterloot, J. G. A., Walmsley, C. M., 1986, A&A, 168, 237.

Wouterloot, J.G.A., Henkel, C., Brand, J., 1988, A&A, 191, 323.

Wood, D. O. S., Churchwell, E. 1989, ApJ, 340, 265.

Wu et al. 1996 (JO: XXX).

Zinnecker, H., Mc Caughrean, M.J., Wilking, B.A., 1993, The Initial Stellar Population. In: Protostars and Planets III, Levy E.H., Lunine J.I. (eds.) (Tucson: University of Arizona Press), p. 429.

Zinnecker, H., Mc Caughrean, M.J., Rayner, J., 1997, HH212: A prototype molecular hydrogen jet from a deeply embedded protostar. In: Low Mass Star Formation from Infall to Outflow, Poster Proceedings of IAU Symp. No. 182, On Herbig-Haro Objects and the Birth Of Low Mass Stars, 20-24 Jan. 1997, Chamonix, France, F. Malbet & A. Castets, eds., p. 198.

Appendix A

Direct Images

This Appendix compares the optical maps and NIR color composite images in a $3.6' \times 3.6'$ field of view.

Optical images were obtained from the Advanced Sky-View survey (http://skyview.gsfc.nasa.gov/cgi-bin/skvadvanced.pl) centered in the IRAS point source coordinates.

NIR color composite images (red = K', green = H and blue = J) were obtained from our observations of the 38 regions. We cut edges that showed offsets from CAMILA positioning.

Additionally, we show 8 NIR color composite images (red=H,green=H_2,blue=ck) for regions with posible HH features.

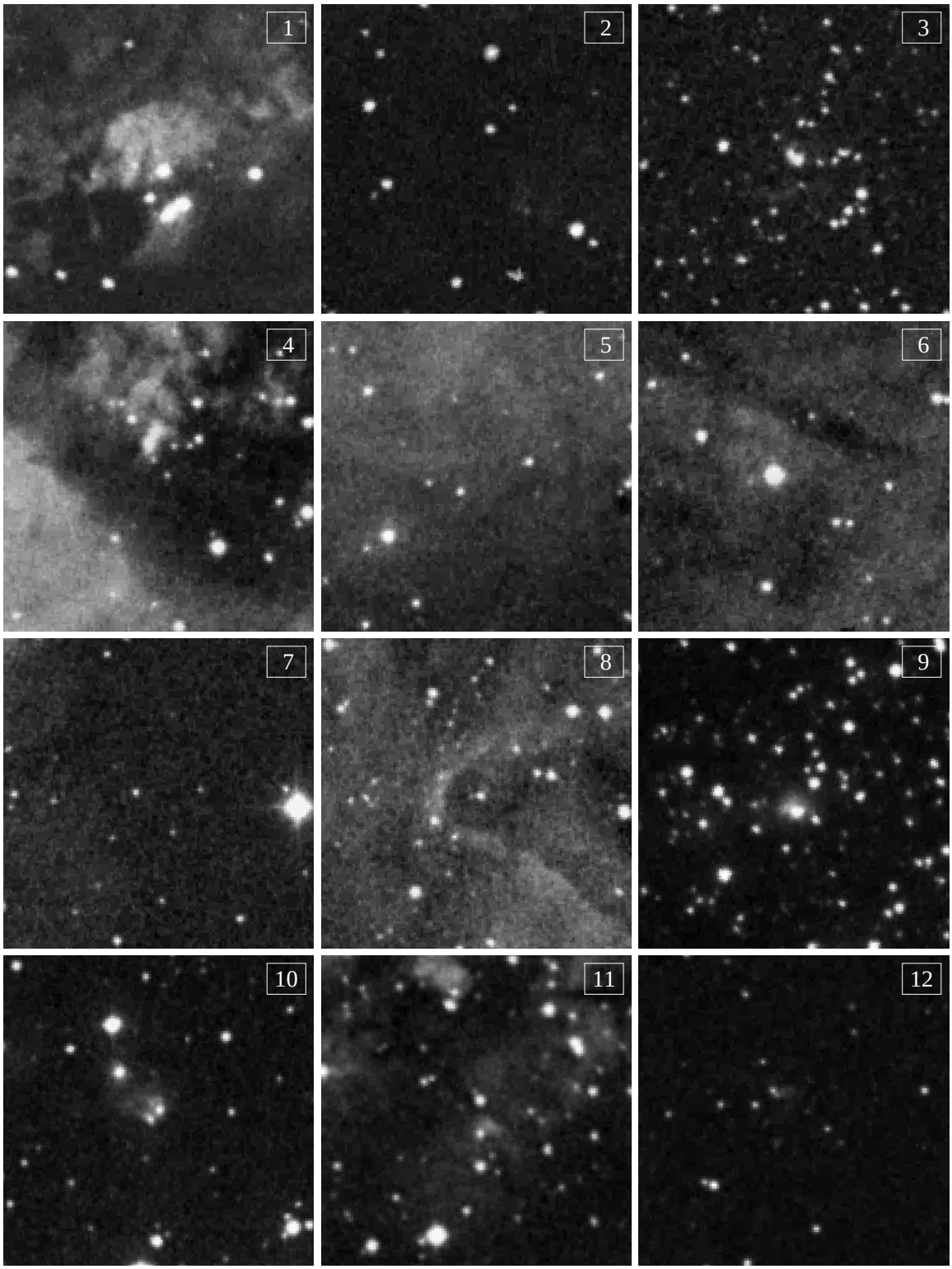

Figure A.1 Optical counterpart and color composite images of the 38 sources in the sample. Identification numbers in upper right corners correspond to those in Table 2.2

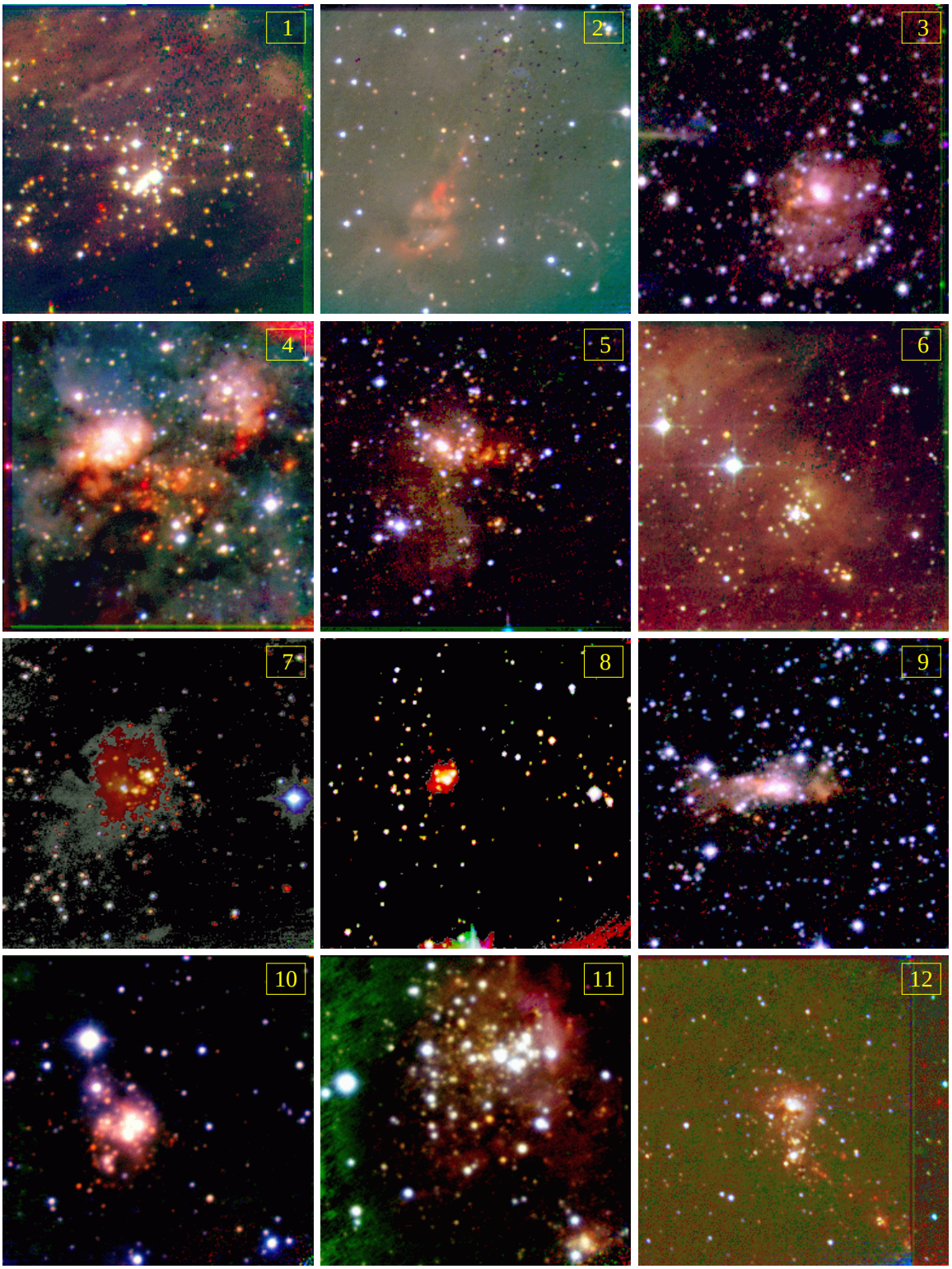
1
2
3
4
5
6
7
8
9
10
11
12

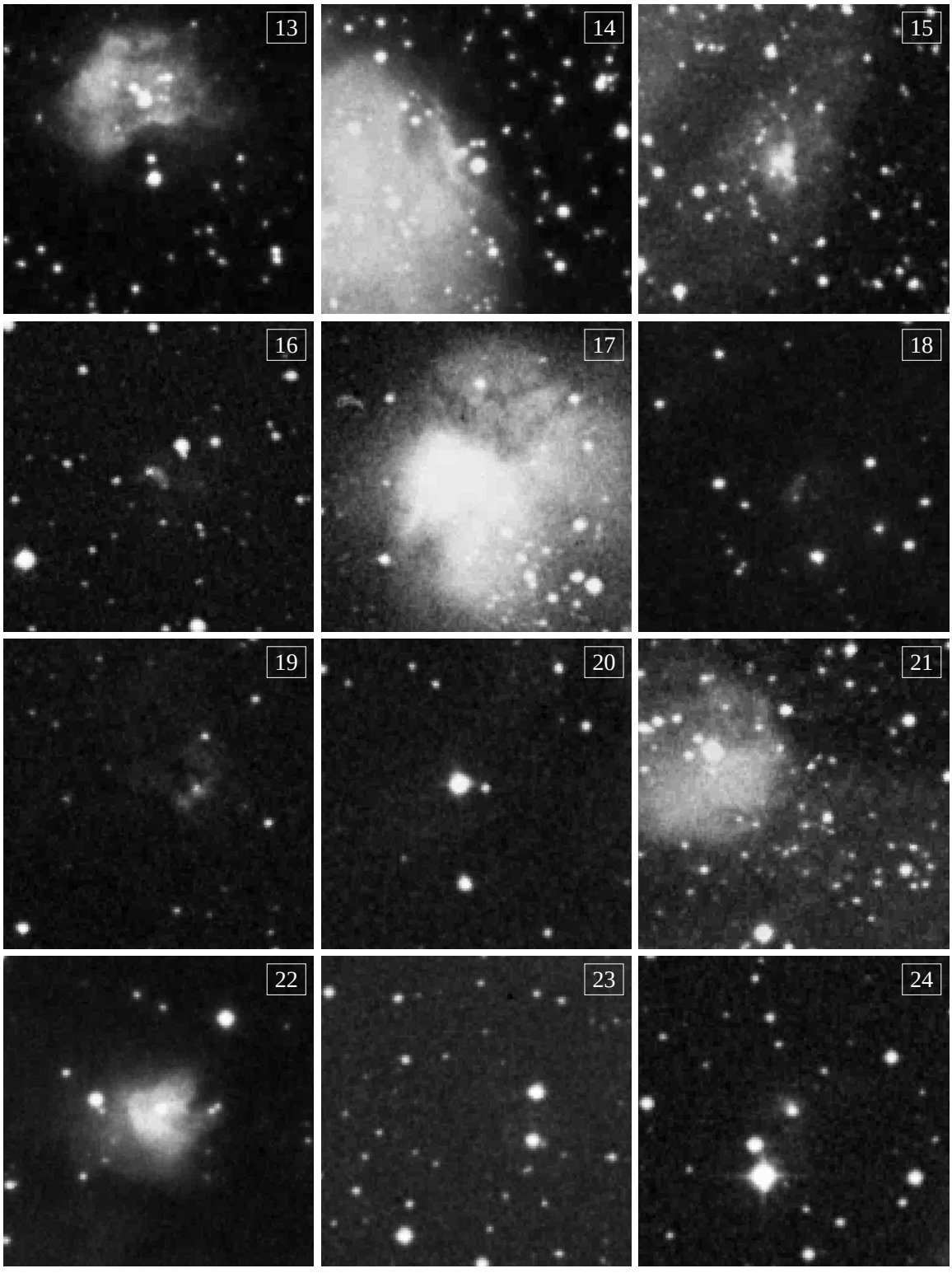
13
14
15
16
17
18
19
20
21
22
23
24

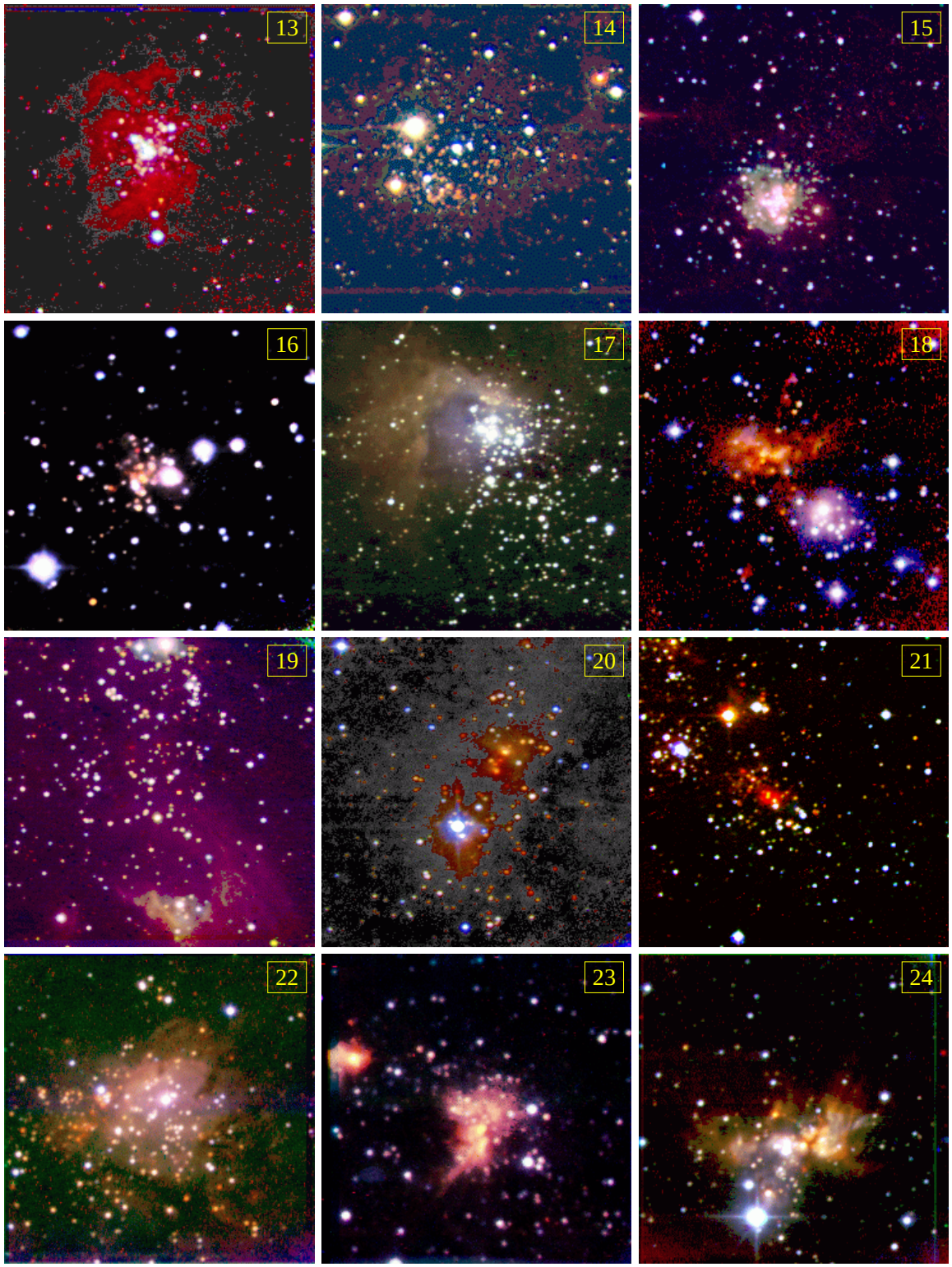
13
14
15
16
17
18
19
20
21
22
23
24

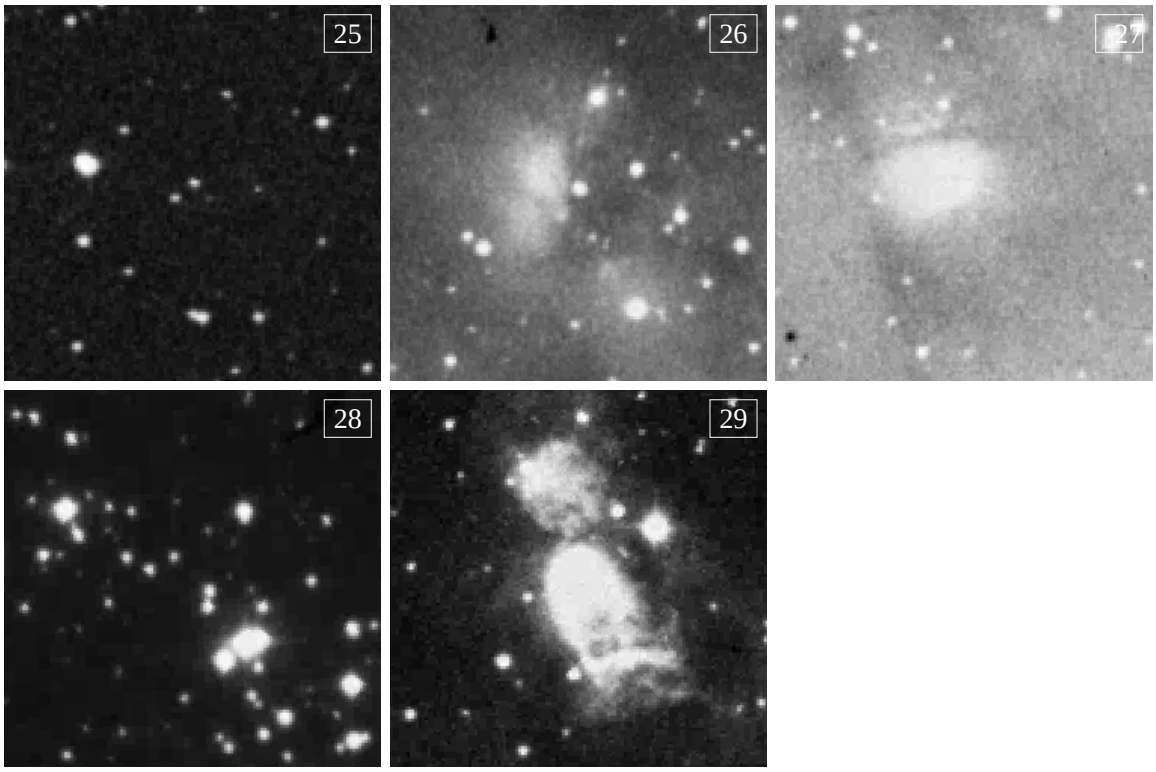
25
26
27
28
29

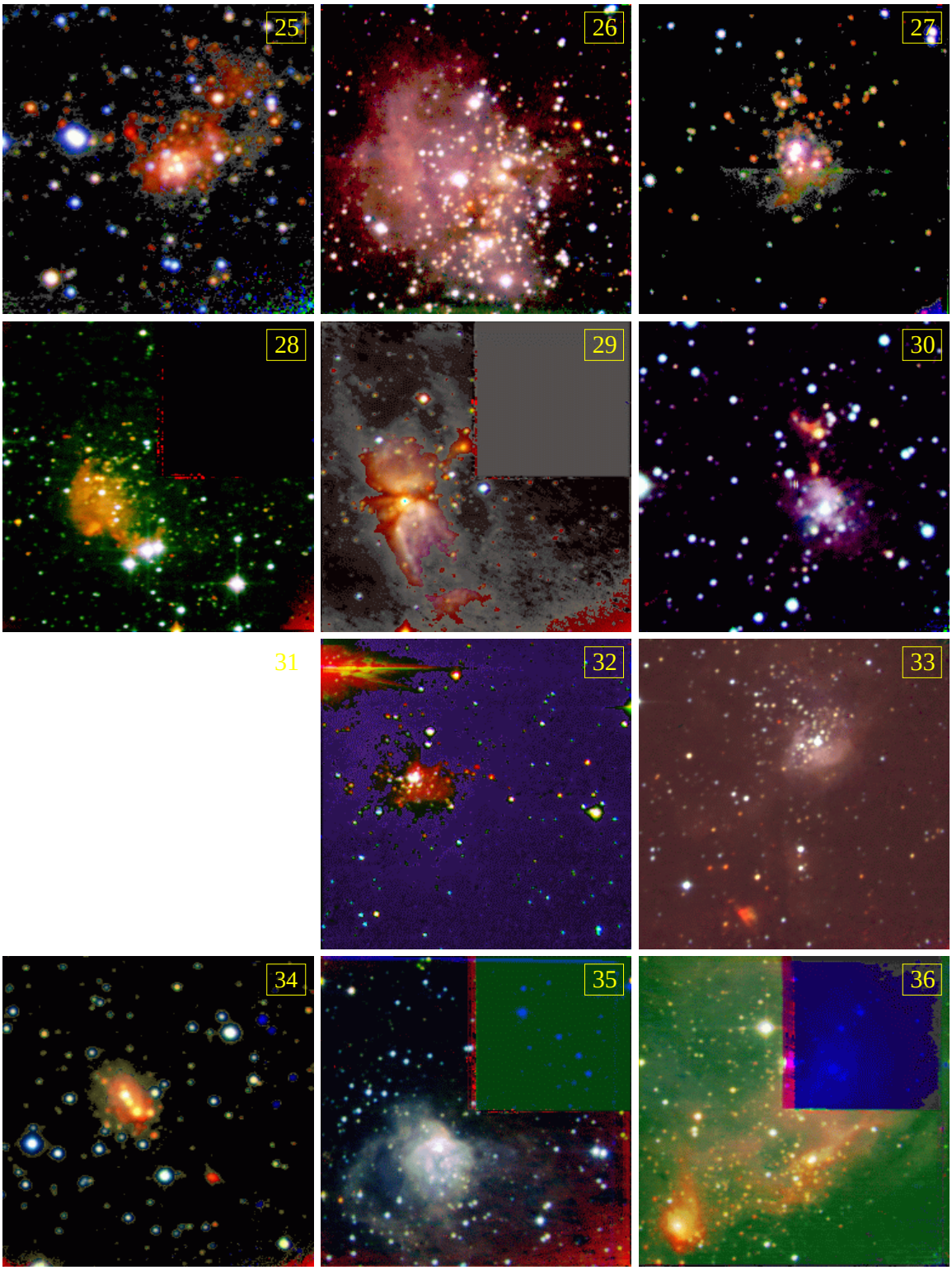
25
26
27
28
29
30
31
32
33
34
35
36

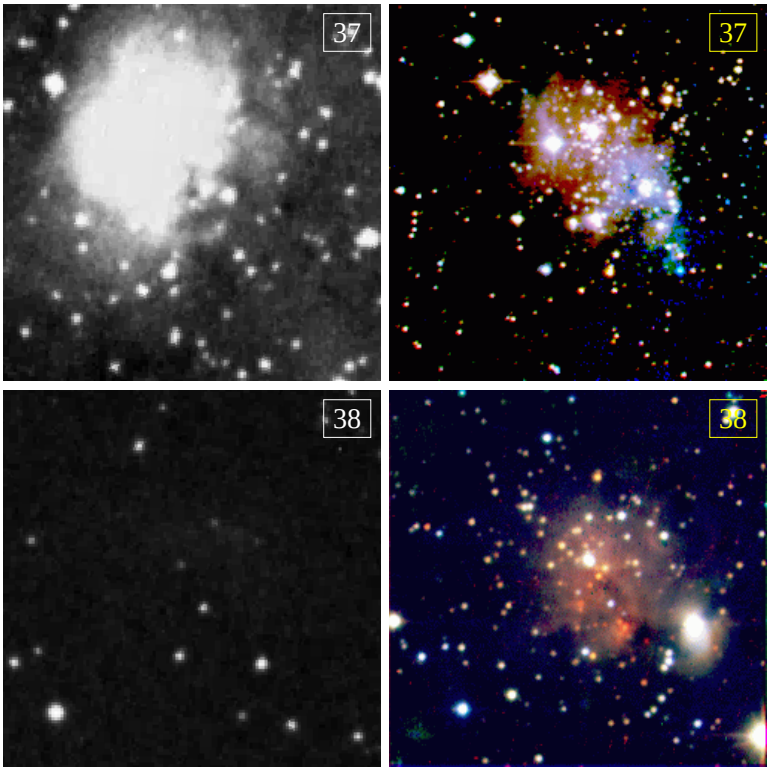
37
37
38
38

Appendix B

IDL/DAOPHOT Reduction Procedures

The data reduction process was described in general §3.4. The main YSC reduction routines are summarized here. The IDL / DAOPHOT data reduction procedures written by W.B. Landsman 1993 are described, together with programs created with the valuable help of L. Georgiev[a]. Our aim in developing this complete software was to have a fast and accurate reduction process. The routines application is for stellar crowded fields with a gas component, which is the case for young stellar clusters, subject of our work.

IDL is a very versatile software package that allows to manage large amounts of data with the following advantages: it is fast, changes in all programs can be done because they are available (in C), contains interactive tasks, has several graphics aids and is user friendly. The developed routines can easily be applied and provided to any user.

B.1 The main procedure

The goal of this procedure is to get the photometry values of a large number of crowded stars in a frame. Photometry on all stars in the field makes use of a "model" star. This "model" star, known as PSF[b], is formed by the sum of several clear and isolated stars. Photometrical errors arise from the fitting of PSF to all stars in a group.

[a]IA-UNAM researcher

[b]The point-spread function "is the two-dimensional brightness distribution produced in the detector by the image of a resolved source, such as a star" (Stetson 1987).

To be compatible with the IDL tasks, we use as input frame: (frame + 10 σ) $* t_{int}$, where σ is the mean sky variation and t_{int} is the integration time. The sum of 10 σ was done to avoid working with negative numbers in the calculation of errors, and multiply by t_{int} is neccesary because the units of our raw frames are in counts/s.

The procedure used for H-filter frames is presented in §B.3 (**AUTOH**). Note that similar procedures for J and K frames apply. Note that this program calls to several Landsman tasks.

After raw data in JHK is obtained the procedure **STAR_COREL** is used to correlate the position of stars found simultaneously in the three frames. The resulting files for each YSC contain position and instrumental photometry values.

B.2 Procedures called by main procedure

The seven standard procedures used, plus some others called by these, can be obtained via ftp from The IDL Astronomy User's Library by W. Landsman in *http://idlastro.gsfc.nasa.gov/* and they are: **SKY, FIND, APER, GETPSF, GROUP, NSTAR,** and **SUBSTAR**.

Function **CLEANPSF** and procedure **DISP2**, as well as final procedure **STAR_ COREL** will be soon included in the manual "Fotometría de campos llenos con IDL / DAOPHOT" (in spanish), available in *http://www.inaoep.mx/∼aporras* and *http://www.astroscu.unam.mx/∼porras*.

Alternatively, there is also a CCDPHOT photometry data reduction package from the Marc Buie's IDL library, that can be useful. Information about is available in *http://www.lowell.edu/users/buie/idl*.

B.3 Programs

```
pro autoh, imah, hh, fwh, aph

;+
; NAME:
; AUTOH
;
; PURPOSE:
; Complete stellar photometry acquisition in a crowded frame.
;
; CALLING SEQUENCE:
; pro autoh, imah, hh, fwh, aph
;
; INPUTS:
; imah - image array.
; hh - image header.
; fwh - approximate full width at high maximum for the image (in pixel units).
; aph - aperture radius or radii (in pixel units).
;
; OPTIONAL KEYWORD INPUT:
;
; REVISION HISTORY:
; A. Porras INAOE January, 1998.
; L. Georgiev IA-UNAM and ; A. Porras INAOE April, 1997.

tpoh = sxpar( hh,'EXPTIME')
nh = sxpar( hh,'NOBS')
sky,imah,smh,sdh,circ=1
imah = (imah + 10*sdh) * tpoh
nh=nh+4
ruidoh=40*sqrt(nh)
fotadu=15
medh=median(imah,17)
imalh=imah-medh
sky,imalh,smh,sdh,circ=1
thh=3.0*sdh + smh
find,imah,xch,ych,fluh,sharph,roundh,thh,fwh
;
idh=indgen(n_elements(xch))
aper,imah,xch,ych,magh,emagh,cieh,ecieh,fotadu,aph,[6,8]
;
aper,imalh,xch,ych,maglh,emaglh,cielh,ecielh,fotadu,aph,[6,8]
;
hzzh=where((magh lt 50) and (maglh lt 50) and (abs(magh-maglh) lt 0.1))
cleh=cleanpsf(xch,ych,magh,hzzh,10)
hih=hzzh(cleh)
lim=avg(magh(where(magh ne 99.999)))
hihb=where((magh(hih) gt (lim-3)) and (sharph(hih) lt 0.7) and (sharph(hih) gt 0.5)
and (abs(roundh(hih)) lt 0.081),count)
count1=0.01
```

```
if count eq 0 then hihb=where((magh(hih) gt (lim-4)) and (sharph(hih) lt 0.75) and
(sharph(hih) gt 0.45) and (abs(roundh(hih)) lt 0.4),count1) else ah=[hih(hihb)]
if count1 eq 0 then ah=hih else ah=[hih(hihb)]
help,hihb
print,hih & print,hihb & print,ah
print,avg(magh(ah)) & print,magh(ah)
disp2,imalh,0
;
xyouts,xch(hih)*2,ych(hih)*2,idh(hih),alignment=1,/device,color=230
ahs=ah(sort(magh(ah)))
forprint,idh(ahs),xch(ahs),ych(ahs),magh(ahs)
hihs=hih(sort(magh(hih)))
forprint,idh(hihs),xch(hihs),ych(hihs),magh(hihs)
;
getpsf,imah,xch,ych,magh,cieh,ruidoh,fotadu,ga,psfh,ah,7,3,'tht.hhh'
rdpsf,epsfh,hpsfh,'tht.hhh'
window,3,xsi=600,ysi=600
surface,epsfh,charsize=2
tv,bytscl(rebin(epsfh,180,180),0,50000),2
window,4,xsi=555,ysi=555
surface,psfh,charsize=2
tv,bytscl(rebin(psfh,185,185),0,50000),2
;
group,xch,ych,9,ngh
;
idh1=idh
xch1=xch
ych1=ych
magh1=magh
nstar, imah, idh1, xch1, ych1, magh1, cieh, ngh, fotadu, ruidoh, 'tht', emagh1, iterh,
chih, picoh, /varsky
forprint, idh1, xch1, ych1, magh1, emagh1, cieh(idh1), iterh, chih, picoh,
f='(I6,2F9.2,2F9.3,F10.1,I4,F9.2,F9.3)', textout='firh'
;
nameh = sxpar(hh,'IRAFNAME')
nameh = string(nameh)
iih=where(emagh1 lt 0.3)
window,2,xsi=500,ysi=500
plot, magh1(iih)-5+2.5*alog10(tpoh), emagh1(iih), psym=5, xtitle='H', ytitle='error
H', charsize=2, title=nameh, symsize=0.5
xyouts, magh1(iih)-5+2.5*alog10(tpoh), emagh1(iih), idh1(iih), alignment=1
```

Appendix C

Stellar Photometry Tables

NIR photometry tables of the 38 YSCs. Columns include:

(1) source number;

(2) and (3) position in the frame; (0,0) is in the lower right corner of images, and grow towards North and East directions;

(4), (5) and (6) are JHK magnitudes and errors;

(7) and (8) are (J-H) and (H-K) colours; and

(9) and (10) derived individual extinction (§5.5) and stellar mass (§6.1).

Footnotes are in all tables as follows:

a Young stellar cluster member.

b Foreground star.

c Possible HH knot.

d Unresolved pair.

e Very embedded stars lying into the cluster radius, but without J counterpart. Their A_V and M values are roughly estimated from K vs. H-K diagram, assuming they have the cluster age. None IR excess consideration was done, but this contribution may be important. These values were not considered into the IMF study.

f Young stellar cluster member of a second subcluster (only in YSC 4 and YSC 18).

g Young stellar cluster member of a third subcluster (only in YSC 4).

Table C.1: Photometry table for IRAS 01198+6136. **YSC 1.**

#	x (pix)	y (pix)	j	h	k	J - H	H - K	A_V	M ($M_\odot$)
(1)	(2)	(3)	(4)	(5)	(6)	(7)	(8)	(9)	(10)
1	102.7	24.4	17.75 ± 0.04	15.58 ± 0.04	14.32 ± 0.11	2.16	1.27	—	—
2	72.8	32.6	17.09 ± 0.03	15.10 ± 0.03	14.42 ± 0.11	1.99	0.68	15.61	2.50
3	77.7	35.7	19.44 ± 0.23	17.57 ± 0.12	16.64 ± 0.25	1.87	0.93	10.96	0.80
4	54.3	39.9	16.89 ± 0.03	14.98 ± 0.03	14.34 ± 0.07	1.91	0.64	14.91	2.50
5	51.8	44.6	19.31 ± 0.26	17.59 ± 0.10	16.47 ± 0.14	1.71	1.12	5.37	0.16
6	191.5	48.7	13.22 ± 0.04	12.70 ± 0.03	12.83 ± 0.10	0.52	-0.13	2.24	2.50
7	169.1	57.1	17.89 ± 0.06	16.20 ± 0.04	15.61 ± 0.07	1.69	0.58	10.08	1.50[a]
8	129.6	56.8	18.11 ± 0.07	15.49 ± 0.02	14.50 ± 0.13	2.62	0.99	19.49	2.50[a]
9	186.8	56.0	17.21 ± 0.04	15.03 ± 0.05	14.03 ± 0.12	2.19	1.00	16.25	2.50
10	229.7	56.3	12.56 ± 0.05	11.39 ± 0.05	11.60 ± 0.14	1.17	-0.21	10.82	20.00
11	84.4	56.9	18.19 ± 0.05	15.39 ± 0.04	13.85 ± 0.09	2.80	1.54	15.52	0.61
12	99.0	63.5	17.55 ± 0.07	15.74 ± 0.04	15.29 ± 0.09	1.81	0.45	15.40	3.00[a]
13	156.7	65.0	17.45 ± 0.06	15.33 ± 0.04	13.87 ± 0.10	2.12	1.46	7.75	0.62[a]
14	114.0	68.1	16.02 ± 0.03	13.73 ± 0.06	13.06 ± 0.07	2.29	0.67	18.77	10.00[a]
15	119.0	73.3	16.09 ± 0.03	13.92 ± 0.05	13.13 ± 0.08	2.17	0.78	18.82	10.00[a]
16	140.4	71.7	16.13 ± 0.02	14.81 ± 0.04	14.38 ± 0.08	1.33	0.43	12.31	4.00[a]
17	158.1	79.9	15.25 ± 0.04	13.60 ± 0.04	13.14 ± 0.08	1.64	0.46	15.64	10.00[a]
18	154.1	86.0	15.98 ± 0.05	14.52 ± 0.07	14.46 ± 0.10	1.46	0.06	13.14	5.00[a]
19	211.3	81.3	19.21 ± 0.20	16.21 ± 0.04	14.91 ± 0.15	3.00	1.30	23.24	2.50
20	128.2	81.1	16.97 ± 0.07	15.22 ± 0.04	14.31 ± 0.07	1.75	0.91	15.36	4.00[a]
21	87.3	84.8	17.12 ± 0.04	14.39 ± 0.02	13.28 ± 0.08	2.73	1.11	22.59	10.00[a]
22	143.6	85.0	15.92 ± 0.01	14.38 ± 0.02	13.76 ± 0.13	1.54	0.61	11.56	2.50[a]
23	233.5	86.2	14.84 ± 0.04	13.02 ± 0.03	12.75 ± 0.09	1.82	0.27	14.63	10.00
24	202.7	90.1	16.79 ± 0.04	15.41 ± 0.02	14.87 ± 0.10	1.38	0.54	8.80	2.00[a]
25	46.9	91.0	18.92 ± 0.14	17.60 ± 0.06	16.76 ± 0.13	1.32	0.84	2.65	0.15
26	83.5	92.4	18.85 ± 0.11	16.64 ± 0.04	15.67 ± 0.11	2.20	0.97	13.61	1.50[a]
27	127.3	93.1	14.73 ± 0.05	13.26 ± 0.06	12.85 ± 0.11	1.48	0.41	13.88	10.00[a]
28	146.5	100.3	13.36 ± 0.07	12.13 ± 0.20	11.03 ± 0.19	1.22	1.10	0.56	3.42[a]
29	130.0	101.3	13.99 ± 0.07	12.66 ± 0.17	12.49 ± 0.19	1.33	0.17	11.46	10.00[a]
30	138.1	100.3	15.17 ± 0.17	12.91 ± 0.21	10.95 ± 0.13	2.26	1.96	5.69	2.80[a]
31	143.1	103.9	10.75 ± 0.08	9.93 ± 0.17	9.48 ± 0.04	0.83	0.45	5.14	20.00[a]
32	139.2	107.4	10.24 ± 0.11	10.03 ± 0.29	8.73 ± 0.02	0.21	1.30	—	—[a,c]
33	162.1	105.0	16.33 ± 0.07	14.08 ± 0.09	13.42 ± 0.13	2.26	0.66	19.64	10.00[a]
34	163.5	108.2	16.21 ± 0.07	14.74 ± 0.11	14.04 ± 0.17	1.47	0.70	12.73	4.00[a]
35	215.3	98.4	19.17 ± 0.14	16.35 ± 0.03	15.24 ± 0.13	2.83	1.11	24.41	5.00
36	220.9	102.2	19.25 ± 0.15	17.39 ± 0.06	16.28 ± 0.16	1.86	1.10	7.32	0.18
37	52.0	99.0	16.97 ± 0.03	15.42 ± 0.03	14.82 ± 0.08	1.55	0.60	13.34	3.00
38	60.9	100.2	18.84 ± 0.16	17.53 ± 0.10	16.61 ± 0.14	1.31	0.92	1.92	0.15
39	72.5	101.4	15.75 ± 0.03	13.85 ± 0.03	13.06 ± 0.10	1.90	0.80	17.44	10.00
40	111.2	100.9	15.18 ± 0.03	13.27 ± 0.05	12.72 ± 0.16	1.91	0.55	15.78	10.00[a]
41	114.6	101.9	14.05 ± 0.02	12.19 ± 0.04	11.74 ± 0.13	1.86	0.45	16.18	20.00[a]
42	231.8	108.3	16.16 ± 0.02	14.01 ± 0.03	13.11 ± 0.09	2.15	0.91	18.98	10.00
43	204.3	103.7	17.75 ± 0.04	16.38 ± 0.04	15.69 ± 0.10	1.37	0.70	6.69	1.00[a]
44	204.2	110.7	18.28 ± 0.07	15.95 ± 0.03	14.84 ± 0.07	2.33	1.11	19.99	4.00[a]
45	153.0	104.6	13.54 ± 0.12	11.92 ± 0.24	11.39 ± 0.22	1.62	0.53	14.31	20.00[a]
46	45.1	106.0	17.92 ± 0.07	15.95 ± 0.03	15.61 ± 0.09	1.97	0.34	16.71	3.00
47	98.3	109.2	16.27 ± 0.04	14.51 ± 0.03	13.98 ± 0.07	1.76	0.53	12.88	2.50[a]
48	70.0	111.3	16.19 ± 0.03	14.47 ± 0.03	13.97 ± 0.11	1.72	0.50	12.59	2.50
49	63.7	114.0	15.96 ± 0.02	14.07 ± 0.02	13.50 ± 0.10	1.90	0.57	18.09	10.00
50	223.8	111.6	19.19 ± 0.17	15.53 ± 0.03	13.69 ± 0.14	3.65	1.85	29.95	10.00
51	51.5	114.4	14.36 ± 0.12	12.65 ± 0.19	12.22 ± 0.21	1.70	0.44	16.90	20.00
52	180.7	114.2	18.45 ± 0.14	16.01 ± 0.04	14.60 ± 0.12	2.44	1.41	12.13	0.42[a]
53	156.4	117.5	11.47 ± 0.02	10.59 ± 0.12	11.12 ± 0.22	0.87	-0.53	7.20	20.00[a]
54	203.8	119.1	19.21 ± 0.30	16.78 ± 0.04	15.94 ± 0.08	2.44	0.84	17.37	2.00[a]
55	205.0	123.9	18.06 ± 0.11	17.51 ± 0.07	16.88 ± 0.16	0.55	0.63	5.16	0.14[a]
56	120.9	120.4	14.66 ± 0.03	12.71 ± 0.04	12.06 ± 0.11	1.96	0.64	18.11	20.00[a]
57	118.2	124.6	15.73 ± 0.05	13.93 ± 0.06	12.99 ± 0.15	1.80	0.94	17.27	10.00[a]
58	123.5	127.7	16.93 ± 0.09	15.37 ± 0.09	14.61 ± 0.21	1.56	0.76	13.22	3.00[a]
59	113.5	130.5	14.94 ± 0.04	12.95 ± 0.06	12.23 ± 0.14	1.98	0.72	18.97	20.00[a]
60	114.8	135.0	15.39 ± 0.04	13.75 ± 0.07	13.45 ± 0.17	1.64	0.30	16.05	10.00[a]
61	98.7	123.8	18.04 ± 0.09	16.73 ± 0.06	16.24 ± 0.16	1.30	0.49	6.04	0.80[a]
62	146.4	120.6	14.09 ± 0.06	12.21 ± 0.10	11.42 ± 0.16	1.88	0.79	16.31	20.00[a]
63	130.4	123.7	15.10 ± 0.05	13.39 ± 0.08	12.94 ± 0.14	1.71	0.45	15.27	10.00[a]
64	70.9	125.1	17.10 ± 0.05	15.17 ± 0.03	14.46 ± 0.11	1.93	0.71	17.06	5.00
65	51.2	146.2	17.35 ± 0.05	15.22 ± 0.02	14.75 ± 0.17	2.13	0.46	16.60	2.50
66	100.9	131.2	17.61 ± 0.09	16.26 ± 0.06	15.85 ± 0.18	1.35	0.41	6.24	1.00[a]
67	169.7	144.7	13.98 ± 0.02	13.14 ± 0.03	13.00 ± 0.11	0.85	0.14	4.92	2.50[a]
68	155.2	135.4	13.99 ± 0.03	12.62 ± 0.03	12.49 ± 0.10	1.37	0.13	11.51	10.00[a]
69	71.1	136.8	12.50 ± 0.03	11.95 ± 0.04	12.41 ± 0.08	0.55	-0.46	6.03	10.00
70	183.2	136.5	15.91 ± 0.02	14.32 ± 0.03	13.99 ± 0.11	1.59	0.33	11.59	2.50[a]
71	185.3	138.3	16.20 ± 0.03	14.63 ± 0.03	14.38 ± 0.14	1.57	0.25	13.91	5.00[a]
72	122.8	136.9	15.20 ± 0.03	13.58 ± 0.03	13.14 ± 0.11	1.63	0.43	15.48	10.00[a]
73	202.9	137.1	13.80 ± 0.02	12.49 ± 0.03	12.17 ± 0.10	1.31	0.32	10.87	10.00
74	212.0	139.1	15.71 ± 0.03	13.88 ± 0.03	13.79 ± 0.11	1.83	0.09	17.26	10.00
75	145.3	140.2	10.92 ± 0.06	10.33 ± 0.17	10.26 ± 0.10	0.59	0.07	5.21	20.00[a]
76	21.2	140.7	15.50 ± 0.02	13.55 ± 0.03	13.42 ± 0.14	1.95	0.13	16.76	10.00
77	23.1	146.6	16.25 ± 0.03	14.45 ± 0.04	13.82 ± 0.14	1.80	0.63	12.90	2.50

continued on next page

Table C.1: *continued*

#	x (pix)	y (pix)	j	h	k	J - H	H - K	A_V	M ($M_\odot$)
(1)	(2)	(3)	(4)	(5)	(6)	(7)	(8)	(9)	(10)
78	26.9	152.4	14.60 ± 0.01	12.74 ± 0.04	12.67 ± 0.11	1.86	0.07	17.79	20.00
79	96.6	142.4	14.04 ± 0.01	12.48 ± 0.05	11.91 ± 0.12	1.57	0.57	15.77	20.00[a]
80	110.3	144.2	15.47 ± 0.02	14.76 ± 0.04	14.60 ± 0.15	0.71	0.16	1.60	—[b]
81	110.0	148.5	15.37 ± 0.02	13.95 ± 0.03	13.86 ± 0.12	1.42	0.09	9.78	2.50[a]
82	103.8	150.3	16.91 ± 0.06	15.36 ± 0.05	14.95 ± 0.20	1.56	0.40	13.17	3.00[a]
83	160.4	145.5	16.09 ± 0.03	14.80 ± 0.05	14.47 ± 0.13	1.29	0.32	10.38	3.00[a]
84	179.4	146.0	18.43 ± 0.09	16.54 ± 0.06	15.15 ± 0.18	1.89	1.39	5.47	0.31[a]
85	180.9	150.6	16.79 ± 0.02	14.44 ± 0.02	13.43 ± 0.12	2.35	1.01	21.13	10.00[a]
86	119.2	152.2	14.76 ± 0.02	13.34 ± 0.03	13.18 ± 0.14	1.42	0.16	13.89	10.00[a]
87	118.5	163.6	16.53 ± 0.04	15.20 ± 0.04	15.11 ± 0.23	1.33	0.09	7.94	2.00
88	165.1	152.7	17.88 ± 0.06	16.66 ± 0.05	16.17 ± 0.10	1.22	0.49	5.47	0.80[a]
89	189.3	153.0	16.34 ± 0.04	14.64 ± 0.04	14.01 ± 0.09	1.70	0.63	13.00	2.50
90	214.0	154.4	18.81 ± 0.21	17.00 ± 0.12	16.08 ± 0.10	1.81	0.92	10.41	1.00
91	146.5	156.7	16.02 ± 0.03	14.73 ± 0.03	14.39 ± 0.11	1.29	0.34	11.92	4.00[a]
92	152.1	156.5	15.83 ± 0.03	15.00 ± 0.03	15.27 ± 0.15	0.84	-0.27	2.85	1.50[a]
93	90.6	158.5	16.42 ± 0.02	14.78 ± 0.03	14.35 ± 0.12	1.63	0.43	14.67	5.00
94	195.5	159.3	16.04 ± 0.02	14.67 ± 0.04	14.04 ± 0.15	1.37	0.63	12.08	4.00
95	212.5	164.0	19.01 ± 0.19	18.16 ± 0.22	16.89 ± 0.15	0.86	1.26	6.22	0.12
96	28.3	175.6	18.67 ± 0.14	16.73 ± 0.08	16.09 ± 0.15	1.94	0.64	12.73	1.50
97	107.2	164.3	15.18 ± 0.02	13.62 ± 0.03	13.44 ± 0.21	1.56	0.18	15.31	10.00
98	127.8	169.3	16.91 ± 0.04	15.81 ± 0.04	15.10 ± 0.17	1.10	0.71	1.03	0.39
99	53.2	172.2	16.13 ± 0.03	14.70 ± 0.03	14.53 ± 0.13	1.43	0.17	12.42	4.00
100	200.9	172.1	19.21 ± 0.29	17.57 ± 0.09	16.13 ± 0.12	1.64	1.44	2.05	0.17
101	102.7	183.8	18.20 ± 0.05	16.44 ± 0.04	15.64 ± 0.10	1.76	0.80	11.13	1.50
102	223.3	173.7	15.53 ± 0.03	13.52 ± 0.04	12.93 ± 0.11	2.01	0.59	16.92	10.00
103	173.0	176.8	18.24 ± 0.07	17.03 ± 0.06	16.87 ± 0.25	1.20	0.16	4.48	0.60
104	170.5	184.8	18.27 ± 0.08	17.28 ± 0.08	16.02 ± 0.14	1.00	1.26	4.46	0.20
105	166.7	189.9	15.62 ± 0.01	14.13 ± 0.03	13.43 ± 0.08	1.49	0.70	10.61	2.50
106	159.2	179.3	18.37 ± 0.08	16.86 ± 0.07	16.21 ± 0.14	1.51	0.65	7.31	0.80
107	46.5	180.4	18.87 ± 0.14	17.17 ± 0.06	16.18 ± 0.26	1.70	0.99	6.25	0.19
108	231.6	180.6	18.05 ± 0.08	16.54 ± 0.08	16.36 ± 0.26	1.51	0.18	7.77	1.00
109	229.0	184.4	16.75 ± 0.03	15.18 ± 0.05	14.47 ± 0.12	1.57	0.70	12.72	3.00
110	135.8	185.1	14.67 ± 0.02	13.27 ± 0.04	13.11 ± 0.10	1.40	0.16	13.59	10.00
111	206.7	190.1	16.53 ± 0.03	15.86 ± 0.04	15.50 ± 0.09	0.67	0.36	0.75	—[b]
112	128.1	194.0	19.45 ± 0.26	17.47 ± 0.08	16.65 ± 0.14	1.99	0.81	11.15	0.80
113	31.6	206.4	18.15 ± 0.15	16.93 ± 0.10	16.58 ± 0.18	1.22	0.35	4.24	0.60
114	45.8	204.1	16.11 ± 0.03	15.22 ± 0.12	14.77 ± 0.26	0.89	0.45	3.77	1.50
115	94.9	204.0	18.26 ± 0.10	16.85 ± 0.05	16.14 ± 0.12	1.41	0.72	6.84	0.80
116	60.4	208.8	16.30 ± 0.04	15.09 ± 0.05	14.28 ± 0.17	1.21	0.81	1.48	0.59
117	230.2	208.6	17.68 ± 0.07	14.62 ± 0.05	13.51 ± 0.14	3.07	1.11	24.72	10.00
118	220.7	218.2	18.16 ± 0.07	16.19 ± 0.04	15.48 ± 0.10	1.97	0.71	13.64	2.00
119	119.9	219.6	16.22 ± 0.05	14.24 ± 0.06	13.59 ± 0.14	1.98	0.65	18.97	10.00
120	226.5	233.8	19.14 ± 0.23	16.31 ± 0.05	14.91 ± 0.10	2.84	1.39	24.33	5.00
121	169.9	20.3	—	18.56 ± 0.16	15.41 ± 0.08	—	3.15	—	—
122	179.6	30.6	—	17.70 ± 0.10	15.58 ± 0.11	—	2.13	—	—
123	25.3	37.3	—	17.81 ± 0.08	17.17 ± 0.23	—	0.64	—	—
124	109.8	42.3	—	17.44 ± 0.10	15.88 ± 0.08	—	1.57	—	—
125	48.3	49.1	—	17.74 ± 0.10	16.69 ± 0.13	—	1.05	—	—
126	164.6	45.1	—	17.36 ± 0.07	16.12 ± 0.05	—	1.25	—	—
127	176.6	49.4	—	15.94 ± 0.04	14.53 ± 0.10	—	1.42	—	—
128	233.2	60.0	—	14.39 ± 0.09	13.26 ± 0.14	—	1.13	—	—
129	136.8	53.7	—	18.28 ± 0.18	17.04 ± 0.14	—	1.24	—	—
130	34.4	57.5	—	18.59 ± 0.25	16.80 ± 0.12	—	1.79	—	—
131	86.9	59.1	—	15.81 ± 0.05	14.54 ± 0.11	—	1.28	—	—
132	128.4	66.2	—	17.56 ± 0.07	16.18 ± 0.16	—	1.38	—	—
133	186.8	67.9	—	17.54 ± 0.08	16.57 ± 0.12	—	0.97	—	—
134	28.8	69.1	—	18.23 ± 0.17	16.79 ± 0.18	—	1.44	—	—
135	219.0	74.7	—	17.39 ± 0.10	16.33 ± 0.17	—	1.06	—	—
136	86.1	72.4	—	17.57 ± 0.07	16.16 ± 0.08	—	1.41	—	—
137	78.6	73.2	—	17.82 ± 0.10	16.47 ± 0.14	—	1.35	—	—
138	67.0	85.0	—	17.66 ± 0.11	16.76 ± 0.16	—	0.89	—	—
139	176.6	76.3	—	16.31 ± 0.05	14.41 ± 0.11	—	1.91	—	—
140	171.1	79.4	—	16.34 ± 0.04	15.11 ± 0.14	—	1.23	—	—
141	172.7	85.5	—	15.80 ± 0.04	13.70 ± 0.09	—	2.09	—	—
142	174.8	88.9	—	16.38 ± 0.05	14.02 ± 0.12	—	2.36	—	—
143	227.0	84.8	—	16.75 ± 0.10	15.59 ± 0.22	—	1.16	—	—
144	230.2	89.1	—	15.10 ± 0.05	14.43 ± 0.14	—	0.67	—	—
145	39.6	86.0	—	18.66 ± 0.16	17.22 ± 0.19	—	1.44	—	—
146	167.0	97.8	—	17.36 ± 0.07	16.55 ± 0.14	—	0.81	—	—
147	191.1	113.8	—	17.63 ± 0.10	16.56 ± 0.17	—	1.07	—	—
148	89.9	114.4	—	17.77 ± 0.12	16.90 ± 0.17	—	0.87	—	—
149	55.5	128.3	—	17.48 ± 0.11	16.79 ± 0.20	—	0.69	—	—
150	154.5	143.7	—	16.72 ± 0.11	15.82 ± 0.24	—	0.90	—	—
151	119.4	173.8	—	17.36 ± 0.06	16.48 ± 0.21	—	0.89	—	—
152	212.1	199.7	—	17.49 ± 0.09	16.62 ± 0.14	—	0.87	—	—
153	206.4	205.1	—	17.60 ± 0.11	16.74 ± 0.23	—	0.85	—	—
154	140.8	210.5	—	17.69 ± 0.11	16.66 ± 0.13	—	1.03	—	—

continued on next page

Table C.1: *continued*

#	x (pix)	y (pix)	j	h	k	J - H	H - K	A_V	M ($M_\odot$)
(1)	(2)	(3)	(4)	(5)	(6)	(7)	(8)	(9)	(10)
155	28.2	215.5	—	18.61 ± 0.26	16.97 ± 0.18	—	1.64	—	—
156	205.0	221.9	—	17.60 ± 0.14	16.38 ± 0.20	—	1.22	—	—
157	193.7	230.5	—	17.71 ± 0.12	16.73 ± 0.12	—	0.99	—	—

Table C.2: Photometry table for IRAS 01202+6133. **YSC 2.**

#	x (pix)	y (pix)	j	h	k	J - H	H - K	A_V	M ($M_\odot$)
(1)	(2)	(3)	(4)	(5)	(6)	(7)	(8)	(9)	(10)
1	34.1	21.7	15.91 ± 0.13	14.40 ± 0.12	12.76 ± 0.13	1.51	1.64	—	—
2	131.9	27.8	17.62 ± 0.04	15.50 ± 0.03	14.57 ± 0.04	2.12	0.93	12.98	0.80[a]
3	118.9	32.6	17.21 ± 0.03	15.62 ± 0.02	14.97 ± 0.05	1.59	0.65	6.67	0.40[a]
4	55.3	34.3	14.61 ± 0.02	13.99 ± 0.02	13.91 ± 0.07	0.62	0.08	2.06	1.00[a]
5	58.5	36.6	16.11 ± 0.04	14.34 ± 0.03	13.35 ± 0.06	1.77	0.99	7.04	0.25[a]
6	191.0	36.2	18.77 ± 0.08	15.93 ± 0.02	14.63 ± 0.04	2.84	1.31	18.74	1.00[a]
7	222.6	35.1	19.03 ± 0.12	17.04 ± 0.05	16.21 ± 0.11	1.99	0.83	10.27	0.40
8	68.6	45.3	12.00 ± 0.06	11.69 ± 0.08	11.65 ± 0.07	0.31	0.03	2.80	2.50[a]
9	36.1	50.7	18.15 ± 0.08	16.79 ± 0.04	16.28 ± 0.26	1.37	0.50	5.65	0.20[a]
10	208.0	53.3	15.14 ± 0.02	14.12 ± 0.03	13.80 ± 0.04	1.02	0.31	4.16	0.80[a]
11	172.7	55.4	17.33 ± 0.04	14.48 ± 0.04	12.64 ± 0.07	2.84	1.85	13.69	0.29[a]
12	23.1	57.5	17.33 ± 0.07	15.78 ± 0.03	14.73 ± 0.10	1.55	1.05	3.89	0.11
13	45.6	57.7	14.65 ± 0.03	13.22 ± 0.03	12.58 ± 0.05	1.43	0.64	7.19	1.50[a]
14	121.8	58.1	18.22 ± 0.05	16.61 ± 0.04	15.96 ± 0.06	1.61	0.65	9.75	0.40[a]
15	123.0	62.1	18.09 ± 0.05	16.47 ± 0.04	15.50 ± 0.05	1.61	0.98	5.17	0.07[a]
16	152.8	58.1	18.43 ± 0.10	15.35 ± 0.04	13.93 ± 0.08	3.08	1.42	22.96	2.00[a]
17	35.0	59.0	18.65 ± 0.19	17.61 ± 0.09	15.42 ± 0.19	1.04	2.19	—	—[a,c]
18	109.0	61.0	13.47 ± 0.02	12.16 ± 0.04	11.53 ± 0.03	1.31	0.64	11.45	4.00[a]
19	178.4	62.4	18.75 ± 0.16	16.50 ± 0.04	15.50 ± 0.08	2.25	1.00	14.48	0.60[a]
20	78.7	63.6	17.47 ± 0.04	15.39 ± 0.04	14.30 ± 0.09	2.08	1.09	12.47	0.80[a]
21	161.2	68.4	18.88 ± 0.21	16.97 ± 0.09	16.31 ± 0.20	1.91	0.66	12.07	0.40[a]
22	59.9	68.7	17.94 ± 0.06	16.12 ± 0.05	15.43 ± 0.07	1.82	0.70	9.16	0.40[a]
23	49.2	70.0	17.62 ± 0.06	15.81 ± 0.03	14.71 ± 0.09	1.82	1.10	6.79	0.11[a]
24	108.0	71.8	17.58 ± 0.05	14.74 ± 0.03	13.17 ± 0.06	2.84	1.56	15.85	0.23[a]
25	233.3	74.8	13.26 ± 0.04	12.30 ± 0.07	11.85 ± 0.07	0.96	0.45	8.65	3.00
26	71.1	77.2	18.00 ± 0.10	17.17 ± 0.06	16.84 ± 0.12	0.83	0.32	0.81	—[b]
27	201.5	76.6	19.17 ± 0.15	18.22 ± 0.14	17.41 ± 0.12	0.95	0.80	1.62	0.03[a]
28	223.1	84.3	13.61 ± 0.03	13.13 ± 0.04	13.10 ± 0.04	0.49	0.02	3.91	1.50
29	175.0	87.4	18.84 ± 0.17	17.44 ± 0.21	15.71 ± 0.28	1.39	1.74	—	—[a,c]
30	52.7	85.9	18.98 ± 0.14	17.11 ± 0.06	16.29 ± 0.07	1.86	0.82	8.76	0.20[a]
31	117.1	87.2	17.51 ± 0.03	16.88 ± 0.03	16.64 ± 0.09	0.63	0.23	1.17	—[b]
32	20.4	92.0	19.10 ± 0.14	17.67 ± 0.08	16.82 ± 0.11	1.44	0.85	4.01	0.04
33	128.0	89.3	18.95 ± 0.14	15.45 ± 0.03	13.68 ± 0.06	3.49	1.77	28.85	3.00[a]
34	39.7	93.4	18.96 ± 0.11	17.45 ± 0.08	16.64 ± 0.10	1.51	0.80	8.25	0.20[a]
35	43.4	95.8	17.92 ± 0.04	16.07 ± 0.04	14.93 ± 0.05	1.85	1.14	6.93	0.10[a]
36	40.2	99.6	18.02 ± 0.05	16.55 ± 0.04	15.88 ± 0.07	1.48	0.67	5.44	0.20[a]
37	148.3	94.0	17.91 ± 0.05	14.44 ± 0.03	12.30 ± 0.04	3.47	2.14	19.22	0.32[a]
38	131.8	94.5	17.04 ± 0.03	15.41 ± 0.03	14.54 ± 0.03	1.63	0.87	6.24	0.13[a]
39	170.6	108.4	18.40 ± 0.10	16.68 ± 0.05	15.96 ± 0.03	1.71	0.72	10.39	0.40[a]
40	94.7	114.3	18.54 ± 0.11	17.07 ± 0.06	15.90 ± 0.06	1.48	1.16	2.14	0.06[a]
41	226.4	113.8	18.50 ± 0.08	16.04 ± 0.03	15.04 ± 0.03	2.45	1.00	15.45	1.00
42	232.3	115.5	18.70 ± 0.08	17.87 ± 0.10	17.36 ± 0.12	0.83	0.51	0.85	0.03
43	136.1	122.0	18.03 ± 0.07	16.69 ± 0.09	16.15 ± 0.24	1.34	0.53	5.24	0.20[a]
44	100.8	126.1	18.61 ± 0.10	16.19 ± 0.04	15.07 ± 0.06	2.42	1.12	14.28	0.60[a]
45	138.3	127.5	14.44 ± 0.02	13.88 ± 0.03	13.77 ± 0.12	0.56	0.11	1.49	—[b]
46	76.8	127.5	18.93 ± 0.14	16.70 ± 0.04	15.17 ± 0.04	2.24	1.52	8.72	0.08[a]
47	58.7	130.3	19.17 ± 0.23	18.41 ± 0.21	17.12 ± 0.12	0.77	1.29	—	0.03[a]
48	188.2	130.5	17.33 ± 0.03	15.71 ± 0.02	14.76 ± 0.02	1.62	0.95	5.51	0.11[a]
49	97.4	134.4	19.18 ± 0.20	18.04 ± 0.11	16.09 ± 0.08	1.14	1.95	—	—[a,c]
50	211.8	137.3	17.76 ± 0.05	16.20 ± 0.03	15.03 ± 0.03	1.56	1.17	3.03	0.09
51	131.2	142.1	16.98 ± 0.03	15.67 ± 0.04	15.15 ± 0.08	1.31	0.51	5.61	0.40[a]
52	132.7	145.4	15.62 ± 0.02	14.12 ± 0.02	13.64 ± 0.05	1.50	0.48	7.60	1.00[a]
53	37.9	144.8	19.64 ± 0.30	18.30 ± 0.13	16.12 ± 0.13	1.33	2.18	—	—[c]
54	120.5	143.9	14.63 ± 0.02	13.90 ± 0.02	13.77 ± 0.04	0.73	0.13	0.28	—[b]
55	58.0	149.0	17.89 ± 0.07	16.96 ± 0.06	16.57 ± 0.04	0.92	0.39	4.37	0.20[a]
56	91.3	149.5	18.14 ± 0.10	16.26 ± 0.09	15.37 ± 0.04	1.89	0.88	9.83	0.40[a]
57	95.8	148.7	18.00 ± 0.09	15.59 ± 0.07	14.30 ± 0.03	2.40	1.30	12.51	0.13[a]
58	93.2	156.1	19.18 ± 0.21	16.51 ± 0.04	15.20 ± 0.03	2.67	1.31	16.30	0.60[a]
59	146.6	149.7	18.16 ± 0.08	16.16 ± 0.04	15.28 ± 0.03	2.00	0.88	10.04	0.40[a]
60	155.2	150.7	16.57 ± 0.03	13.78 ± 0.03	12.55 ± 0.05	2.79	1.23	22.23	2.50[a]
61	204.1	152.0	18.03 ± 0.07	17.36 ± 0.08	17.09 ± 0.09	0.67	0.27	1.93	0.20
62	222.0	153.1	15.59 ± 0.02	14.81 ± 0.03	14.61 ± 0.04	0.78	0.20	0.60	—[b]

continued on next page

Table C.2: *continued*

#	x (pix)	y (pix)	j	h	k	J - H	H - K	A_V	M ($M_\odot$)
(1)	(2)	(3)	(4)	(5)	(6)	(7)	(8)	(9)	(10)
63	51.9	156.1	14.16 ± 0.02	13.10 ± 0.05	12.82 ± 0.03	1.06	0.28	8.49	2.00
64	76.5	156.9	17.14 ± 0.04	16.58 ± 0.05	16.36 ± 0.05	0.57	0.22	1.28	—[b]
65	70.4	161.7	17.50 ± 0.03	16.68 ± 0.04	16.34 ± 0.06	0.82	0.34	3.07	0.20[a]
66	91.2	167.7	17.72 ± 0.07	15.02 ± 0.04	13.37 ± 0.04	2.70	1.65	13.48	0.20[a]
67	59.0	174.3	18.03 ± 0.07	17.00 ± 0.05	16.67 ± 0.10	1.03	0.33	2.29	0.20
68	164.9	176.4	18.40 ± 0.09	16.26 ± 0.02	15.22 ± 0.03	2.14	1.04	12.32	0.80
69	73.5	178.7	19.09 ± 0.15	17.08 ± 0.08	16.02 ± 0.13	2.01	1.06	10.48	0.40
70	117.0	179.2	17.50 ± 0.04	15.55 ± 0.03	14.65 ± 0.05	1.95	0.91	10.36	0.60[a]
71	179.0	181.0	17.78 ± 0.05	15.53 ± 0.02	14.60 ± 0.02	2.25	0.93	13.06	1.00
72	210.3	182.6	18.03 ± 0.07	15.49 ± 0.03	13.91 ± 0.05	2.54	1.57	12.14	0.15
73	215.6	188.5	15.39 ± 0.03	14.76 ± 0.06	14.29 ± 0.03	0.62	0.47	3.09	0.17
74	227.3	190.3	13.82 ± 0.04	12.85 ± 0.05	12.48 ± 0.04	0.98	0.37	8.70	2.50
75	56.3	188.8	19.00 ± 0.17	18.02 ± 0.29	17.88 ± 0.24	0.98	0.14	1.25	—[b]
76	58.5	199.2	16.87 ± 0.05	14.64 ± 0.04	13.89 ± 0.03	2.23	0.75	18.09	2.00
77	224.1	198.8	18.66 ± 0.11	17.90 ± 0.10	17.21 ± 0.12	0.76	0.69	3.01	0.03
78	169.6	209.0	18.97 ± 0.16	16.75 ± 0.04	15.90 ± 0.04	2.22	0.85	12.53	0.60
79	139.8	210.7	15.61 ± 0.01	13.83 ± 0.03	12.91 ± 0.05	1.77	0.92	15.05	2.50
80	138.2	216.1	18.78 ± 0.12	18.14 ± 0.30	16.19 ± 0.14	0.64	1.95	—	—[c]
81	93.2	217.5	18.19 ± 0.08	16.30 ± 0.05	14.94 ± 0.05	1.89	1.36	5.76	0.09
82	63.0	219.3	17.79 ± 0.11	15.76 ± 0.03	15.01 ± 0.05	2.03	0.75	12.80	1.00
83	104.6	225.2	13.73 ± 0.02	12.10 ± 0.03	11.71 ± 0.06	1.63	0.38	13.75	5.00
84	101.3	228.2	16.71 ± 0.06	15.46 ± 0.06	14.89 ± 0.14	1.25	0.57	4.55	0.60
85	126.1	225.7	16.79 ± 0.02	16.05 ± 0.07	15.88 ± 0.03	0.73	0.17	2.04	0.40
86	186.9	228.6	15.70 ± 0.08	14.86 ± 0.06	14.76 ± 0.16	0.84	0.10	1.01	—[b]
87	191.6	231.6	12.44 ± 0.04	11.55 ± 0.03	11.47 ± 0.06	0.89	0.08	7.85	4.00
88	206.6	229.1	19.38 ± 0.16	18.25 ± 0.11	17.57 ± 0.12	1.13	0.69	1.46	0.03
89	74.9	232.7	17.96 ± 0.07	15.77 ± 0.02	14.56 ± 0.05	2.19	1.21	10.46	0.12
90	164.7	232.2	15.59 ± 0.03	13.38 ± 0.03	12.62 ± 0.04	2.21	0.76	18.91	4.00
91	22.3	233.5	12.66 ± 0.03	11.64 ± 0.04	11.42 ± 0.06	1.02	0.22	8.68	4.00
92	113.3	234.7	19.07 ± 0.17	17.26 ± 0.09	16.26 ± 0.06	1.80	1.01	7.33	0.05
93	179.2	20.4	— ± —	18.21 ± 0.14	16.51 ± 0.13	—	1.70	—	—
94	211.6	22.4	— ± —	18.22 ± 0.13	16.87 ± 0.08	—	1.35	—	—
95	143.8	27.6	— ± —	17.50 ± 0.06	15.74 ± 0.05	—	1.76	—	—
96	220.5	40.6	— ± —	17.35 ± 0.06	16.00 ± 0.10	—	1.35	—	—
97	100.7	45.2	— ± —	17.83 ± 0.15	17.42 ± 0.17	—	0.42	—	—
98	166.3	48.7	— ± —	17.74 ± 0.11	14.81 ± 0.09	—	2.93	—	—
99	33.3	56.3	— ± —	17.55 ± 0.08	15.29 ± 0.17	—	2.26	—	—
100	40.2	65.6	— ± —	18.03 ± 0.12	16.80 ± 0.20	—	1.23	—	—
101	76.0	70.0	— ± —	18.40 ± 0.14	16.74 ± 0.18	—	1.66	—	—
102	133.2	79.2	— ± —	18.42 ± 0.14	16.36 ± 0.04	—	2.06	—	—
103	69.1	95.8	— ± —	18.22 ± 0.10	16.68 ± 0.11	—	1.54	—	—
104	75.9	96.2	— ± —	17.38 ± 0.09	15.60 ± 0.03	—	1.78	—	—
105	189.8	99.1	— ± —	18.28 ± 0.17	16.49 ± 0.04	—	1.79	—	—
106	221.0	100.3	— ± —	16.30 ± 0.04	14.80 ± 0.09	—	1.50	—	—
107	177.4	101.9	— ± —	17.35 ± 0.06	15.96 ± 0.08	—	1.38	—	—
108	156.9	103.9	— ± —	16.81 ± 0.12	11.93 ± 0.14	—	4.88	—	—
109	148.5	105.4	— ± —	17.76 ± 0.11	14.69 ± 0.09	—	3.07	—	—
110	108.6	113.5	— ± —	16.72 ± 0.04	14.76 ± 0.04	—	1.97	—	—
111	118.6	110.6	— ± —	17.90 ± 0.07	15.61 ± 0.04	—	2.29	—	—
112	141.5	131.6	— ± —	16.55 ± 0.10	14.32 ± 0.15	—	2.22	—	—
113	199.8	122.2	— ± —	18.61 ± 0.18	16.89 ± 0.14	—	1.72	—	—
114	214.2	125.4	— ± —	17.12 ± 0.06	15.37 ± 0.06	—	1.75	—	—
115	137.7	155.7	— ± —	17.58 ± 0.10	15.19 ± 0.04	—	2.39	—	—
116	160.5	134.9	— ± —	17.82 ± 0.15	16.31 ± 0.11	—	1.51	—	—
117	156.7	142.2	— ± —	16.60 ± 0.04	15.38 ± 0.03	—	1.21	—	—
118	174.6	144.3	— ± —	17.58 ± 0.07	15.65 ± 0.03	—	1.93	—	—
119	191.2	143.9	— ± —	18.10 ± 0.12	17.12 ± 0.08	—	0.98	—	—
120	111.1	160.5	— ± —	18.01 ± 0.10	16.22 ± 0.04	—	1.80	—	—
121	61.9	163.1	— ± —	18.63 ± 0.16	16.26 ± 0.08	—	2.37	—	—
122	163.5	164.0	— ± —	17.51 ± 0.07	15.62 ± 0.03	—	1.89	—	—
123	219.4	164.4	— ± —	18.58 ± 0.19	17.16 ± 0.07	—	1.42	—	—
124	111.3	171.8	— ± —	17.09 ± 0.10	15.82 ± 0.06	—	1.28	—	—
125	102.8	183.4	— ± —	17.71 ± 0.11	15.82 ± 0.06	—	1.88	—	—
126	130.6	188.7	— ± —	17.36 ± 0.06	15.41 ± 0.04	—	1.95	—	—
127	201.7	192.7	— ± —	17.89 ± 0.10	16.34 ± 0.06	—	1.54	—	—
128	211.0	215.7	— ± —	18.10 ± 0.12	16.99 ± 0.11	—	1.11	—	—
129	104.5	216.3	— ± —	16.71 ± 0.08	15.93 ± 0.06	—	0.78	—	—
130	227.6	217.3	— ± —	18.24 ± 0.13	17.49 ± 0.15	—	0.75	—	—
131	22.9	229.7	— ± —	14.55 ± 0.09	12.71 ± 0.08	—	1.83	—	—
132	132.6	229.7	— ± —	18.02 ± 0.15	17.60 ± 0.11	—	0.42	—	—

Table C.3: Photometry table for IRAS 02044+6031. **YSC 3.**

#	x (pix)	y (pix)	j	h	k	J - H	H - K	A_V	M ($M_\odot$)
(1)	(2)	(3)	(4)	(5)	(6)	(7)	(8)	(9)	(10)
1	116.5	28.3	15.45 ± 0.02	14.91 ± 0.02	14.83 ± 0.06	0.54	0.08	—	—[a]
2	133.0	34.6	15.83 ± 0.02	15.17 ± 0.03	14.84 ± 0.06	0.66	0.33	6.28	4.00[a]
3	113.2	34.9	17.99 ± 0.11	15.94 ± 0.04	14.90 ± 0.06	2.05	1.04	14.12	2.50[a]
4	119.3	38.3	17.89 ± 0.08	16.27 ± 0.06	15.77 ± 0.11	1.63	0.49	13.67	4.00[a]
5	144.5	38.7	19.11 ± 0.27	17.35 ± 0.15	16.31 ± 0.08	1.76	1.05	6.48	0.40[a]
6	136.4	40.8	15.13 ± 0.01	14.46 ± 0.02	14.27 ± 0.06	0.67	0.19	3.82	2.50[a]
7	113.9	42.5	17.58 ± 0.07	16.27 ± 0.06	15.49 ± 0.09	1.31	0.78	3.05	0.68[a]
8	124.5	43.5	18.04 ± 0.11	16.21 ± 0.06	15.45 ± 0.10	1.83	0.76	13.98	2.50[a]
9	130.5	45.7	18.05 ± 0.11	16.13 ± 0.06	15.48 ± 0.10	1.92	0.65	14.12	2.50[a]
10	143.6	45.1	18.99 ± 0.26	17.08 ± 0.12	15.90 ± 0.07	1.91	1.18	7.32	0.48[a]
11	130.4	51.1	17.94 ± 0.10	16.36 ± 0.07	15.73 ± 0.11	1.58	0.63	13.73	4.00[a]
12	48.0	26.6	17.79 ± 0.09	16.85 ± 0.10	16.52 ± 0.14	0.94	0.33	3.44	0.80
13	146.0	23.6	18.83 ± 0.20	17.20 ± 0.12	16.99 ± 0.15	1.63	0.22	8.68	1.00
14	91.5	24.9	17.36 ± 0.06	15.65 ± 0.04	14.99 ± 0.10	1.71	0.66	11.80	2.50[a]
15	87.8	30.7	17.54 ± 0.08	15.67 ± 0.04	14.74 ± 0.07	1.86	0.94	12.55	2.50[a]
16	105.1	33.7	17.59 ± 0.07	16.83 ± 0.11	16.46 ± 0.09	0.77	0.37	1.19	—[b]
17	124.5	27.7	16.17 ± 0.03	15.32 ± 0.03	15.18 ± 0.08	0.85	0.14	7.52	4.00[a]
18	223.2	32.4	18.07 ± 0.07	17.02 ± 0.08	16.72 ± 0.08	1.05	0.30	4.42	0.80
19	218.3	46.7	18.54 ± 0.10	17.44 ± 0.11	16.83 ± 0.15	1.10	0.61	1.74	0.33
20	185.7	33.3	14.97 ± 0.02	14.24 ± 0.02	14.10 ± 0.05	0.73	0.14	6.28	4.00
21	37.1	35.9	18.27 ± 0.11	17.28 ± 0.18	16.78 ± 0.19	0.99	0.50	3.07	0.60
22	208.9	36.8	17.78 ± 0.07	16.86 ± 0.08	16.54 ± 0.14	0.91	0.32	3.36	0.80
23	28.2	38.9	16.68 ± 0.03	15.96 ± 0.04	15.81 ± 0.06	0.72	0.15	1.09	—[b]
24	25.0	45.6	17.13 ± 0.05	16.19 ± 0.04	16.15 ± 0.08	0.94	0.04	2.73	1.00
25	21.8	47.6	17.57 ± 0.08	16.94 ± 0.08	16.57 ± 0.11	0.63	0.37	2.31	0.42
26	72.7	38.8	14.30 ± 0.01	13.74 ± 0.01	13.74 ± 0.04	0.56	- —	7.18	10.00[a]
27	72.6	43.8	17.53 ± 0.17	16.20 ± 0.08	15.66 ± 0.11	1.33	0.54	12.22	4.00[a]
28	64.8	41.3	14.64 ± 0.02	13.86 ± 0.06	13.77 ± 0.04	0.79	0.09	8.46	10.00[a]
29	201.5	42.2	17.81 ± 0.09	16.91 ± 0.08	16.82 ± 0.14	0.90	0.09	1.61	—[b]
30	169.7	42.5	16.08 ± 0.02	15.37 ± 0.03	15.07 ± 0.07	0.71	0.30	1.37	—[b]
31	87.2	46.0	16.42 ± 0.05	15.47 ± 0.04	14.99 ± 0.07	0.95	0.48	8.40	4.00[a]
32	93.8	51.4	17.68 ± 0.12	16.83 ± 0.11	16.50 ± 0.19	0.85	0.33	1.58	—[b]
33	61.8	49.1	13.53 ± 0.02	12.86 ± 0.04	12.77 ± 0.06	0.67	0.10	5.01	10.00[a]
34	49.8	50.1	15.19 ± 0.02	14.71 ± 0.03	14.38 ± 0.05	0.48	0.32	3.74	1.45[a]
35	54.8	54.9	16.39 ± 0.03	15.73 ± 0.05	15.37 ± 0.08	0.66	0.36	2.39	2.00[a]
36	109.4	52.7	18.74 ± 0.17	17.31 ± 0.14	16.61 ± 0.19	1.43	0.70	8.02	1.50[a]
37	156.2	54.7	18.54 ± 0.10	17.50 ± 0.09	17.21 ± 0.15	1.04	0.29	4.34	1.00[a]
38	160.9	54.7	18.59 ± 0.11	17.01 ± 0.06	16.64 ± 0.09	1.58	0.36	7.90	1.00
39	158.9	61.6	17.91 ± 0.06	16.32 ± 0.03	15.98 ± 0.06	1.59	0.34	13.68	4.00[a]
40	205.5	55.7	17.73 ± 0.07	16.67 ± 0.11	16.14 ± 0.11	1.06	0.54	4.67	1.00
41	146.8	54.2	18.66 ± 0.20	16.89 ± 0.06	16.12 ± 0.06	1.77	0.77	14.41	3.00[a]
42	228.6	55.1	18.32 ± 0.09	16.85 ± 0.08	15.96 ± 0.07	1.48	0.88	4.29	0.51
43	30.1	58.5	17.22 ± 0.05	16.48 ± 0.05	16.44 ± 0.07	0.74	0.04	1.47	—[b]
44	138.0	62.5	15.60 ± 0.01	14.17 ± 0.02	13.53 ± 0.03	1.43	0.64	12.12	10.00[a]
45	130.3	62.9	16.73 ± 0.03	15.34 ± 0.03	14.65 ± 0.06	1.39	0.69	9.52	2.50[a]
46	127.8	68.0	17.67 ± 0.08	16.33 ± 0.08	15.26 ± 0.07	1.34	1.08	1.05	0.71[a]
47	137.5	72.0	18.08 ± 0.10	16.42 ± 0.09	15.69 ± 0.09	1.65	0.73	14.25	4.00[a]
48	50.2	63.4	13.20 ± 0.02	12.71 ± 0.03	12.67 ± 0.06	0.49	0.04	3.77	10.00[a]
49	148.2	63.9	17.10 ± 0.05	15.56 ± 0.04	14.98 ± 0.04	1.54	0.58	10.81	2.50[a]
50	205.3	65.9	18.27 ± 0.13	16.42 ± 0.05	15.61 ± 0.06	1.85	0.81	11.94	2.50
51	189.0	67.3	16.40 ± 0.02	15.66 ± 0.02	15.41 ± 0.05	0.74	0.24	2.36	1.50
52	193.3	72.2	17.87 ± 0.07	16.80 ± 0.07	16.25 ± 0.09	1.07	0.55	3.82	0.80
53	190.1	79.7	18.73 ± 0.17	17.66 ± 0.14	16.91 ± 0.12	1.07	0.75	0.25	0.31
54	167.9	68.6	17.97 ± 0.13	17.00 ± 0.11	16.46 ± 0.22	0.97	0.54	0.68	0.42
55	56.9	70.1	16.43 ± 0.03	15.00 ± 0.05	14.32 ± 0.04	1.43	0.67	14.62	10.00[a]
56	98.7	71.0	15.79 ± 0.05	15.07 ± 0.02	15.47 ± 0.20	0.72	-0.40	6.22	4.00[a]
57	159.1	75.3	16.43 ± 0.02	14.97 ± 0.05	14.33 ± 0.04	1.46	0.65	14.68	10.00[a]
58	180.6	74.5	18.05 ± 0.11	16.89 ± 0.11	16.25 ± 0.10	1.16	0.64	2.19	0.46
59	33.5	78.2	16.88 ± 0.05	16.16 ± 0.09	15.99 ± 0.06	0.73	0.17	1.59	—[b]
60	143.3	77.8	16.83 ± 0.06	16.20 ± 0.06	15.59 ± 0.07	0.63	0.61	4.03	0.68[a]
61	48.5	80.4	17.67 ± 0.09	16.84 ± 0.08	16.76 ± 0.14	0.84	0.07	1.52	—[b]
62	213.0	79.9	16.05 ± 0.02	15.44 ± 0.02	15.41 ± 0.05	0.61	0.03	1.13	—[b]
63	233.6	80.5	17.59 ± 0.10	16.58 ± 0.10	16.45 ± 0.11	1.01	0.13	4.18	1.00
64	23.7	82.8	17.06 ± 0.07	16.27 ± 0.10	15.97 ± 0.05	0.79	0.31	2.31	1.00
65	122.8	99.3	17.43 ± 0.06	15.43 ± 0.06	13.34 ± 0.18	2.00	2.08	—	—[a,c]
66	179.5	84.6	16.66 ± 0.03	15.82 ± 0.05	15.42 ± 0.05	0.84	0.40	3.27	1.50
67	161.7	86.9	18.85 ± 0.19	17.60 ± 0.16	16.90 ± 0.19	1.24	0.70	2.79	0.31[a]
68	161.6	92.5	17.28 ± 0.04	15.78 ± 0.03	15.30 ± 0.05	1.49	0.48	11.27	2.50[a]
69	122.4	88.0	16.49 ± 0.09	14.50 ± 0.03	13.55 ± 0.06	1.98	0.96	19.34	20.00[a]
70	84.0	89.3	15.42 ± 0.02	14.90 ± 0.03	15.13 ± 0.26	0.53	-0.23	4.89	4.00[a]
71	106.6	91.6	14.36 ± 0.04	12.85 ± 0.04	12.36 ± 0.07	1.51	0.49	12.35	20.00[a]
72	147.0	88.9	18.55 ± 0.15	16.93 ± 0.07	16.68 ± 0.14	1.61	0.25	13.85	3.00[a]
73	72.7	90.7	15.03 ± 0.02	14.29 ± 0.02	14.15 ± 0.04	0.73	0.14	3.65	2.50[a]
74	52.8	93.4	14.97 ± 0.02	14.36 ± 0.01	14.18 ± 0.05	0.61	0.19	3.29	2.50[a]
75	30.2	96.7	17.42 ± 0.05	16.59 ± 0.05	16.42 ± 0.08	0.83	0.17	2.17	0.80

continued on next page

Table C.3: *continued*

#	x (pix)	y (pix)	j	h	k	J - H	H - K	A_V	M ($M_\odot$)
(1)	(2)	(3)	(4)	(5)	(6)	(7)	(8)	(9)	(10)
76	36.8	97.0	18.34 ± 0.09	17.01 ± 0.08	16.60 ± 0.10	1.33	0.41	6.70	1.50[a]
77	31.9	106.2	16.07 ± 0.02	15.45 ± 0.03	15.18 ± 0.04	0.62	0.27	5.20	3.00[a]
78	65.7	96.8	14.42 ± 0.03	13.53 ± 0.02	13.43 ± 0.07	0.89	0.10	7.90	10.00[a]
79	162.4	103.3	12.60 ± 0.02	12.03 ± 0.02	11.98 ± 0.05	0.57	0.05	5.91	20.00[a]
80	73.1	103.4	17.74 ± 0.06	16.88 ± 0.10	16.65 ± 0.10	0.86	0.23	1.76	—[b]
81	137.2	105.9	16.57 ± 0.04	15.58 ± 0.04	15.31 ± 0.07	0.99	0.27	8.92	4.00[a]
82	119.0	110.6	15.14 ± 0.01	14.53 ± 0.03	14.26 ± 0.05	0.61	0.27	3.78	2.50[a]
83	124.7	113.3	17.19 ± 0.06	15.99 ± 0.07	15.73 ± 0.13	1.20	0.26	11.04	4.00[a]
84	45.4	112.9	17.95 ± 0.08	16.93 ± 0.09	16.49 ± 0.09	1.02	0.44	5.14	1.50[a]
85	63.0	113.0	18.64 ± 0.21	17.29 ± 0.09	16.81 ± 0.14	1.35	0.49	7.62	1.50[a]
86	182.3	116.8	18.31 ± 0.09	17.40 ± 0.14	16.49 ± 0.09	0.91	0.91	2.85	0.37
87	154.8	118.1	18.47 ± 0.14	17.69 ± 0.12	16.88 ± 0.13	0.78	0.81	3.77	0.31[a]
88	210.1	117.9	17.99 ± 0.11	16.93 ± 0.11	16.54 ± 0.12	1.06	0.39	4.18	0.80
89	107.6	118.8	18.89 ± 0.21	17.86 ± 0.28	16.18 ± 0.09	1.03	1.68	—	—[a, c]
90	90.7	120.8	15.07 ± 0.04	14.46 ± 0.07	14.21 ± 0.08	0.62	0.25	3.58	2.50[a]
91	99.1	121.2	14.64 ± 0.02	14.15 ± 0.02	14.02 ± 0.08	0.49	0.14	2.17	2.50[a]
92	232.8	122.0	17.35 ± 0.06	16.22 ± 0.04	16.04 ± 0.07	1.13	0.18	5.69	1.50
93	225.3	123.5	16.68 ± 0.03	15.69 ± 0.03	15.69 ± 0.06	0.99	—	4.84	2.00
94	231.4	141.0	16.80 ± 0.04	16.04 ± 0.04	16.17 ± 0.17	0.76	-0.13	1.48	—[b]
95	164.4	127.4	17.85 ± 0.08	16.92 ± 0.10	16.45 ± 0.09	0.93	0.47	1.77	0.60
96	79.5	131.4	15.09 ± 0.01	14.53 ± 0.02	14.38 ± 0.05	0.56	0.15	3.57	2.50[a]
97	80.6	137.1	16.63 ± 0.04	15.98 ± 0.05	15.46 ± 0.10	0.65	0.52	3.18	0.75[a]
98	203.7	131.0	17.69 ± 0.08	16.95 ± 0.10	16.29 ± 0.07	0.74	0.67	3.18	0.45
99	218.0	135.9	17.77 ± 0.10	16.57 ± 0.09	15.99 ± 0.10	1.20	0.58	4.95	1.00
100	218.5	140.1	17.24 ± 0.06	16.58 ± 0.09	15.90 ± 0.10	0.66	0.68	4.22	0.56
101	113.8	137.3	15.67 ± 0.02	15.02 ± 0.02	14.64 ± 0.08	0.65	0.39	2.07	1.23[a]
102	37.1	144.3	16.25 ± 0.02	15.53 ± 0.04	15.43 ± 0.05	0.72	0.10	1.87	1.50
103	131.9	138.3	16.89 ± 0.04	16.09 ± 0.04	15.68 ± 0.10	0.80	0.41	4.07	2.00[a]
104	103.2	140.4	15.15 ± 0.02	13.99 ± 0.04	12.91 ± 0.04	1.16	1.08	1.13	2.68[a]
105	193.2	142.4	15.19 ± 0.02	14.49 ± 0.02	14.32 ± 0.05	0.70	0.17	6.90	4.00
106	69.8	142.8	17.70 ± 0.09	17.36 ± 0.23	16.80 ± 0.15	0.34	0.56	—	0.35[a]
107	80.0	146.0	15.57 ± 0.02	15.07 ± 0.03	14.69 ± 0.07	0.50	0.38	3.97	1.20[a]
108	205.2	153.5	16.68 ± 0.07	15.68 ± 0.04	15.11 ± 0.06	1.00	0.56	0.85	0.90
109	95.4	148.9	17.26 ± 0.06	16.36 ± 0.13	15.99 ± 0.07	0.90	0.37	2.95	1.50[a]
110	149.7	149.1	17.75 ± 0.05	17.02 ± 0.07	16.77 ± 0.11	0.73	0.25	1.20	—[b]
111	155.9	150.0	18.21 ± 0.07	17.30 ± 0.09	16.95 ± 0.12	0.91	0.35	2.80	0.60
112	153.7	161.0	18.62 ± 0.12	17.90 ± 0.19	16.84 ± 0.11	0.71	1.06	6.45	0.29
113	76.0	159.4	13.74 ± 0.01	12.91 ± 0.02	12.84 ± 0.05	0.83	0.07	9.67	20.00
114	119.9	156.1	18.04 ± 0.11	16.95 ± 0.12	16.08 ± 0.10	1.09	0.87	0.44	0.47[a]
115	193.4	155.5	17.97 ± 0.10	16.67 ± 0.08	16.09 ± 0.08	1.30	0.59	5.68	1.00
116	91.8	160.8	18.46 ± 0.13	17.76 ± 0.27	16.84 ± 0.19	0.70	0.92	5.63	0.30
117	201.2	161.5	17.09 ± 0.04	16.40 ± 0.07	16.04 ± 0.07	0.69	0.36	1.03	—[b]
118	60.3	166.5	17.02 ± 0.02	16.28 ± 0.05	16.11 ± 0.07	0.74	0.18	0.88	—[b]
119	68.3	169.6	16.61 ± 0.02	15.74 ± 0.02	15.41 ± 0.05	0.87	0.33	3.15	1.50
120	62.8	174.4	17.67 ± 0.05	16.74 ± 0.06	16.62 ± 0.09	0.93	0.12	3.05	0.80
121	112.9	164.9	18.62 ± 0.17	17.75 ± 0.22	16.92 ± 0.18	0.87	0.83	2.78	0.30
122	108.4	168.7	17.00 ± 0.04	16.30 ± 0.06	15.89 ± 0.09	0.70	0.41	1.60	0.60
123	219.7	166.9	17.04 ± 0.06	15.92 ± 0.04	15.61 ± 0.08	1.12	0.32	4.76	1.50
124	27.2	168.7	16.70 ± 0.03	15.78 ± 0.05	15.55 ± 0.04	0.92	0.23	3.49	1.50
125	135.5	174.2	14.71 ± 0.01	13.97 ± 0.01	13.74 ± 0.03	0.74	0.23	2.15	3.00
126	140.3	179.8	17.09 ± 0.05	16.15 ± 0.06	15.92 ± 0.11	0.94	0.23	2.61	1.00
127	43.7	171.1	18.20 ± 0.09	17.12 ± 0.14	16.67 ± 0.08	1.09	0.45	4.85	0.80
128	166.3	171.3	17.23 ± 0.05	16.36 ± 0.04	16.21 ± 0.09	0.87	0.14	2.91	1.00
129	20.0	183.5	16.96 ± 0.04	16.21 ± 0.05	16.19 ± 0.13	0.75	0.02	1.98	1.00
130	52.1	181.4	15.50 ± 0.02	14.98 ± 0.02	14.94 ± 0.05	0.53	0.03	0.73	—[b]
131	69.2	180.4	15.34 ± 0.12	14.82 ± 0.03	14.44 ± 0.05	0.53	0.38	3.55	1.38
132	103.0	180.6	18.09 ± 0.11	17.16 ± 0.09	16.66 ± 0.15	0.93	0.50	2.46	0.60
133	232.5	181.3	17.59 ± 0.08	16.58 ± 0.08	16.20 ± 0.10	1.01	0.38	4.19	1.00
134	150.4	182.8	15.57 ± 0.01	15.00 ± 0.02	14.63 ± 0.03	0.57	0.37	2.95	1.25
135	150.7	190.0	17.67 ± 0.07	16.62 ± 0.06	16.18 ± 0.07	1.05	0.44	4.46	1.00
136	110.3	183.9	18.69 ± 0.16	18.16 ± 0.23	17.26 ± 0.20	0.54	0.90	—	0.24
137	127.8	199.3	16.74 ± 0.02	16.20 ± 0.04	16.26 ± 0.07	0.55	-0.07	4.27	2.00
138	130.6	206.6	16.58 ± 0.02	15.84 ± 0.03	15.62 ± 0.04	0.74	0.22	0.85	—[b]
139	172.1	194.5	17.54 ± 0.06	16.70 ± 0.06	16.30 ± 0.09	0.84	0.40	2.56	0.80
140	119.3	196.5	17.78 ± 0.07	16.68 ± 0.12	16.46 ± 0.11	1.10	0.21	4.87	1.00
141	26.2	199.0	16.49 ± 0.04	15.59 ± 0.02	15.25 ± 0.06	0.90	0.34	4.17	2.00
142	77.1	203.0	14.56 ± 0.01	13.91 ± 0.01	13.94 ± 0.05	0.65	-0.03	1.57	—[b]
143	83.0	207.5	17.98 ± 0.11	17.14 ± 0.09	16.60 ± 0.20	0.84	0.54	0.88	0.39
144	20.5	210.7	16.59 ± 0.02	16.07 ± 0.04	15.63 ± 0.09	0.52	0.44	4.16	0.69
145	195.2	209.7	16.35 ± 0.04	15.58 ± 0.04	15.54 ± 0.04	0.77	0.04	2.25	1.50
146	172.8	212.9	17.09 ± 0.05	16.50 ± 0.06	15.99 ± 0.07	0.59	0.52	3.82	0.55
147	167.1	215.5	14.94 ± 0.01	14.51 ± 0.01	14.38 ± 0.03	0.43	0.12	4.43	5.00
148	160.3	216.6	17.84 ± 0.08	17.06 ± 0.11	16.55 ± 0.14	0.77	0.52	1.59	0.40
149	203.8	215.8	14.51 ± 0.02	13.89 ± 0.02	13.56 ± 0.06	0.62	0.34	1.41	—[b]
150	146.5	223.7	18.26 ± 0.09	17.37 ± 0.10	17.10 ± 0.15	0.89	0.27	2.92	0.60
151	126.0	223.4	17.66 ± 0.07	17.02 ± 0.11	16.47 ± 0.09	0.64	0.55	3.52	0.42

continued on next page

Table C.3: *continued*

# (1)	x (pix) (2)	y (pix) (3)	j (4)	h (5)	k (6)	J - H (7)	H - K (8)	A_V (9)	M ($M_\odot$) (10)
152	61.8	224.2	16.45 ± 0.04	15.60 ± 0.03	15.30 ± 0.06	0.85	0.30	2.66	1.50
153	56.0	225.9	15.98 ± 0.02	14.93 ± 0.02	14.55 ± 0.04	1.04	0.38	9.67	4.00
154	77.2	227.0	14.61 ± 0.02	14.10 ± 0.01	13.94 ± 0.04	0.51	0.16	4.93	4.00
155	71.5	232.5	16.95 ± 0.11	16.20 ± 0.07	15.75 ± 0.11	0.75	0.46	1.42	0.65
156	118.9	228.2	17.73 ± 0.08	16.74 ± 0.08	16.60 ± 0.15	1.00	0.14	3.32	0.80
157	220.9	234.6	16.34 ± 0.02	15.61 ± 0.09	15.28 ± 0.06	0.73	0.33	2.18	1.50
158	130.4	23.4	—	17.26 ± 0.11	16.65 ± 0.22	—	0.61	—	—
159	84.3	31.7	—	16.42 ± 0.09	14.97 ± 0.08	—	1.46	—	—
160	177.7	34.6	—	17.90 ± 0.24	16.82 ± 0.29	—	1.08	—	—
161	93.9	38.9	—	17.31 ± 0.17	16.54 ± 0.12	—	0.77	—	—
162	153.0	50.7	—	17.54 ± 0.09	16.97 ± 0.13	—	0.57	—	—
163	134.0	70.0	—	17.07 ± 0.15	16.22 ± 0.15	—	0.85	—	—
164	118.3	65.9	—	17.08 ± 0.16	16.34 ± 0.13	—	0.74	—	—
165	126.8	85.2	—	15.61 ± 0.09	14.30 ± 0.09	—	1.31	—	—
166	130.6	85.0	—	16.52 ± 0.19	14.06 ± 0.08	—	2.46	—	—
167	230.6	160.7	—	17.63 ± 0.13	16.75 ± 0.09	—	0.88	—	—
168	131.0	169.2	—	17.75 ± 0.19	16.39 ± 0.15	—	1.36	—	—
169	72.1	181.8	—	15.03 ± 0.03	15.06 ± 0.08	—	-0.03	35.46	20.00
170	137.9	208.8	—	17.84 ± 0.20	17.20 ± 0.15	—	0.65	—	—
171	41.1	195.8	—	17.89 ± 0.21	16.99 ± 0.12	—	0.90	—	—
172	65.8	229.0	—	17.27 ± 0.12	16.53 ± 0.16	—	0.74	—	—

Appendix D

The Catalog

This is the result of the complete study and main information of each YSC in a graphic way: The Catalog. Its detailed content is as follows (see Fig. D.1):

1. RGB image. Is the composite color image made with the three NIR filters, K-red, H-green, and J-blue on a 3.6×3.6 arcmin field aproximatelly, the borders in some images have been removed, and central coordinates may be shifted from that of the IRAS source (see Table 2.2). See also the optical frames in Appendix A for comparison.

2. J vs. J-H color-magnitude diagram. MS is represnted with a long dash - dotted line; addopted isochrone with mass values along it, and the shifted isochrone to the average value of extinction $< A_V >$ are in solid lines; yellow dashed line connecting these isochrones show the completeness mass limit value. Also shown are the completeness limit, the extinction vector of 10 mag and the average error cross. Blue points correspond to stars lying along the reddened MS in color-color diagram, while red dots correspond to reddened CTT+Ae/Be stars; both into the cluster radius. Small black dots correspond to field (or extended population) stars.

3. J-H vs. H-K color-color diagram. Solid line represents the MS and the GB from Bessell and Brett 1988; dahed line shows the CTTS+Ae/Be loci (Meyer 1996), extended up to H-K=1.5; dotted lines are along the extinction vector direction. Also average error cross is shown. Blue and red points correspond to reddened MS and CTT+Ae/Be stars respectively, these are two groups very well defined here. Small black dots correspond to field (or extended population) stars.

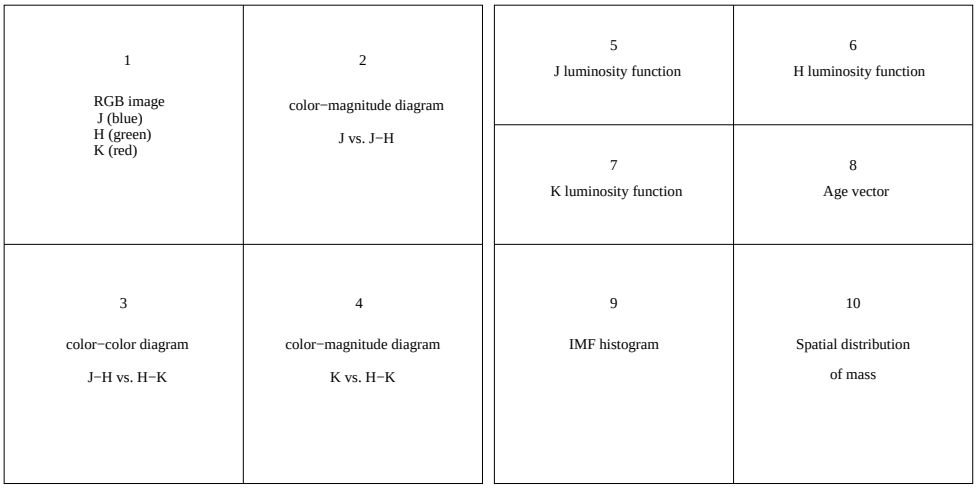

Figure D.1 Frames content in the Catalog of the 38 YSCs.

4. K vs. H-K color-magnitude diagram. Same as J vs. J-H diagram, except for the magent dots which correspond to stars with H and K photometry but without J counterpart.

5. J luminosity function (JLF). Histogram of the number of stars into the radius cluster (grey) and into the completeness area (blue), see §7.1.1. Red dashed line shows the diferential completeness limit.

6. H luminosity function. Same as JLF.

7. K luminosity function. Same as JLF.

8. Age vector. This is the plot of the vector obtained by the inverse matrix transformation of the observed-JLF. Matrix is formed with theoretical values of JLF at six different ages (see §6.2).

9. IMF histogram. Log-log plot of the mass histogram of stars from the mass completened cluster.

10. Spatial distribution of mass. Aqui falta definir colores para masas.

Additionally, at top of frames there is information of source names and physical parameters calculated along this work. They are: YSC number, associated IRAS source, nearest Sharpless HII region, distance in kpc and distance modulus in parentesis, number of stars into the cluster radius with JHK photometry,

cluster radius in pc, average surface density in pc^{-2}, average extinction in magnitudes, estimated age in Myr and age of the associated isochrone in parentesis, mass completeness limit in $M_{\odot}$, number of stars from the mass completened cluster, slope value for IMF power law, total mass in the completened cluster, and number of massive stars into the cluster.

Sh-187	D = 3.0 kpc (12.39 mag)
N = 71	r_C = 0.79 pc
$<\Sigma>$ = 36.10 pc^{-2}	$< A_V >$ = 12.15±4.89 mag

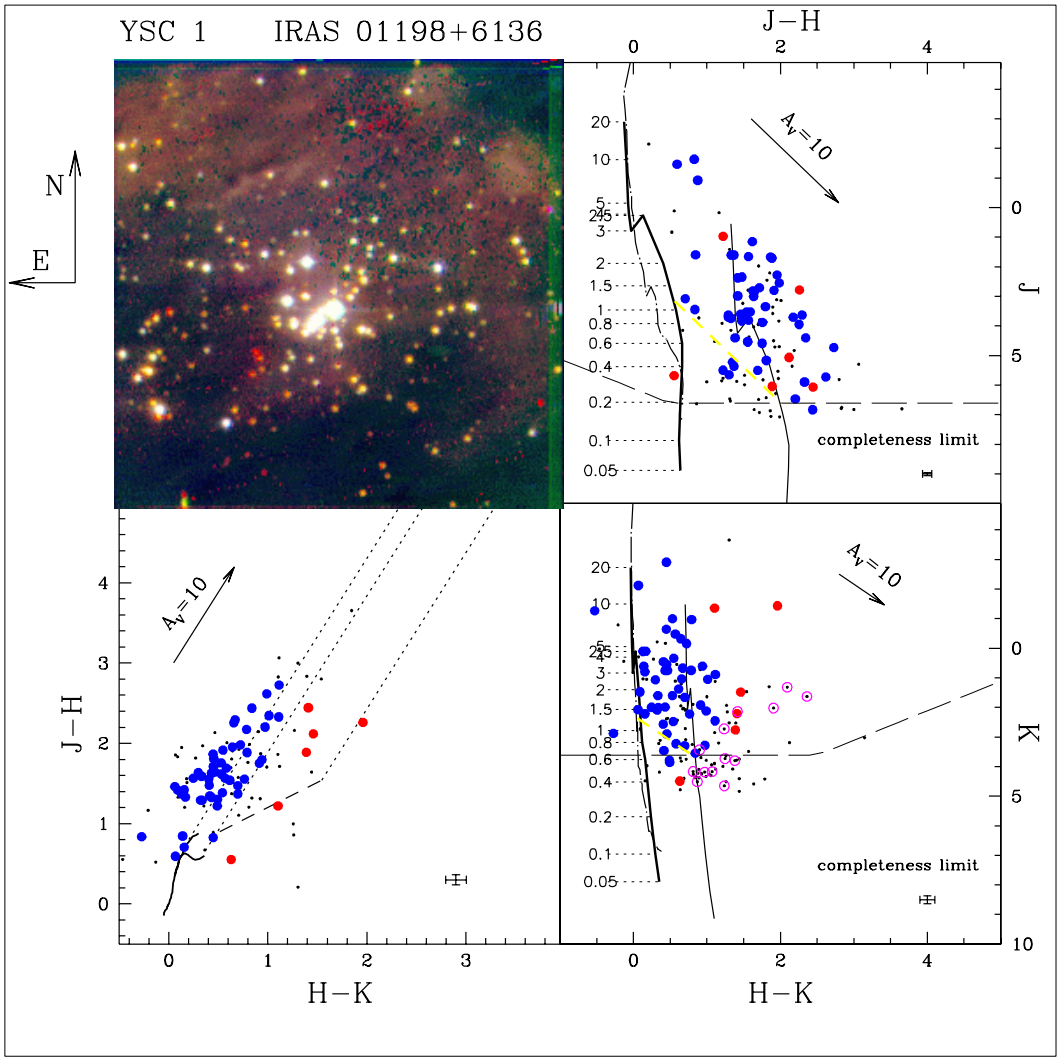

E = 2.2 Myr (3 Myr)	M_{lim} = 1.03 $M_\odot$
N_C = 45	Γ = 0.18±0.24
M_T = 298.2 $M_\odot$	N_M = 7

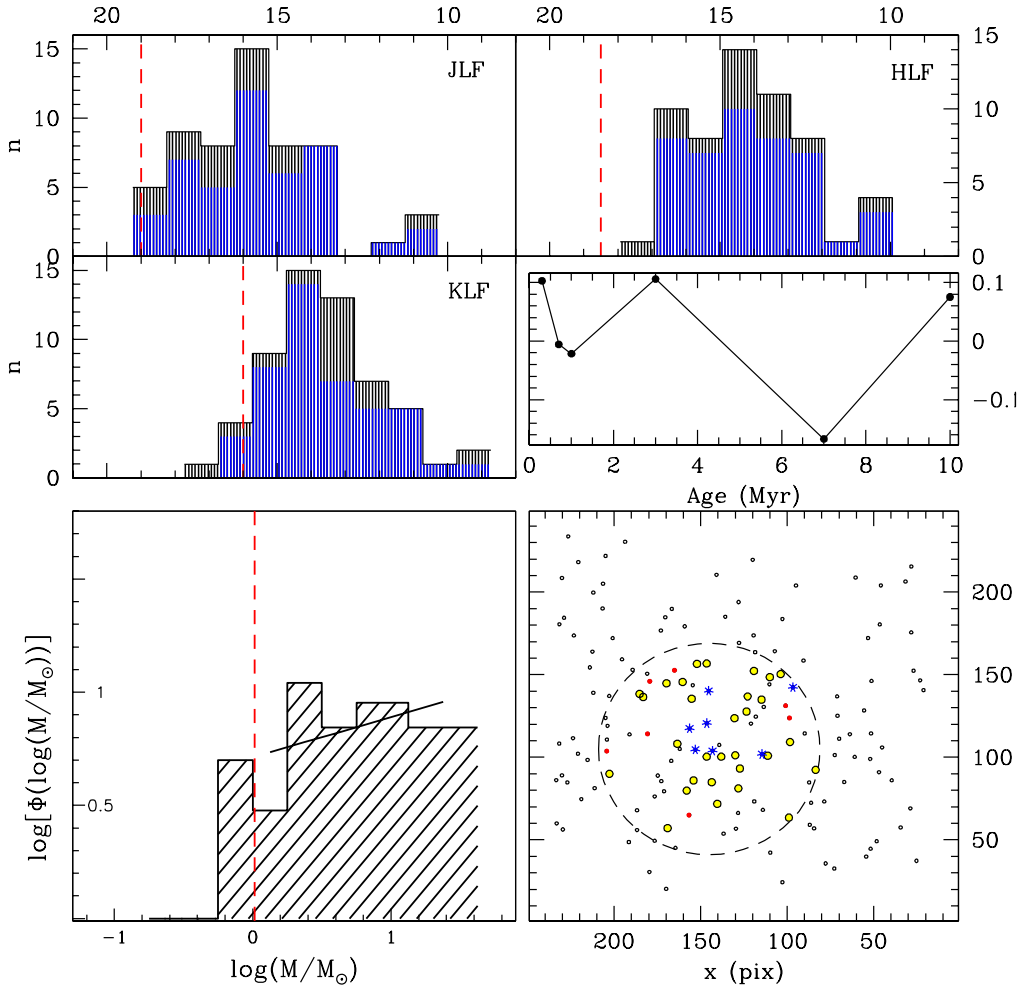

Sh-187	D = 1.0 kpc (10.00 mag)
N = 86	r_C = 0.40 pc
$< \Sigma >$ = 171.32 pc^{-2}	$< A_V >$ = 8.9±4.5 mag

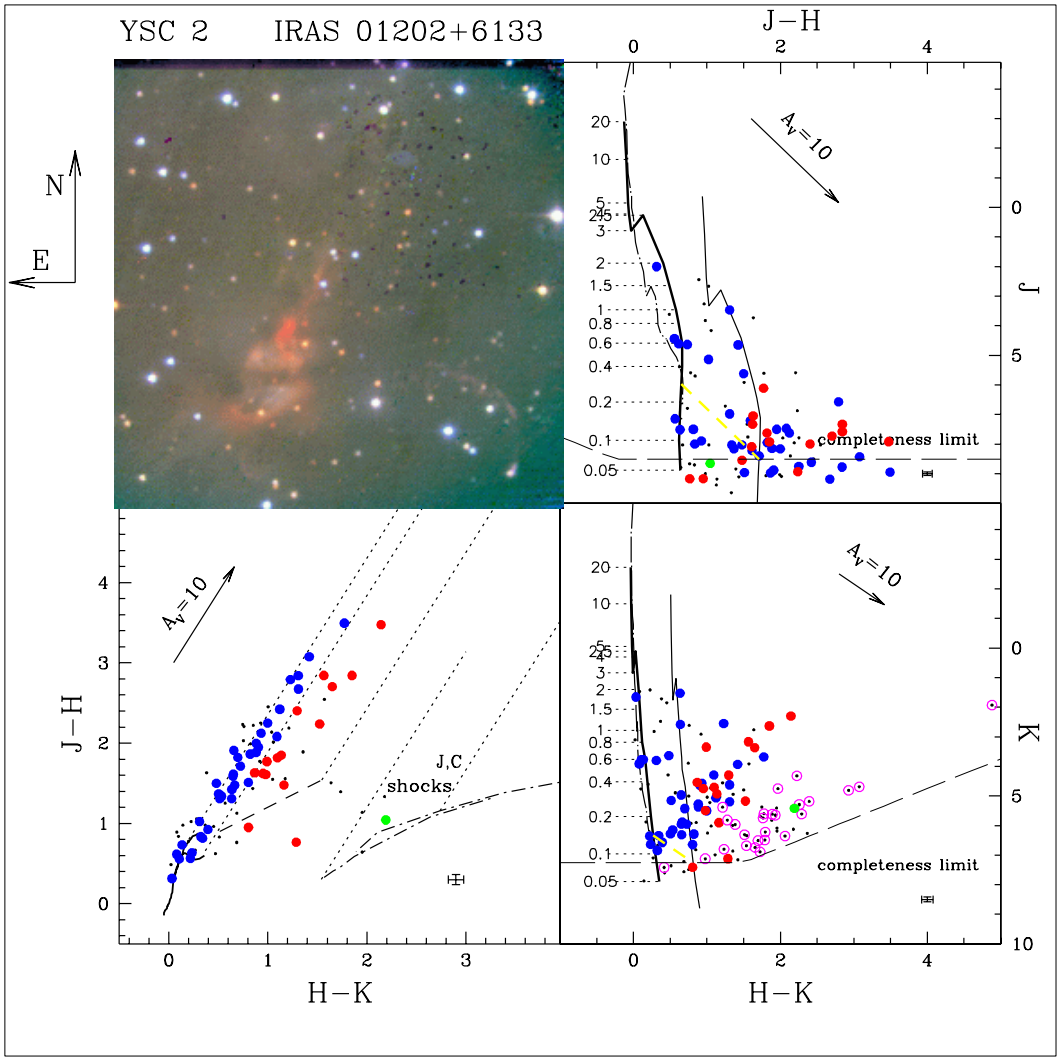

E = 2.0 Myr (3 Myr)	M_{lim} = 0.3 $M_\odot$
N_{CC} = 34	Γ = -0.93±0.54
M_T = 18.2 $M_\odot$	N_M = 0

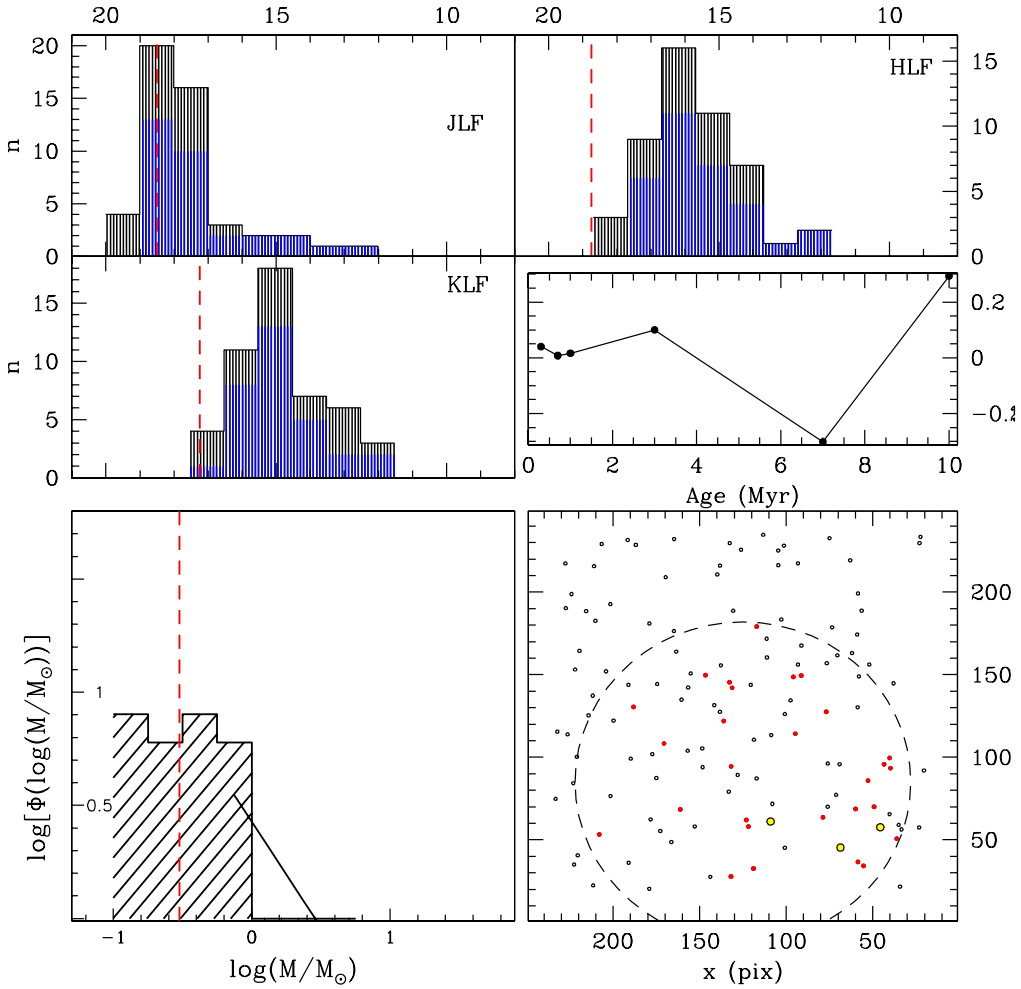

Sh-189	D = 5.8 kpc (13.82 mag)
N = 78	r_C = 1.67 pc
$< \Sigma >$ = 8.87 pc^{-2}	$< A_V >$ = 7.6±4.6 mag

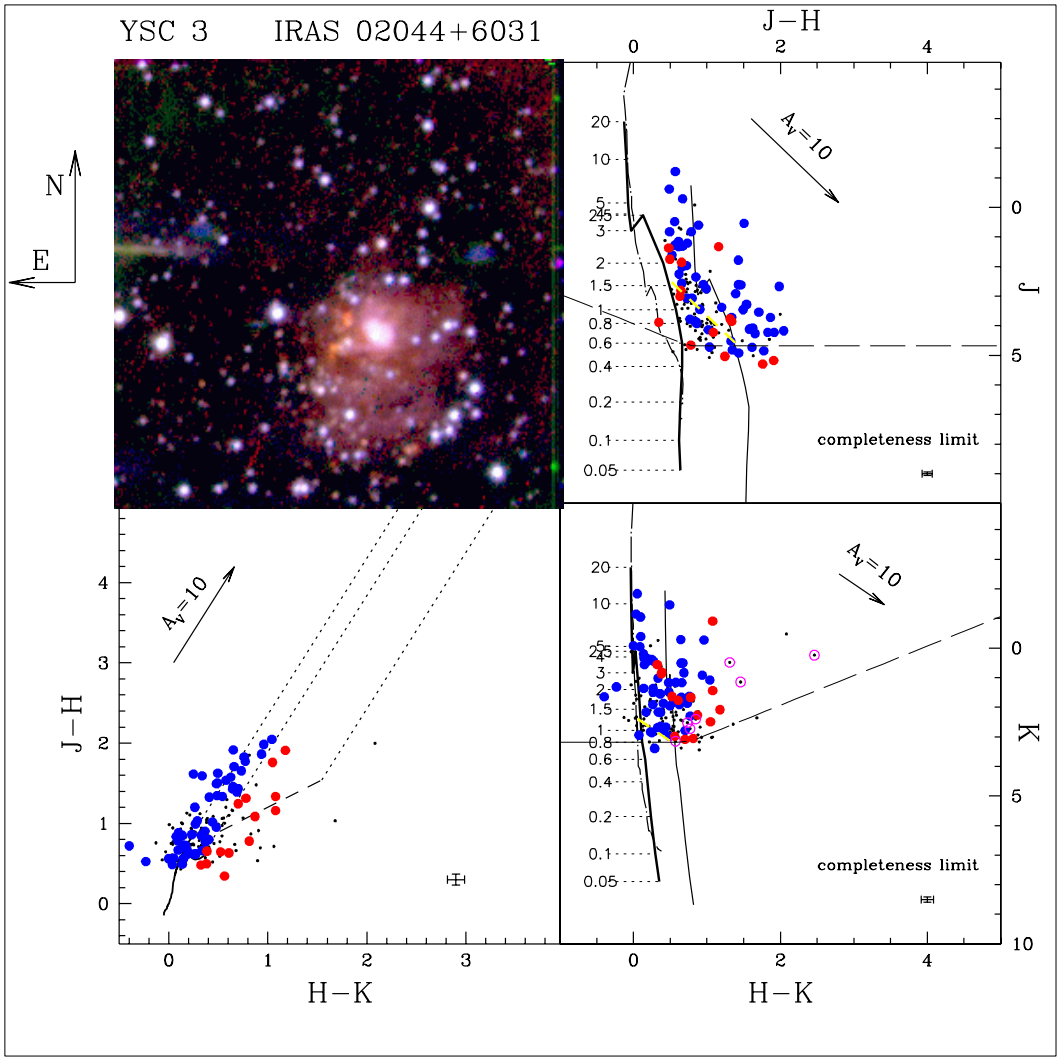

E = 2.1 Myr (3 Myr)	M_{lim} = 1.2 $M_\odot$
N_{CC} = 47	Γ = -1.14±0.17
M_T = 162.2 $M_\odot$	N_M = 1

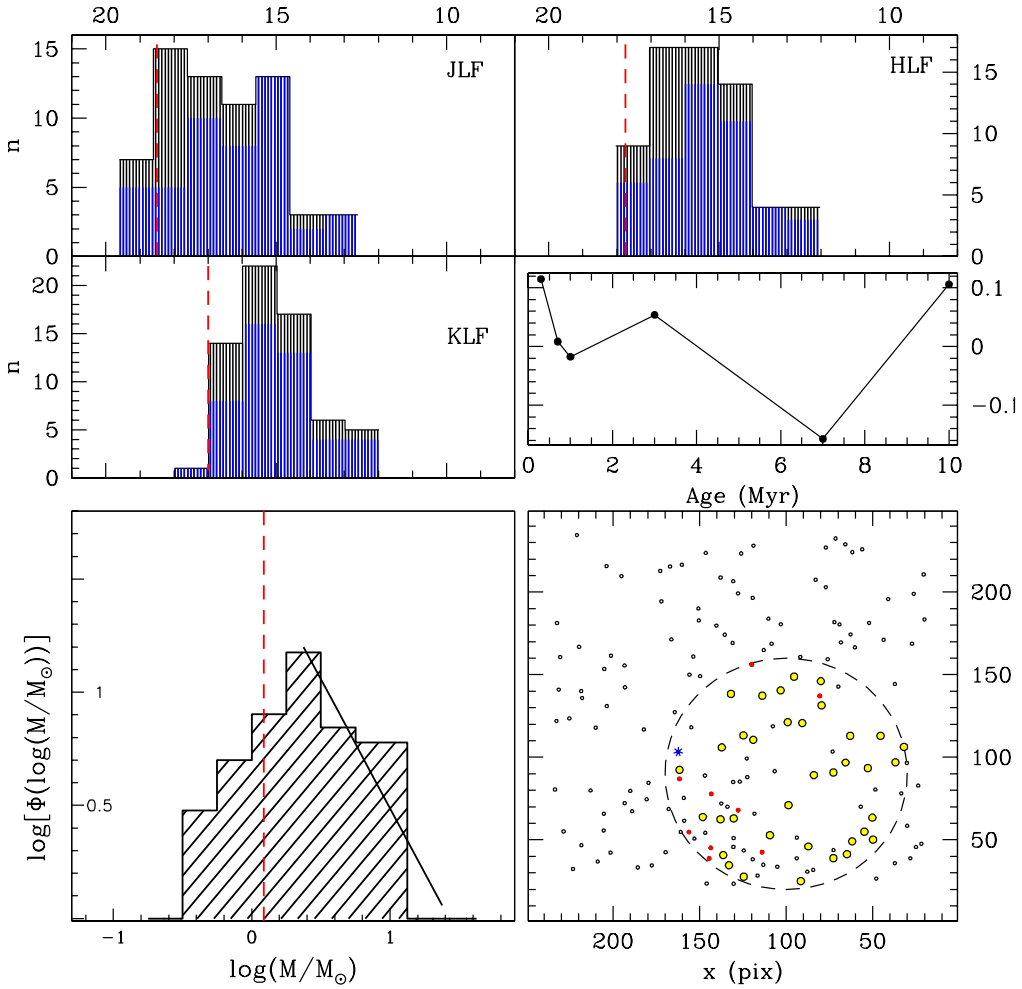

Appendix E

Resúmen extenso en español

E.1 Introducción

Observacionalmente se ha constatado que las estrellas se forman en grupos; en cúmulos ricos de cientos a muchos miles de estrellas, o en pequeños grupos conteniendo del orden de 10 a unas decenas de estrellas. Es solo recientemente, sin embargo, que las propiedades de los cúmulos jóvenes están siendo bien caracterizadas. Los cúmulos de estrellas jóvenes profundamente enterrados ofrecen un excelente laboratorio para estudiar las fases mas tempranas en la evolucion estelar. Estos cúmulos ricos han sido revelados a través de observaciones con detectores sensibles en el infrarrojo cercano (NIR = near infra-red) de nubes moleculares cercanas.

La colección de estrellas jóvenes con edades de 10 Myr o menos halladas en asociación con mubes moleculares son referidas como la "población estelar inicial". Estudiando la población estelar inicial en nuestra Galaxia es un problema fundamental, porque la determinación de las características globales e individuales pueden proveer un mejor entendimiento de los efectos de la fragmentación de nubes moleculares en la formación de cúmulos estelares jóvenes (YSCs = young stellar clusters) y de cómo las masas estelares individuales son adquiridas y distribuidas. Mas aun, ellas nos pueden llevar al conocimiento de la contribución de masa de la población estelar joven en la Vía Láctea y en otras galaxias.

Una característica global de los YSCs es como la masa de la nube paterna se distribuye en estrellas. Esta distribución inicial de las masas estelares es conocida como la función inicial de masa (IMF= initial mass function). Nuestro conocimiento de la IMF viene de estudios de muestras de estrellas limitadas en volúmen. La IMF se estudió primero en la vecindad solar y en este caso las correcciones evolutivas a la distribución de masa observada fueron necesarias. En los

cúmulos estelares jóvenes las distribuciones de masa observadas revelan la historia de la formación estelar desde la fragmentación de la nube hasta ahora, pero ya que el proceso de formación estelar continúa, el resultado final integrado de la nube en formación y en consecuencia la IMF verdadera, son realmente desconocidas.

Sin embargo, hasta ahora, los cúmulos estelares jóvenes proveen los mejores laboratorios para estudiar la IMF en un rango de 0.5 a 15 $M_{\odot}$. Las ventajas observacionales son las siguientes (Meyer et el. 2000): 1) debido a su juventud, hay un mínimo de correcciones evolutivas a la distribución de masa al momento actual, y por lo tanto la distribución de masa actual puede ser considerada como la IMF; 2) su juventud excluye la posibilidad de que los miembros del cúmulo vayan muy lejos de su lugar de nacimiento debido a movimientos propios; 3) las observaciones son mas sensibles a objetos de baja - masa porque la relación masa - luminosidad, M-L, para estrellas en la fase pre - secuencia principal (PMS = Pre main sequence) no es una función tan empinada de la masa como para estrellas en la secuencia principal (MS = main sequence); 4) ellos no están contaminados por estrellas en la línea de visión debido a que son compactos; y 5) no están contaminados por estrellas de fondo debido a la presencia de gas molecular, el cual provee un velo natural para evitarlas.

El concepto generalmente aceptado de la IMF es, el número de estrellas por intervalo logarítmico de masa. La notación en ley de potencias mas comunmente usada es:

$$\Gamma = \frac{d\,log\Phi(logM)}{d\,logM}, \tag{E.1}$$

donde Γ es conocido como el **índice de la IMF**. Otra notación usada es $\gamma = d\phi/dM$ y por lo tanto, Γ y γ se relacionan por $\Gamma = \gamma + 1$.

En esta notación la IMF de Salpeter (1955) sería Γ_{Sal} = -1.35 en un intervalo de masa de 3 a 10 $M_{\odot}$. Miller & Scalo hallaron una IMF de tres segmentos o leyes de potencia: Γ=-0.4 en un intervalo de 0.1 to 1 $M_{\odot}$, -1.5 en un intervalo de 1 to 10 $M_{\odot}$ y -2.3 para masas $>$ 10 $M_{\odot}$. Este tercer intervalo fue mas tarde corregido al valor de Γ = -1.2 por Scalo en 1986. El estudio de Kroupa et al. en 1993 de estrellas en la vecindad solar (dentro de un radio de 5.2 pc del Sol) con masas entre 0.08 y 100 $M_{\odot}$, muestra que la IMF puede ser aproximada con Γ: 0.3 a -0.85 para $0.08 < M < 0.5$ $M_{\odot}$, -1.2 para $0.5 \leq M \leq 1$ $M_{\odot}$ y -1.7 para $M >$1 $M_{\odot}$. Cualquiera de estas IMFs, especialmente la dos primeras, han sido usadas en la literatura y asumidas como leyes universales, sin embargo la universalidad de la IMF es todavia un tema abierto (e.g. Scalo 1998).

Revisiones recientes sobre la IMF basadas en trabajo teórico y observacional han sido presentadas por Scalo 1998, Clarke 1998, Larson 1998 y 1999, Elmegreen

1999 y Meyer et al. 2000. Revisiones importantes de la IMF en el contexto galáctico y extragálactico están contenidas en la conferencia de la ASP por Gilmore & Howell 1998.

El índice de la IMF como una función del promedio de log M de los 61 cúmulos y asociaciones en la Vía Láctea y la LMC (Large Magellanic Cloud) presentada por Scalo 1998 (Fig.5) y reproducida aquí en la Fig. 1.1, resume varios artículos sobre la IMF en un amplio intervalo de masa e incluye tanto estrellas de campo, como cúmulos jóvenes y mas viejos. Esta gráfica sugiere que $0< \Gamma <$-0.5 para $0.1< M <0.8$ $M_\odot$, lo cual está en concordancia con las estrellas de campo. Arriba de ~ 1 $M_\odot$, la dispersion de valores del índice de la IMF es muy grande ($\Delta\Gamma \sim 1$). Scalo concluye que no hay evidencia para una acumulación de puntos alrededor del valor de Salpeter (-1.35). También que las incertidumbres son tan grandes que la IMF todavía no se conoce o que las variaciones significativas observadas son reales. Mas adelante él hace notar que si las variaciones en la IMF son reales, ellas "aparentemente no dependen mucho de la metalicidad, densidad estelar, o el radio galactocéntrico, sino que debe depender de alguna combinación desconocida de variables del ambiente o si no, la IMF, como es concevida usualmente, no es una función de probabilidad estadísticamente bien definida". Este punto de vista contrasta don el de Larson 1999, quien basado en la misma figura concluye que "ninguna evidencia clara ha sido hallada de cualquier dependencia sistemática de la IMF con cualquier propiedad de los sistemas estudiados, y esto ha llevado al punto de vista ampliamente sostenido actualmente de que la IMF es universal, al menos en el universo local".

Para los estudios de evolución galáctica Scalo 1998 sugiere el uso de la siguiente forma de la ley de potencias en tres segmentos:

$$\begin{array}{rcll} \Gamma & = & -0.2 \pm 0.3 & 0.1 - 1\ M_\odot \\ & & -1.7 \pm 0.5 & 1 - 10\ M_\odot \\ & & -1.3 \pm 0.5 & 10 - 100\ M_\odot \end{array} \qquad \text{(E.2)}$$

donde los símbolos $\pm$ pueden ser interpretados como una medida de las incertidumbres empíricas y/o las variaciones reales de la IMF.

El requerimiento mínimo para que el colapso ocurra es el criterio de Jeans clásico de que la auto-gravedad de un núcleo denso debe sobrepasar su presión térmica. Para una temperatura y densidad dadas, esta masa de Jeans esta fijada. Considerando una "esfera de Bonnor-Ebert" críticamente estable (Larson 1998), con una temperatura de nube molecular típica (10K) y una presión no-térmica (3×10^5 cm $^{-3}$ K), el radio resultante y la masa de Jeans son cerca de 0.03 pc

y 0.7 $M_\odot$, respectivamente. Lo último es típicamente observado en la estructura de las nubes moleculares (ver revisiones de Evans 1999 y Williams et al. 2000).

Las nubes moleculares son dominadas por presiones turbulenta y magnética a grandes escalas y por presión térmica a pequeñas escalas. La transición entre los dos regímenes es de hecho lo que define la escala de Jeans cuando la última es calculada asumiendo un balance de presión entre un grumo isotérmico soportado térmicamente y el medio ambiente turbulento. La masa de Jeans es proporcional a $T^2/P^{1/2}$, donde T es la temperatura y P la presión en nubes con formación estelar. En estos términos, las nubes con temperaturas mas altas se esperaría que formaran estrellas con una masa característica mayor (Larson 1985). Pero de hecho, las nubes con temperaturas mas altas generalmente también tienen presiones mucho mas altas, así que hay una cancelación parcial de este efecto cuando la masa de Jeans es calculada (Larson 1999). Esto sugiere que $T^2/P^{1/2}$ es aproximadamente constante para diferentes ambientes (Elmegreen 1999). Sin embargo, una pregunta abierta y difícil es si la distribución de masas estelares depende ligera o fuertemente de las condiciones físicas iniciales en el ambiente de la mube molecular (e.g. temperatura y densidad del ambiente, condiciones de fragmentacion, etc.).

Por otro lado, los procesos de acreción y aglomeración son importantes en particular para formar estrellas masivas, pero un claro entendimiento de este proceso es un problema abierto. Asi que, un modelado confiable de la parte superior de la IMF es necesario. Las observaciones ciertamente proveeran restricciones importantes. También, los estudios teóricos que proveen trazas evolutivas PMS son crucialmente necesarias para estrellas con masas mayores que 5 $M_\odot$. Evidencia observacional relevante muestra que las estrellas masivas recientemente formadas siempre estan rodeadas por cúmulos de estrellas menos masivas, donde las estrellas mas masivas tienden a estar asociadas con cúmulos mas grandes (Hillenbrand 1995, Testi et al. 1999, Garay & Lizano 1999).

Con el uso de los arreglos IR, en los últimos 10 años, los estudios de la población estelar inicial, i.e. la coleccion de estrellas jóvenes con edades $\leq$10 Myr halladas en asociación con nubes moleculares, proveen una información muy valiosa acerca de la IMF. Este tema de investigación es actualmente muy activo con la mayoria de los estudios llevandose a cabo en el IR-cercano. Una revisión de este tema esta presentado en Zinnecker et al. 1993, donde el trabajo inicial teórico y observacional está resumido tanto en nubes moleculares gigantes donde se encuentran las asociaciones OB, como en complejos de nubes de masa intermedia.

En una revisión mas reciente, Meyer et al. 2000, se presenta la mayoria del trabajo reciente relacionado con la IMF, tanto teórico como observacional.

Meyer et al. 2000 señalan que una cuestión fundamental en los estudios de la formación estelar es la distribución de masas estelares formadas dentro de las nubes moleculares. Estimaciones cuantitativas de la IMF han sido hechas con técnicas de paralaje, fotométricas y espectroscópicas, así como de combinaciones de ellas. Dos puntos importantes son resaltados por estos autores: si, los cambios de la IMF de una sola ley de potencias a una distribución mas compleja entre 1-5 $M_{\odot}$ es crucial, ya que provee una restricción importante en las teorías para el origen de las masas estelares; y, la demostración clara de un pico en la IMF en el extremo de las masas bajas. Un esfuerzo observacional considerable ha sido enfocado en establecer si o no tal pico existe, y si es así, en caracterizar su localización y ancho. Por ejemplo, un survey espectroscópico óptico de cerca de 1000 estrellas localizadas $\sim$ 2 pc de las estrellas del Trapecio, revelan que la función de masa del cúmulo cambia en $\sim$0.2 $M_{\odot}$ (Hillenbrand 1997).

Ya que la IMF detallada no está disponible para muchos cúmulos estelares jóvenes, Meyer y sus colaboradores proveen una gruesa estimación de la IMF por el cociente del número de estrellas de alta a intermedia-baja masa en los pocos YSCs cercanos estudiados. Ellos "conservativamente" concluyen que "la mayoría de las regiónes de formación estelar compactas, extremadamente jóvenes, exhiben distribuciónes de masa emergente consistentes con las que han sido encontradas de la IMF de estrellas de campo dentro de nuestra habilidad de distinguir cualquier diferencia". Esto refuerza la universalidad de la IMF, pero su muestra de cúmulos es muy pequeña y mas trabajo es aun necesario. Finalmente, ellos mencionan la complejidad del marco teórico en el formidable problema de el origen de la IMF.

En esta tesis nosotros estudiamos la IMF en una muestra de 40 cúmulos estelares jóvenes a lo largo del Brazo de Perseo. El Brazo de Perseo fué seleccionado porque está localizado lejos del centro galáctico y de la región de Orión, evitando asi su posible contaminación. También, estudios previos muestran evidencia de que la formación estelar se esta llevando a cabo a lo largo de él y una región en los brazos externos de la Galaxia provee un conjunto de YSCs en un intervalo de distancias pequeño (Capítulo 2). La descripción de las observaciones y el proceso de reducción de datos son presentados en el Capítulo 3. El estudio provee información de 6298 estrellas en los YSCs. Nosotros proponemos un metodo fotométrico multicolor para estimar los tamaños de los cúmulos, densidades estelares (Capítulo 4) y edades (Capítulo 5), así como la extinción y masa individual de estrellas de cúmulo (Capítulos 5 y 6). Nosotros usamos las funciones de luminosidad para estimar la edad de los cúmulos y diagramas de diagnóstico para distinguir las poblaciones estelares en ellos. Las edades de la población distribuida o estrellas de campo local son obtenidas y comparadas con las edades de los cúmulos. Las masas estelares son obtenidas para con-

struir distribuciónes de masa que llevan a la IMF de los YSCs, confiando en un tratamiento uniforme de los datos. Una comparación entre cúmulos es discutida tanto en el índice de la IMF como en la distribución espacial de masas (Capítulo 6). Las imágenes, programas y tablas de datos fotométricos son presentadas en los Apéndices A, B y C respectivamente. Nosotros hemos compilado un catálogo presentado en el Apéndice D, que contiene todos los datos importantes de los 40 cúmulos -individualmente-, obtenidos en nuestro trabajo, los cuales creemos que serán útiles para trabajo futuro. Finalmente, un resúmen y las conclusiones se presentan en el Capítulo 7.

E.2 Criterios de selección de la muestra

Nuestra meta principal en este trabajo es el estudio de la población estelar en regiónes de formación estelar (SFR, star forming región). Hemos escogido buscar fuentes en el Brazo de Perseo porque contiene varias SFRs (por ej. W3-5, Gem OB1, Cyg OB1), su localización en la parte externa de la Galaxia garantiza menor contaminación de las estrellas de Poblacion II y es observable desde un observatorio norteño.

Existen varios criterios para la búsqueda de trazadores de formación estelar, basados principalmente en los flujos de fuentes infrarrojas del catálogo de fuentes puntuales PSC/IRAS (Point Source Catalog / Infra - Red Astronomical Satellite). La Tabla 2.1 resume algunos criterios adoptados por diferentes grupos de investigación donde los trazadores de formación estelar tales como las protoestrellas, máseres de H_2O, núcleos de nubes moleculares gigantes, regiónes HII ultracompactas, regiónes HII, fuentes IRAS brillantes, han sido hallados exitosamente (ver también a tabla 4 de Palagi et al. 1993).

Nosotros adoptamos los siguientes cuatro criterios para las fuentes IRAS que pudieran estar asociadas a cúmulos de estrellas recién formados.

1. **Que estuvieran en el Brazo de Perseo**. La zona en la que se extienden nuestras fuentes observadas en coordenadas galácticas es $\boldsymbol{l} \epsilon$ (70°,200°) y $\boldsymbol{b}$ ϵ (-5°,5°).

2. **Cerca de una región HII pequeña**. Buscamos en el catálogo de Sharpless 1959, y escogimos regiónes HII con diámetro menor que 6 pc (a la distancia que hallamos en la literatura), que puedieran estar provocando nueva formación estelar en sus alrededores, hasta un radio de 60 pc.

3. **Colores infrarrojos (IR)**. Escogimos fuentes con una distribución espectral de energia creciente hacia el lejano IR de tal forma que $1\ Jy \lessapprox F_{12\mu m} <$

$F_{25\mu m} < F_{60\mu m} < F_{100\mu m}$, esta es una característica general de los objetos estelares jóvenes (YSOs = Young Stellar Objects, Chan & Henning 1996). Además restringimos los colores IR con:

$$\begin{aligned} log(F_{60\mu m}/F_{25\mu m}) &\gtrsim 0.3 \\ log(F_{25\mu m}/F_{12\mu m}) &\gtrsim 0.4 \end{aligned} \tag{E.3}$$

4. **Flujo en 100μ m alto**. Consideramos las fuentes con $F_{100\mu m}$ de 500 a 1000 Jy, porque los granos de polvo de las nubes moleculares absorben la radiación de las estrellas enterradas y la re - emiten en el lejano IR.

De este modo, obtuvimos 150 fuentes candidatas a ser cúmulos jóvenes enterrados. De éstos, 50 regiónes fueron observadas con filtros J,H y K (i.e. 30% de hallazgos exitosos). De las fuentes restantes cerca de un 10-15% son buenas candidatas para observar en el futuro. También de nuestra muestra estimamos que cerca del 10% pueden ser YSOs profundamente enterrados y serian buenos candidatos a ser observados en el IR medio (MIR = Mid Infra-Red).

De las 50 fuentes IRAS observadas, restringimos nuestra muestra a 38 porque algunas caian fuera de los limites del Brazo de Perseo, la fotometría no estaba completa o el número de estrellas detectadas era demasiado pequeño. La Tabla 2.2 lista estas 38 fuentes donde se encontró clara evidencia de contener un cúmulo estelar joven. Las distancias varian de 1 a 9 kpc en toda la muestra y el valor promedio es de 3.4 $\pm$ 1.6 kpc. Las luminosidades varian de 2 - 900 $\times$ 10^3 $L_\odot$.

E.3 Observaciones y reducción de datos

Las observaciones se llevaron a cabo con la cámara IR CAMILA, instalada en el telescopio de 2.1 m en San Pedro Mártir, operado por el Observatorio Astronómico Nacional, en Baja California, México. Una descripción general del instrumento se presenta en Cruz-González et al. 1994.

Se uso el reductor focal f/4.5 de CAMILA, dando una escala de placa de 0.86 "/ pix y un campo de visión de 3.6' $\times$ 3.6' para el detector NICMOS 3 (HgCdTe) de 256 $\times$ 256 pixeles. La longitud de onda central y el ancho de banda de las bandas mas observadas son las siguientes: K' (2.125 μm, $\Delta\lambda = 0.35$ μm, Mauna Kea K'), H (1.60 μm, $\Delta\lambda = 0.27$ μm) y J (1.20 μm, $\Delta\lambda = 0.28$ μm).

Las imagenes fueron tomadas en cinco temporadas de observación: en 1996, Noviembre 2-5 (N/96); en 1997, Enero 23-27 (E/97), Junio 25-30 (J/97) y Diciembre 7-12 (D/97); y en 1998, Enero 5-8 (E/98). Durante la cobertura de la

tercera temporada, J/97, el cuarto cuadrante de CAMILA estuvo "ciego", por eso obtuvimos imagenes en forma de "L".

Para cada campo (150) a observar se siguió un procedimiento de dos pasos. Primero, tomamos exposiciones de corto-tiempo (snap-shots) en la fuente y en el cielo, de 24 seg en el filtro K, para seleccionar regiónes donde un patrón de varias estrellas acumuladas era evidente. Después las regiónes con estas características (50) fueron seleccionadas para exposiciones mas largas en los filtros J,H y K. Algunas regiónes que mostraron nebulosidades interesantes tambien fueron seleccionadas para observarse con el filtro de banda angosta de hidrógeno molecular H_2 v=1-0 S(1) (2.122 μm, $\Delta\lambda = 0.02$ μm) (ver Salas et al. 1998 y Porras et al. 2000).

Se tomaron un conjunto de 9 imagenes por región, 5 en fuente y 4 en cielos aledaños formando una cruz. Las imagenes en fuente fueron procesadas restandoles la mediana de los cielos, y las imagenes resultantes fueron "aplanadas" usando conjuntos de campos planos de alta y baja iluminación al anochecer. La Tabla 3.1 resume los datos observacionales de las 38 regiónes que presentamos en este trabajo.

Las imágenes individuales sirvieron para construir mosaicos RGB con K (Red), H (Green) y J (Blue). Casi todas las fuentes caen en regiónes de alta extinción y los cúmulos son prácticamente invisibles en el óptico. En NIR, los cúmulos exhiben muchas estrellas, uno o varios objetos muy enrojecidos, y nebulosidades características de estas zonas, donde el gas no ha sido convertido completamente en estrellas y/o barrido por vientos estelares y jets.

La reducción de datos observacionales se llevo a cabo con el paquete de rutinas de fotometría para campos llenos de IDL/DAOPHOT. Algunas adaptaciones fueron necesarias debido a la presencia de gas y polvo en las regiónes que dificultaba la construcción de la PSF (point spread function), es decir, el modelo del perfil de la luz estelar en una imagen dada. Como resultado, obtuvimos listas de la posición de 6298 estrellas y su magnitud (instrumental) en los tres filtros con un error fotométrico $< 7\%$, presentandose los errores mas grandes en estrellas inmersas en zonas con nebulosidad o con compañeras muy cercanas.

La calibración de flujo se obtuvo de la observación de las estrellas estándares de UKIRT, y después las magnitudes se transformaron al sistema homogeneo de Glass-Johnson, usando las ecuaciones de transformación de Bessell y Brett 1988.

E.4 Densidad superficial de estrellas

Por lo pronto, la única estimación de distancia que tenemos para nuestras fuentes proviene de la literatura, pero no una estimación bajo el mismo método es necesaria. Si existiera un error en la estimación de la distancia de $\pm$ 1 kpc, esto implicaría un error en $\pm$ 1 pc en el radio de la región observada dentro del campo de CAMILA. La distribución de distancias muestra dos concentraciones, una a $\sim$ 2 kpc, y otra menos prominente a $\sim$ 6 kpc, en concordancia con la presencia de dos brazos espirales externos de la Galaxia.

Resulta interesante colocar una submuestra de YSCs a la distancia promedio de 3.5 kpc, (ver Fig. 4.2) y observar las similitudes de estos YSCs. Todos estan asociados a una nebulosidad roja con una concentración estelar en una distribución casi circular. Para calcular el radio de los cúmulos, suponemos una distribución esférica de estrellas con mayor número en su centro. La Fig. 4.3 muestra los perfiles de densidad superficial de estrellas, las líneas punteadas corresponden al radio del cúmulo que le asociamos a cada YSC y que definimos como el 15% ($\sim 3\,\sigma$) de su pico de densidad superficial. De esta forma, obtuvimos valores de radios que están listados en la Tabla 4.1. La mayoría de los cúmulos tienen radios entre 0.5 y 2 pc, y el valor promedio en toda la muestra es de 0.89 $\pm$ 0.47 pc.

La densidad superficial promedio de los cúmulos, $< \Sigma > = \mathrm{N} \,/\, \pi\ \mathrm{r}_C^2$, varía de 3 a 220 estrellas / pc^2, y su concentración estelar es menor por un factor ~ 3 que la de los cúmulos globulares.

E.5 Resultados fotométricos: edad y masa

Desde los años 60's y especialmente a través de los 70's (e.g. Grasdalen et al. 1973, Strom et al. 1975, Vrba et al. 1975), los diagramas J-H vs. H-K han sido usados como diagramas de diagnóstico para estudiar la población estelar joven enterrada en una región particular. En la Fig. 5.1 se muestran cuatro zonas para distinguir poblaciones estelares de acuerdo con la localización de estrellas en este diagrama (e.g. Meyer 1996; Hillenbrand et al. 1995; Carpenter et al. 1993). El diagrama incluye la secuencia principal (MS), la rama de las gigantes (GB = giant branch) tomada de Koorneef 1983 y Bessell & Brett 1988 y transformada al sistema Glass-Johnson. La ley de enrojecimiento estándar (Bessell & Brett 1988) está representada por el vector de extinción $\vec{A}_V$=10 mag.

La región **A** corresponde a las estrellas de la ZAMS enrojecidas a lo largo del vector A_V. Esta zona puede contener estrellas enrojecidas de tipo temprano y

tardío, así como algunas estrellas T-Tauri desnudas (WTTS = weak T-Tau stars).

La región **B** está poblada por estrellas T-Tauri clásicas (CTTS = classical T-Tau stars), por encima del CTTS loci (extendido a H-K = 1.5 mag) descrito por Meyer 1996 y Hillenbrand et al. 1995; es decir, aquellas estrellas de baja masa que están en el proceso de acrecer material y con un disco de polvo característico que produce su exceso infrarrojo.

La región **C** está poblada por estrellas con exceso IR debido a una geometría mas complicada que un disco, e incluye a estrellas Ae/Be de Herbig y a candidatos a proto - estrellas (con A_V de hasta 20 mag y H-K > 2).

Finalmente la región **D** es el lugar teóricamente determinado por Smith 1995 para choques J y C asociados a componentes intensas de objetos Herbig - Haro (HH) enterrados, en el caso de algunos cumulos si esta zona estaba ocupada, fueron observados en hidrogeno molecular (ver Salas et al. 1998 y Porras et al. 2000).

La población estelar de los YSCs se presenta en la Tabla 5.1. La población de estrellas en cada región puede ser dividida en **miembros del cúmulo** y **estrellas de campo**, las cuales son miembros de la población extendida de fuentes alrededor del cúmulo. También, la Tabla 5.1, muestra el número de estrellas en las regiónes **A**, **B/C** y **D** correspondientes a estrellas MS, estrellas CTT+Ae/Be y candidatos a emisión de objetos HH, respectivamente.

La Fig. 5.4 muestra algunos ejemplos de las funciones de luminosidad en las tres bandas J, H y K. Las líneas verticales punteadas señalan los límites de completez diferenciales, que es la magnitud a la cual el 99% de las estrellas artificialmente añadidas a la imagen, son recuperadas bajo el proceso de reducción fotométrica (Carpenter et al. 1997). En promedio, estos valores para la muestra son 18.2 ± 0.6, 17.6 ± 0.7 y 16.8 ± 0.6 para J, H y K respectivamente.

Hemos desarrollado una forma de estimación de edad de un YSCs en base a su función de luminosidad observada en J. Escogimos el filtro J porque provee una estimación mas confiable de la emisión fotosférica real de las estrellas con exceso IR. Para calcular las edades de los YSCs, proponemos el siguiente método:

1. usamos un intervalo de luminosidad que va de 0.75 a 7.75 magnitudes absolutas, con 26 intervalos de 0.25 mag en los histogramas del modelo de Strom et al. 1993. Este modelo supone formación de estrellas en forma simultánea, usa las isocronas de D'Antona & Mazzitelli y asume la IMF de Miller & Scalo;

2. los histogramas teóricos, 6 en total, a 0.3, 0.7, 1, 3, 7 y 10 Myr, son tratados como columnas de la matriz de transformación $\widehat{M}$, entonces la dimensión de $\widehat{M}$ es de 26×6;

3. es posible recuperar cualquier vector de luminosidad en J, JLF, simplemente por

$$\overrightarrow{JLF} = \widehat{M}\ \overrightarrow{\delta}$$

donde $\overrightarrow{\delta}$ se define como un vector delta de edades (e.g. $\overrightarrow{\delta}$ = [0,0,0,1,0,0] reproduce la JLF teórica a 3 Myr);

4. como contamos con las funciones de luminosidad observadas (JLF_{obs} en cada cúmulo, entonces su edad puede ser calculada por

$$\overrightarrow{E} = \widehat{M}^{-1}\ \overrightarrow{JLF}_{obs}.$$

donde los elementos del vector $\vec{E}$ se pueden interpretar como la distribución de edades de todas las estrellas en el cúmulo, y se puede tomar como la edad representativa (mas probable) del YSC al punto con el valor máximo, evitando los extremos.

Las edades así determinadas aparecen en la Tabla 5.3 y algunos de los vectores de edad están graficados en la Fig. 5.5. Las edades estimadas caen en el intervalo de 1.1 a 5.5 Myr, mientras que para las estrellas de campo la edad varía de 1.2 a 18.1 Myr. Ambos valores son consistentes con la edad esperada de una nube molecular gigante (GMC = giant molecular cloud) de 10^{6-7} Myr.

Queremos ahora estimar las masas de las estrellas en los YSCs, para ello necesitamos conocer la masa de estrellas a lo largo de isocronas PMS en el diagrama J vs. J-H, el cual es el equivalente del diagrama Hertzprung - Russell (HR) pero en infrarrojo.

En la Fig. 5.7 se muestran las escalas de masa de las isocronas a edades de 0.1, 0.3, 1, 3, 10, 30 y 100 Myr. Para construirlas, hicimos uso de la relación

$$J = 4.74 - 2.5\,log\,(L/L_{\odot}) - BC(T_e) - (V - J) \qquad \text{(E.4)}$$

donde L es la luminosidad y BC(T_e) es la corrección bolométrica como función de la temperatura efectiva T_e. Las trazas evolutivas que usamos para estrellas con masa $0.05 < M / M_{\odot} < 2.5$ fueron las de D'Antona & Mazzitelli 1994, y para $2.5 < M / M_{\odot} < 20$, las de Hillenbrand et al. 1995.

Usamos el diagrama J vs. J-H para estimar la extinción de las estrellas MS enrojecidas (región **A**), trayéndolas a lo largo del vector de extinción, hacia la isocrona previamente calculada. Con ayuda del diagrama J-H vs. H-K, estimamos la extinción interestelar de estrellas que caen en la región **B**, trayéndolas a lo largo

del vector de extinción hacia el CTTS loci. El promedio de la extinción $< A_V >$, de todas las estrellas (MS + CTTS + Ae/Be) en los cúmulos se presenta en la columna (2) de la Tabla 6.1. En general, todos los YSCs muestran valores $< A_V >$ mayores que ~ 4 mag y cerca del 20% de la muestra tiene una extinción promedio mayor a 10 mag.

Para la asignación de masa a cada estrella de los cúmulos jóvenes, primero nos fijamos en las estrellas de la región **A** y de la misma manera que encontramos su extinción en el diagrama J vs. J-H, asignamos su masa de acuerdo a la escala de masas a lo largo de la isocrona. Para las estrellas en la región **B**, estimamos su masa usando las relaciones empíricas de Carpenter et al. 1993:

$$\log M = -0.25\ M_H + 0.44$$
$$\log M = -0.24\ M_K + 0.24$$

donde M_H y M_K son las magnitudes de las bandas H y K, no - corregidas por extinción. Debido a que estas relaciones son el resultado de un estudio en estrellas de la nube molecular de Taurus, nosotros estamos intrínsecamente asumiendo que las estrellas CTT y Ae/BE de cúmulos en el Brazo de Perseo, son similares a las de Taurus.

Ahora, definimos el límite de completez en masa, M_{lim}, como el valor de la masa que resulta de la proyección del punto P a lo largo del vector de extinción $\vec{A}_V$ (ver Fig. 6.2); P es la intersección de la isocrona corrida por el valor promedio de la extinción al cúmulo, y el límite de completez fotométrico. M_{lim} es entonces el valor al cual una muestra de estrellas en un cúmulo es considerada completa en masa.

De este modo, encontramos que todos los cúmulos (40) son completos hasta 2 $M_\odot$; de éstos, 29 son completos hasta 1.2 $M_\odot$ y sólo 14 cúmulos son completos hasta una masa de 0.6 $M_\odot$. Los valores de M_{lim} están listados en col. (3) de la Tabla 6.1.

La masa total de los cúmulos completos oscila entre 8 y 320 $M_\odot$, y 14 / 40 YSCs tienen una masa total mayor a 100 $M_\odot$. Mas aun, hacemos notar que 12 / 14 cúmulos masivos, contienen estrellas masivas. El valor de la masa total en cada cumulo esta listada en la col. (5) de la Tabla 6.1.

E.6 Estimación de IMF en YSCs

Los cálculos de la IMF en cúmulos de estrellas tanto en nuestra Galaxia como en las nubes de Magallanes son en general consistentes con la IMF local, y los valores

de las pendientes arriba de una masa solar generalmente se dispersan alrededor del valor de Salpeter (ver Fig. 1.1). En este contexto, Scalo (1998) sugiere una ley de potencias en tres segmentos de la forma

$$\begin{array}{rcll} \Gamma & = & -0.2 \pm 0.3 & 0.1 - 1\ M_{\odot} \\ & & -1.7 \pm 0.5 & 1 - 10\ M_{\odot} \\ & & -1.3 \pm 0.5 & 10 - 100\ M_{\odot} \end{array} \qquad \text{(E.5)}$$

Ahora, nosotros estamos en la posibilidad de derivar la IMF de nuestros YSCs y comparar nuestros resultados con los recientes estudios de otros cúmulos jóvenes.

Nos proponemos hacer los histogramas de masa para cada YSC y calcular la pendiente Γ, que representa al índice de la IMF en diagramas log M vs. log N. Para ello, necesitamos hacer un compromiso con el tamaño del intervalo en log M al momento de construir los histogramas de la funcion inicial de masa.

Para calcular el índice de la IMF de cada cúmulo, hicimos un ajuste de mínimos cuadrados en diferentes intervalos de masa, usando valores por encima de M_{lim}. Los valores de Γ fueron calculados a partir de $M_{lim} = 0.6$ $M_{\odot}$ para 14 YSCs, a partir de $M_{lim} = 1.2$ $M_{\odot}$ para 15 YSCs y de $M_{lim} = 2$ $M_{\odot}$ para los 11 cúmulos restantes.

Con el propósito de seleccionar el tamaño del intervalo mas conveniente, calculamos los índices de la IMF para diferentes intervalos en masa: 0.1, 0.15, 0.2, 0.25, 0.3, 0.35, 0.4, 0.45 y 0.5. La Fig. 6.4 muestra el tamaño del intervalo versus los valores promedio de Γ (Γ_1, Γ_2, Γ_3) para los tres intervalos de ajuste. Las barras de error corresponden al valor promedio de los errores de ajuste. Haciendo un ajuste de promedios pesado, obetuvimos para los tres intervalos:

$< \Gamma_1 >$ = -1.11 $\pm$ 0.23 $< \Gamma_2 >$ = -0.90 $\pm$ 0.15 $< \Gamma_3 >$ = -0.86 $\pm$ 0.23.

y por lo tanto, escogemos como el índice de la IMF en todo el espectro de masas, Γ_{YSC} = -0.96 $\pm$ 0.14, que es consistente con las tres estimaciones. El error corresponde a la desviación estandar en el promedio de los valores de gama.

Alternativamente, como ha sido sugerido por Meyer et al. 2000, un parámetro útil en los YSCs es el cociente de número de estrellas de masa intermedia a baja, el cual tiene la ventaja de minimizar el número de intervalos de masa a sólo dos, así como las incertidumbres en este cociente. Así, nosotros definimos el cociente

$$C = N(1.2 - 20\ M_{\odot})/N(0.6 - 1.2\ M_{\odot}) \qquad \text{(E.6)}$$

basados en los valores de masa mínimo y máximo que obtuvimos en nuestra muestra. Podemos calcular este cociente solamente en los 14 YSCs completos

hasta 0.6 $M_\odot$. Estos valores están incluidos en la última columna de la Tabla 6.1. El valor promedio de estos valores es de $C^{0.6} = 1.04 \pm 0.39$.

Por otro lado, es posible estimar estos cocientes para una IMF dada por medio de la integración de $dN/dM = M^{-\gamma}$, donde $\gamma = \Gamma$ - 1, y N es el número de estrellas en dM. Los valores que encontramos para las funciones de masa de Salpeter, Scalo (1998), Kroupa y la nuestra son: $C^{0.6}_{Sal}$=0.63, $C^{0.6}_{Sc}$=0.64±0.04, $C^{0.6}_{Kr}$=0.50 y $C^{0.6}_{-0.96}$=0.99, respectivamente (ver Fig. 6.9). De estos valores, se observa que mientras los nuestros son cercanos a C $\sim$ 1, los otros autores tienden a tener valores cercanos a $\sim$ 0.6. Esta discrepancia pudiera deberse a que nosotros estamos considerando un solo valor de la pendiente, pero es posible que la IMF contenga mas de una ley de potencias. Para checar esta posibilidad, graficamos el valor de Γ que habría en el extremo de las masas pequeñas versus el valor de la masa en la que se daría este cambio de pendiente, de tal forma que se mantenga el cociente C = 1, bajo una ley de potencias de - 0.96 para M > 2 $M_\odot$. La Fig. 6.10 muestra esta gráfica y notamos que para M < 1 $M_\odot$, existe un valor mínimo de $\Gamma \sim$ -0.75 en M_{brake} $\sim$1±0.07 $M_\odot$. Esto podría implicar una IMF del tipo

$$\begin{aligned} \Gamma &= -0.75 \pm 0.10 \qquad M < 1 M_\odot \\ &\quad -0.96 \pm 0.14 \qquad M > 1 M_\odot \end{aligned} \tag{E.7}$$

Además si $\Gamma = 0$ el cambio de pendiente ocurriría a 0.65 $M_\odot$ y se obtendrían valores positivos de la pendiente si el cambio de pendiente se diera en valores de masa cercanos a 0.6 $M_\odot$.

Si vamos a una masa todavía menor y si realizamos el cociente $C^{0.3} = N(1.2 - 20\ M_\odot)/N(0.3 - 1.2\ M_\odot)$ en los 6 YSCs completos hasta 0.3 $M_\odot$, observamos que el valor promedio, $C^{0.3}$=0.34, es muy cercano al valor de Scalo, $C^{0.3}_{Sc}$=0.29 $\pm$ 0.05 (ver Fig 6.11). Esto sugiere que esta IMF puede ser la IMF de los YSCs en Perseo en el extremo de las masas pequeñas. También es interesante hacer notar que estos valores son muy parecidos a los ejemplos citados en Meyer et al. 2000, en donde definen el cociente R como $R = N(1 - 10\ M_\odot)/N(0.1 - 1\ M_\odot)$ (ver Fig. 6.12).

En resumen, podemos adoptar como la función inicial de masa de los cúmulos estelares jóvenes en el Brazo de Perseo a los tres segmentos de ley de potencias

$$\begin{aligned} \Gamma &= -0.20 \qquad \text{for } 0.3 < M < 0.6 M_\odot \\ &\quad -0.75 \pm 0.10 \qquad \text{for } 0.6 < M < 1 M_\odot \\ &\quad -0.96 \pm 0.14 \qquad \text{for } M > 1 M_\odot \end{aligned} \tag{E.8}$$

La Fig. 6.13 muestra el histograma del"cúmulo promedio" construido con los valores promediados intervalo por intervalo de los 40 cúmulos (con una línea contínua), y de los 14 YSCs completos hasta 0.6 $M_{\odot}$ (línea punteada). Superpuestos están los tres segmentos de ley de potencias de la ecuación E.9, y vemos que coinciden muy bien con el histograma del "cumulo promedio", cuyo ajuste es $\Gamma_{all} = -1.01 \pm 0.09$.

E.7 Distribuciones espaciales de masa

Una vez que conocemos la masa de las estrellas en los cúmulos, es posible localizarlas espacialmente y estudiar su distribución dentro del área del cúmulo. Las figuras Fig. 6.14 a Fig. 6.17 muestran estas distribuciones espaciales. Los puntos negros son estrellas detectadas en el campo observado, los puntos rojos corresponden a estrellas de baja masa ($M < 1M_{\odot}$), los círculos amarillos a las estrellas de masa intermedia ($1M_{\odot} < M < 10M_{\odot}$), y los asteriscos azules corresponden a las estrellas masivas ($M > 10M_{\odot}$). Los círculos de líneas punteadas limitan el área de los cúmulos.

Comparando estas distribuciones, encontramos lo siguiente:

- el 49% de la muestra contienen estrellas masivas, en la mayoría de los casos estan ubicadas en el centro del cúmulo, pero hay también algunos casos en los que caen cerca del borde. El cúmulo con mas estrellas masivas es el YSC 1;

- existe un balance entre la población de estrellas de baja, intermedia y alta masa en 10 de los cúmulos (24% de la muestra), mientras que en el resto de los cúmulos con estrellas masivas (22%) dominan las estrellas de masa intermedia y hay muy pocas o ninguna de baja masa.

- En los cúmulos sin estrellas de alta masa, se puede presentar un balance entre estrellas de masa intermedia (27%) o un dominio de las de baja masa (17%), pero solo en 3 casos (7%) dominan las de masa intermedia.

Un problema importante que ha sido discutido por Stahler et al. 2000 es el de la segregación de masa. La segregación de masa se presenta cuando el promedio de la masa estelar en un YSC se incrementa hacia el centro del cúmulo, el cual es también la región mas densa. Hemos calculado y comparado las masas promedio m_1, m_2 y m_3 dentro del radio $r_1 = r_C/3$, en el anillo entre r_1 y $r_2 = 2r_C/3$, y entre r_2 y r_C, respectivamente. De este modo, la segregación de masa se da

cuando se cumple que $m_1 > m_2 > m_3$, la cual es evidente en 18 YSCs, o 44% de la muestra.

Las figuras Fig. 6.19 y Fig. 6.20 muestran algunas correlaciones que encontramos entre los parámetros de los cúmulos. En la gráfica de N_{CC} vs. M_{tot}, es decir, del número de estrellas en el cúmulo (ver col. (4) en Tabla 6.1) versus la masa total del cúmulo, se aprecia una doble agrupación de puntos, los círculos abiertos corresponden a cúmulos masivos, mientras que los círculos llenos corresponden a cúmulos de baja masa y que por lo general no contienen estrellas masivas.

Otra correlación interesante es la de M_T vs. r_C, que puede interpretarse como el posible estado de virialización de los cúmulos ($M_T \sim r_C$). También vemos en la gráfica de M_T vs. Γ que los cúmulos masivos ($\Gamma \sim$-0.5 y ~ 120 estrellas) tienen una IMF mas aplanada que los cúmulos de baja masa ($\Gamma \sim$-0.9 y ~ 40 estrellas).

E.8 Resúmen y Conclusiones

Hemos llevado a cabo un estudio observacional de cúmulos jóvenes enterrados en sus nubes maternas, con la finalidad de construir y comparar su función inicial de masa (IMF) así como las características físicas que los describen.

Establecimos criterios de selección que nos permitieran tener hallazgos exitosos en la búsqueda de estos cúmulos, basándonos en los flujos IR de fuentes IRAS aledañas a regiones HII pequeñas, cuya existencia pudiera propiciar el desarrollo secuencial de nueva formación estelar en cúmulos.

Llevamos a cabo un programa de observaciones con la cámara infrarroja CAMILA en el telescopio de 2.1 m del OAN/SPM, durante 5 temporadas en las que completamos un survey de 38 regiones de formación estelar en las bandas J, H y K del IR cercano.

El tratamiento de los datos fotométricos fue hecho con el paquete de reducción fotométrica IDL/DAOPHOT por sus ventajas de rapidez y precisión. El error intrínseco alcanzado en la fotometría fue menor que 7%.

Con las distancias obtenidas de la literatura (valor promedio de 3.6±1.8 kpc) estimamos el radio de los cúmulos r_C, encontrando que $0.26 < r_c < 2.34$ pc y la mayoría entre 0.5 y 2 pc. La densidad superficial de estrellas es de $3 < \Sigma < 220$ stars/pc^2 en la muestra y la concentración de estrellas es ~ 3 veces menor que en los cúmulos globulares.

Construimos histogramas de luminosidad y desarrollamos un método de estimación de edad de cúmulos en base a su función de luminosidad en la banda J. El valor promedio de la edad de los cúmulos es de 2.42 ± 1.20 Myr, en un intervalo

de 1.1 a 5.5 Myr. Con esta estimación y con ayuda de las trazas evolutivas de D'Antona & Mazzitelli y de Hillenbrand et al. 1995, derivamos las isocronas para edades de 0.1, 0.3, 1, 3, 10, 30 y 100 Myr en el diagrama J vs. J-H por medio de la relación $J = 4.74 - 2.5\,log\,(L/L_{\odot}) - BC(T_e) - (V - J)$.

Haciendo uso de los diagramas de diagnóstico, J-H vs. H-K y J vs. J-H, y asociando la isocrona correspondiente a la edad estimada de los cúmulos, calculamos la extinción y la masa individual de las estrellas. La masa de las estrellas MS enrojecidas fue tomada de la escala de masas a lo largo de las isocronas al llevarlas desde su posición en el diagrama J vs. J-H en la dirección del vector de extinción A_V. La masa de las estrellas CTT y Ae/Be enrojecidas se estimó por medio de las relaciones empíricas de Carpenter et al. 1993, $\log M = -0.25\ M_H + 0.44$ y $\log M = -0.24\ M_K + 0.24$, donde M_H y M_K son las magnitudes absolutas sin corrección por extinción.

Con el propósito de hacer una comparación realista entre las distribuciones de masa de los cúmulos, definimos el límite de completez en masa M_{lim}, que define el límite al cual una muestra de estrellas en un cúmulo es considerada completa. Encontramos que 14 YSCs son completos hasta $\sim$0.6 $M_{\odot}$, 29 (15 + 14) hasta $\sim$1.2 $M_{\odot}$ y todos, 40 (11 + 15 + 14), hasta $\sim$2 $M_{\odot}$. Calculamos índices de IMF en estos grupos de cúmulos por medio de ajustes lineales de mínimos cuadrados a los histogramas de masa, y el valor promedio de estos valores que es consistente en todo el espectro de masas es Γ = -0.96 $\pm$ 0.14.

Al estimar cocientes de número de estrellas de masa intermedia a baja (Meyer et al. 2000), y comparando con las leyes de potencias de otros autores (Salpeter 1955, Scalo 1998, Kroupa et al. 1993), encontramos que pueden existir cambios en la pendiente de la IMF en el extremo de la baja masa. La función inicial de masa (IMF) que extraemos de la muestra de 40 YSCs en el Brazo de Perseo está compuesta por los tres segmentos mostrados en la ecuación E.9 donde el primer valor, de Scalo 1998, es sugerido del estudio de 6 YSCs, el segundo de 14 YSCs y el último de la muestra de 40 YSCs.

En general, podemos decir que la IMF en el Brazo de Perseo es mas plana en el momento actual, de como fué en la vecindad solar. Coincidimos con otros autores en que existe un cambio de pendiente en el extremo de las masas bajas. Del estudio de sistribuciones espaciales de masa y de correlaciones entre parámetros físicos de los cúmulos, se muestra una bimodalidad en la formación de YSCs, cúmulos masivos ($\sim$ 150 $M_{\odot}$) y cúmulos menos masivos ($\sim$ 50 $M_{\odot}$). Los cúmulos masivos muestran una IMF mas plana que los menos masivos.

Nuestro trabajo muestra que los YSCs ofrecen un excelente laboratorio para el estudio de la IMF, y alentamos a que se haga un mayor trabajo futuro en esta línea de investigación.